Summer 8-15-2022

The Influence of Processing and Additives on Cellulose Nanofiber Properties for Orthopedic Application

Mitchell P. Chesley
University of Maine, mitchell.chesley@maine.edu

THE INFLUENCE OF PROCESSING AND ADDITIVES ON CELLULOSE NANOFIBER PROPERTIES FOR ORTHOPEDIC APPLICATION

By

Mitchell P. Chesley

B.S University of Maine, 2017

M.S University of Maine 2019

A Dissertation

Submitted in Partial Fulfillment of the

Requirement for the Degree of

Doctor of Philosophy

(in Biomaterial Engineering)

The Graduate School

The University of Maine

August 2022

Advisory Committee:

Dr. Michael Mason, Professor of Biomedical and Chemical Engineering, Advisor

Dr. Mehdi Tajvidi, Associate Professor of Renewable Nanomaterials

Dr. Ian Dickey, Assistant Professor of Orthopedic Oncology & Adult Reconstruction, Colorado

Dr. Douglas Bousfield, Professor of Biomedical and Chemical Engineering

Dr. Benjamin Lakin, SVP, Innovation & Technology, Cambridge Innovation Institute

THE INFLUENCE OF PROCESSING AND ADDITIVES ON CELLULOSE NANOFIBER PROPERTIES FOR ORTHOPEDIC APPLICATION

By: Mitchell Chesley
Dissertation Advisor: Dr. Michael D. Mason

An Abstract of the Thesis Presented
In Partial Fulfillment of the Requirements for the
Doctor of Philosophy
(in Biomaterial Engineering)
August 2022

Current orthopedics are separated into three different classes of materials, metals, polymers, and ceramics. While these devices have had success throughout the years they are not without their faults. Metallic devices for example are usually extraordinarily stiff when compared with the surrounding bone. This difference in stiffness induces localized stress-shielding promoting cortical atrophy, which can lead to osteoporosis. Polymers while having the capacity of being biodegradable and bioabsorbable also have the potential to incite localized demineralization and weakness in surrounding bone. A result of breakdown byproducts not efficiently being evacuated from the area, which additionally acts as catalysts expediating the degradation rate. Ceramic devices while providing superior osteointegration, with a potential of being comprised from minerals analogous to naturally sourced bone, tend to be extremely brittle causing premature failure of devices. While materials currently used have their benefits, providing medical

professionals with sufficient alternatives is imperative, for them to have more variety during operations.

Our proposed solution is the use of a recent biopolymer of interest, cellulose nanofibrils (CNF). CNF is a biopolymer that is incredibly naturally abundant, being the base structure sourced from cellulosic materials and byproducts of many agricultural industries. CNF additionally has physical properties that make it a promising material within the orthopedic field. It is morphologically similar to collagen, can be easily chemically modified, and has tunable mechanical properties. CNF, while heavily studied by many research groups has rarely been studied in large bulk. Throughout this thesis processing and additive properties of CNF were determined, including bulk orientation, effects of composites, and crosslinking. Bulk orientation was determined through a multitude of mechanical testing and found an orientation within the large length direction of molds. Composite films were produced under different conditions and tested to view their effects. Crosslinking of CNF was conducted and viewed with an acute submersion and water absorption testing, viewing effects of crosslinker and amount (~2.5 % crosslinker). Finally, a simple computer simulation was made using CNFs now determined properties and placed under known loads experienced by specific orthopedic devices.

ACKNOWLEDGMENTS

First and foremost, I would like to thank my advisor Dr. Michael Mason for allowing me to partake in such an influential project, and for giving me the experience needed to continue in the research field. I would also like to thank him for the enthusiasm and encouragement he has given me throughout these challenging years. I give thanks to Dr. Mehdi Tajvidi, Dr. Douglas Bousfield, Dr. Benjamin Lakin, and Dr. Ian Dickey, who have given me insight into the many different aspects of researching materials for biomedical field. I also am grateful for everyone in my research group Aileen Co, Aimee Co, Jeremy Grant, Travis Haysley, and Kora Kukk, who have helped me and supported me through my graduate career. I am also grateful for the support and help I got from Justin Hardcastle, Madison Mueth, Jordan Miner, Jan Wusik, and Joshua Hamilton. Additionally, I would like to thank all the undergraduate students who have worked with me on this project thought the years, without their help none of this work would have been completed. I would like to thank Emma perry with the ICORE who helped me obtain my images used in this thesis. Lastly, I would also like to thank David Holomakoff for setting the groundwork for this project and for mentoring me during the beginning of my scientific career.

I would like to acknowledge my family who have supported me throughout this endeavor, especially my mother and father who helped me push myself past any boundaries that have been placed in front of my path and encouraging me to achieve my pursuits. And all my friends who have always believed and encouraged me along this journey and who support me in the next chapter of my life.

TABLE OF CONTENTS

LIST OF TABLES

LIST OF FIGURES

LIST OF ABBREVIATIONS

CNF - Cellulose Nano-fibrils

PLA - Poly(Lactic Acid)

PGA - Poly(Glycolic Acid)

PLLA - Poly(L-Lactic Acid)

PDLA - Poly(D-Lactic Acid)

DL-PLA - Poly (D, L-Lactic Acid)

HA - Hydroxyapatite

SEM - Scanning Electron Microscopy

Wt%- Weight Percent

OD-Optical Density

CHAPTER 1

INTRODUCTION

1. Introduction

Current orthopedics are separated into three different classes of materials, metals, polymers, and ceramics. While these devices have had success throughout the years they are not without their faults. Metallic devices for example are usually extraordinarily stiff when compared with the surrounding bone. This difference in stiffness induces localized stress-shielding promoting cortical atrophy, which can lead to osteoporosis. Polymers, while having the capacity of being biodegradable and bioabsorbable, also have the potential to incite localized demineralization and weakness in surrounding bone. There is a result of breakdown byproducts not efficiently being evacuated from the area, which additionally acts as catalysts expediating the degradation rate. Ceramic devices, while providing superior osteointegration, with a potential of being comprised from minerals analogous to naturally sourced bone, tend to be extremely brittle causing premature failure of devices. While materials currently used have their benefits, providing medical professionals with sufficient alternatives is imperative, for them to have more variety during operations.

Our proposed solution is the use of a recent biopolymer of interest cellulose nanofibrils (CNF). CNF is a biopolymer that is incredibly naturally abundant being the base structure sourced from cellulosic materials and byproducts of many agricultural industries. CNF additionally has physical properties that make it a promising material within the orthopedic field. It is morphologically similar to collagen, can be easily chemically modified, and has tunable mechanical properties. CNF while heavily studied by many research groups has rarely been studied in large bulk. Throughout this thesis processing and additive properties of CNF were determined

as well as a brief literature review, discussing bone anatomy, physiology, and the mechanisms for which it senses stimulants. Then discussing the current state of orthopedic materials and their potential complications, discussing CNF, its properties and manufacturing. And finally discussing specific standard testing that is applied to new materials to be presented to the FDA. Later bulk orientation, effects of composites, potential cytotoxicity, and crosslinking will be discussed. Bulk orientation was determined through a multitude of mechanical testing and found an orientation within the large length direction of molds. Composite films were produced under different conditions and tested to view their effects. Crosslinking of CNF was conducted and viewed with an acute submersion and water absorption testing, viewing effects of crosslinker and amount (~2.5 % crosslinker). Finally, a simple computer simulation was made using CNFs now determined properties and placed under known loads experienced by specific orthopedic devices.

CHAPTER 2

LITERATURE REVIEW

2.1. Human Bone

There are 213 bones in the adult body separated into 126 appendicular skeleton, 74 axial skeleton, and 6 auditory ossicles bones[1]. Human bone is classified into two types, cortical and trabecular bone. Cortical bone is a mechanically stiff outer layer of the bone comprised of mineralized collagen, whereas trabecular bone is a spongy opened cell-matrix in which bone vascularization is facilitated. Humans are comprised of ~80% cortical and ~20% trabecular bone, with bone mass depending on location and mechanical loading of the bone[1,2]. Bone mass is comprised of 50-70% mineral, primarily a naturally occurring bone mineral called hydroxyapatite (HA), which is a form of calcium apatite with a chemical structure of ($Ca_5(PO_4)_3$) or ($Ca_{10}(PO_4)_6(OH)_2$) to denote crystal unite cell, 20-40% collagen, and 5-10% water[1,3–5]. Natural hydroxyapatite contains copious substitutional variants brought about through interactions with various electrolytes in the interstitial fluid. One such substitutional variant is carbonated hydroxyapatite which can be found up to 8% in natural HA[1,6,7]. Other ionic substitutions (e.g., F^-, CO_3^{2-}, Na^+, Mg^{2+}, Zn^{2+}, and Sr^{2+}) occur during HA production due to passing fluids[8,9].

Cortical bone is the hard external mineralized shell of the bone, with high mechanical stiffness, while trabecular bone or cancellous bone is a softer vascularized system. Mechanical properties for these tissues have discrepancies depending on the method and condition of mechanical testing, as such an approximation is usually used and is depicted in table 2.1 with modulus, tensile strength, and compressive strength being shown.[10,11]. Trabecular bone is

Table 2.1: Bone Mechanical Properties

Type	Modulus (GPa)	Tensile Strength (MPa)	Compression Strength (MPa)
Cortical bone (Longitudinal Direction)	~17	~133	~193
Cortical Bone (Transverse Direction)	~12	~51	~133
Cancellous Bone	~0.4	~7.4	~50

structured out of cylindrical networks called Haversian canals which are connected by Volkmann's canals seen in figure 2.1. During everyday activities, bone experiences stresses and strains that result in deformations. These deformations create pressure gradients resulting in fluid flow within the pericellular space of the cytoplasmic process which causes drag forces. Drag forces then creates shear stress on osteocytes within the cannel which make up 90-95% of bone cells[12,13]. Osteocytes are the primary mechanosensory cells that use extracellular membrane receptors such as integrins and CD44 receptors as mechanotransducers. Using the information derived from these systems osteocytes then direct osteoblasts and osteoclasts to remodel the bone[12,13].

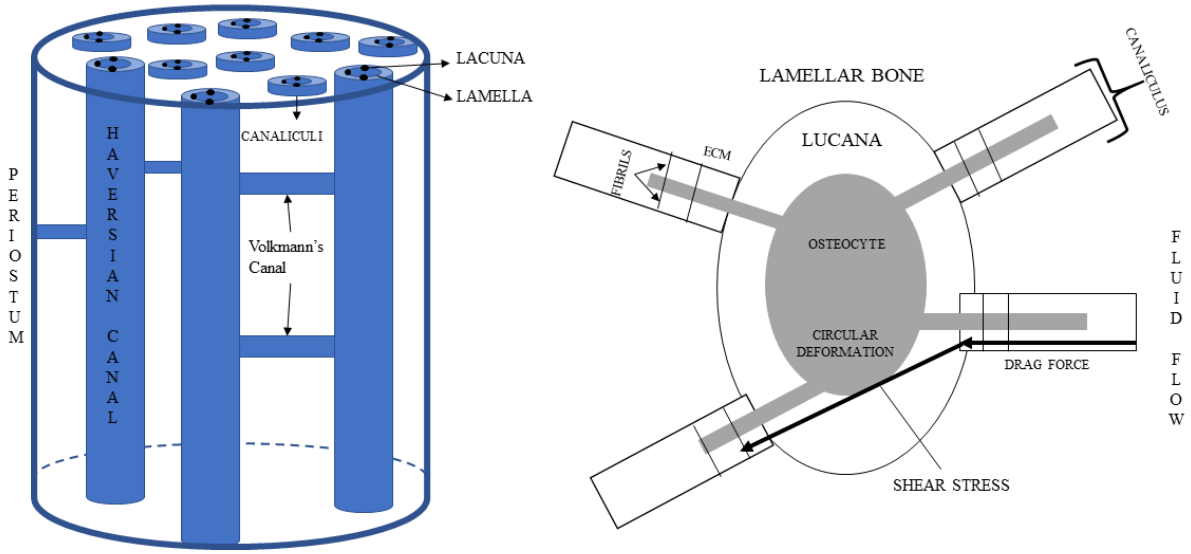

Figure 2.1: Anatomy of Bone Interior (Left), Fluid Flow and Interaction With Osteocyte (Right), Recreated From Ref([12]).

Along with osteocytes, osteoclasts, and osteoblasts, proteins, such as bone morphogenic proteins (BMP), are involved with bone growth. BMPS were discovered in 1960, to date there are 20 identified and characterized BMPs[14]. BMPs have importance in bone development and the development of various tissue outside of bone[14]. It has been shown that BMP 2,4,5,6,7, and 9 have the greatest osteogenic capacity (Table 2.2). Through a process of implanting BMPs into *in vivo* bone induction assay systems, BMP 2 was first shown to induce the formation of cartilage and bone tissue, giving life to the hypothesis these BMP classes of molecules were necessary and held significance for osteoinduction[14]. While research has been done with BMP there is still much not known and there is much speculation about their specific cellular and molecular mechanisms and function of specific BMPs.

Table 2.2: Table of Known BMP and Their Functions, Recreated From Ref([14])

BMP Type	**Function**
BMP-1	Metalloprotease acts on procollagen I, II, and III Involved in cartilage development
BMP-2	Induces bone and cartilage formation by acting as a disulfide-linked homodimer Key role in osteoblast differentiation
BMP-3	Induces bone formation
BMP-4	Regulates formation of teeth, limbs, and bone from mesoderm Role in fracture repair
BMP-5	Cartilage development
BMP-6	Joint integrity in adults
BMP-7	Key role in osteoblast differentiation Renal development and repair
BMP-8	Bone and cartilage development
BMP-9	Chromogenic differentiation of human multipotential mesenchymal cells
BMP-10	Trabeculation of embryonic heart
BMP-15	Role in oocyte and follicular development

Upon fracture of a bone, multiple mechanisms take places for which bone is regenerated and reshaped. This process incorporates 4 phases of healing (figure 2.2) and is considered to primarily occur over a period of 3 to 6 months but can vary by individual. Inflammation and revascularization of bone happens in the first 2 weeks, which is crucial to bone healing. Following the revascularization and inflammatory stage, repair begins. This involves fibroblasts laying down

a stroma that supports vascular ingrowth, after 4 to 6 weeks of healing the callus is mechanically weak and requires adequate forms of protection such as braces or internal fixation. Bone healing is then subsequently finished during the remolding state, in which the bone is restored to its original shape, structure, and mechanical integrity. This is a slow process that can take months or even years and is facilitated by a mechanical stimulus that is placed on the bone, utilizing the osteocytes' mechanotransduction as described above[15].

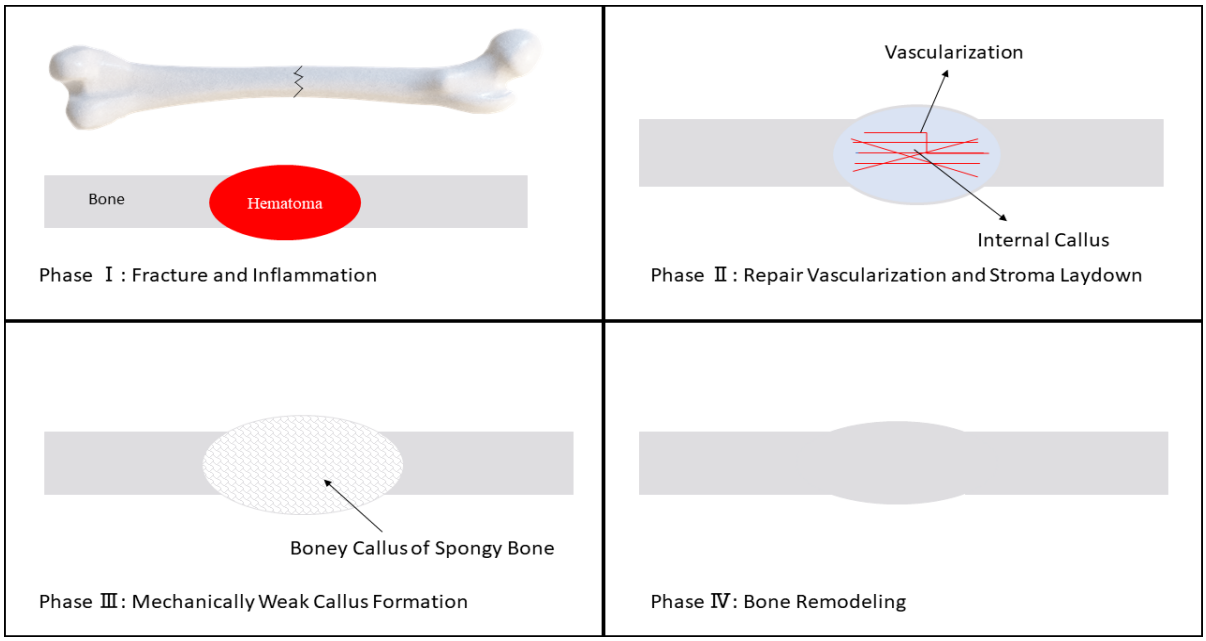

Figure 2.2: Bone Healing and Remolding Process.

2.2 Current Device Materials

Medical devices have made considerable improvements over the millennia, from wooden prostheses 4000 years ago in Egypt, to metallic and plastic implants[16]. The field of orthopedics and biomaterials is a never-ending struggle for perfection, creating materials that seamlessly interact and benefit biology in intended ways. This has been done in small steps, creating materials that are bioabsorbable have, corrosion-resistant, biocompatible, mechanically robust (during required initial healing), and have osteo-conductive and -inductive properties, and controlled

mechanical decay[16–18]. There are three primary categories of biomaterials from which medical devices are manufactured are metals, polymers (including natural polymers), and ceramics. The bulk of devices is made from either metallic or polymeric sources, while ceramics have been used as a method of coating other devices. Materials used within orthopedics and devices can be seen in Figure 2.3 which shows moduli of materials and their density, specific materials such as cortical and cancellous bone have been outlined.

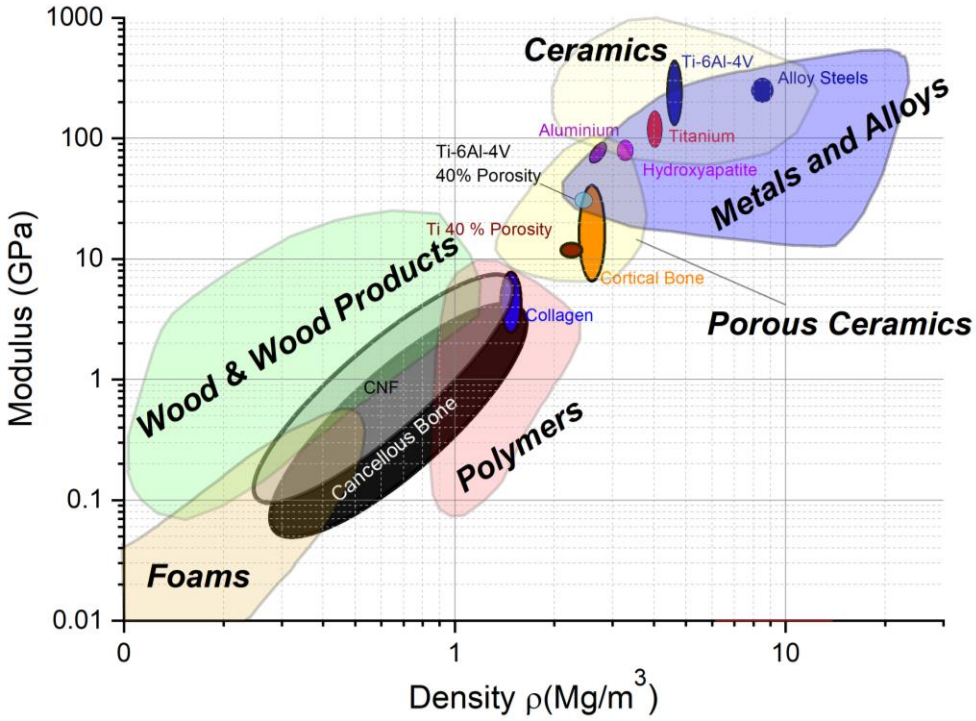

Figure 2.3: Moduli vs Density of Commonly Known Materials and Specific Medical Device Materials.

Ceramics consist of calcium phosphate-sourced minerals. These can be in the form of calcium phosphate both alpha and beta forms, hydroxyapatites, and bioglasses. These materials alone have a low strain when put under loads, however, they have been proven to possess osteoconductive and inductive properties, with their surface chemistry and degradation products providing ideal conditions for bone growth. Commonly modern metallic and polymer devices have

incorporated such ceramics as a surface layer or composites, providing osteoconductive elements to devices during their breakdown, signaling bone formation and growth[19–22]. This allows devices to have the benefit of mechanical robustness coupled with the added osteointegration properties of the bioceramics.

As bone healing is imperative during early fracture and stroma formation, adequate fixation or brace strength is required. However, after a period of time, fixation strength can be detrimental with stress shielding, causing sufficient mechanotransduction stimulation of natural bone to be

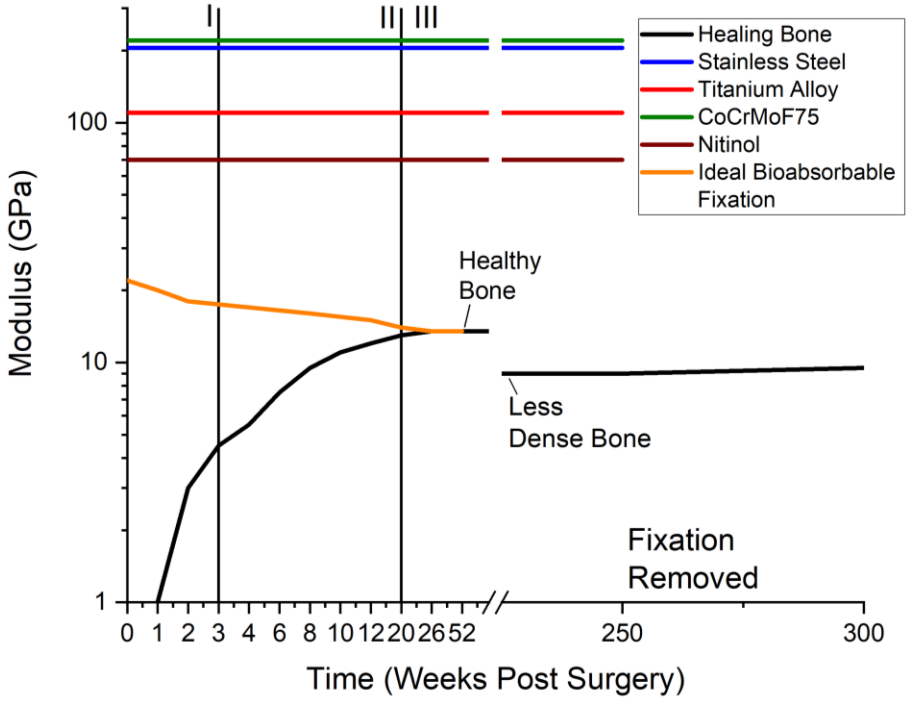

Figure 2.4: Moduli of Known Metals Used in Orthopedics vs Bone Healing and Idealistic Bioabsorbable Devices.

compromised weakening bone by signaling osteoclasts. Designing devices that have a controlled and reproducible mechanical decomposition is important to ensure natural stimulation can be reestablished. Figure 2.4 shows an example of fixation devices' mechanical decay over time versus bone healing.

Orthopedic surgery has become a financial burden on patients receiving these operations, with the cost for primary surgeries increasing yearly. In general healthcare costs have been increasing as a whole, with an increase from $5 billion in 1960 to $515 billion in 2010[23]. In 2010 Sathiyakumar *et al.* estimated that 8.2 billion dollars were spent annually on orthopedic surgeries alone contributing a large percentage of the national healthcare expenditure[23]. This cost is a combination of personnel costs, supplies, medical suite reservation, post-operation and pre-operation imaging (X-ray/MRI), and equipment cost[23,24]. A study by Herzog *et al.* showed that outpatient surgeries for anterior cruciate ligament (ACL) reconstruction surgeries showed a mean increase in the cost of upwards of $4,000 after just 8 years[25]. Bioabsorbable devices, despite having an increased initial price benefit from reducing the need for secondary removal or exploratory surgeries and decreasing the overall price as a whole[26]. While primary device surgeries are expensive, secondary surgeries on average cost more than the initial implantation due to biological overgrowth removal and the subsequent time that is taken to dismantle[24,27]. The cost of secondary surgery is subject to change depending on multiple factors, such as the location and state of the device.

An example of this price discrepancy between primary and secondary surgeries can be seen in total joint replacements of the knee compared to subsequent surgeries of ACL reconstruction. The primary total knee arthroplasty surgery cost for a 90-day average was found to be $17,662 and $24,131 in revision total knee arthroplasty in 2012, which fluctuated between subgroups including age and gender[28]. This trend can again be seen in operations that are considered common such as ACL reconstruction surgeries which have a total healthcare cost of $15,000 for primary procedures and $16,238 for secondary surgeries in 2014[25].

2.2.1 Metals

Metallic medical devices have been used and studied for the past century with the first successful devices being comprised of stainless steel and cobalt-chrome-based alloys, which are desirable materials due to their mechanical robustness[29]. Early metals used in surgeries were stainless steel and cobalt-chromium. More recently metals such as titanium alloys, magnesium alloys, and Nitinol (Nickel Titanium Alloy)[30] have been employed within orthopedic surgeries. Table (2.3) shows Young's moduli, ultimate tensile strength, and fracture toughness. Metals are intended to be left post-operation, not requiring post-operative removal or replacements. The high moduli, yield point, and ductility of metals lead to their inevitable adoption within orthopedic surgeries for high load-bearing replacements[17].

Table 2.3: Table of Metal Mechanical Properties Comparative to Cortical Bone, Recreated from Ref([30])

Materials	Young's Modulus (GPa)	Ultimate Tensile Strength (MPa)	Fracture Toughness (MPa $m^{1/2}$)
CoCrMo Alloys	240	900-1540	~100
316L Stainless Steel	200	540-1000	~100
Ti Alloys	105-125	900	~80
Mg Alloys	40-45	100-250	15-40
NiTi Alloys	30-35	1355	30-60
Cortical Bone	10-30	130-150	2-12

Metallic implants are not without their own set of complications, ranging from stress shielding, aseptic loosening, fracture (from both static and dynamic loading), corrosion, inclusions, debris migration, surgical error, and other immunological issues[17,31,32]. Device failures commonly suffer from compounding issues with one complication leading to another causing failures and rejection. This is especially true of immune responses and reactions, being the common response elicited by device complications. The causes of implant failures and a description of their effects can be seen in figure 2.5. Stress shielding occurs due to metals' superb stiffness, which vastly exceeds that of bone in some cases 10-20 orders of magnitude, creating localized stress shielding within locations of implantation. Stress shielding can interfere with the bone's mechanotransduction processes which can lead to bone remodeling in which total bone density decreases called osteopenia and later osteoporosis weakening the bone which can lead to further damage[10,17,33].

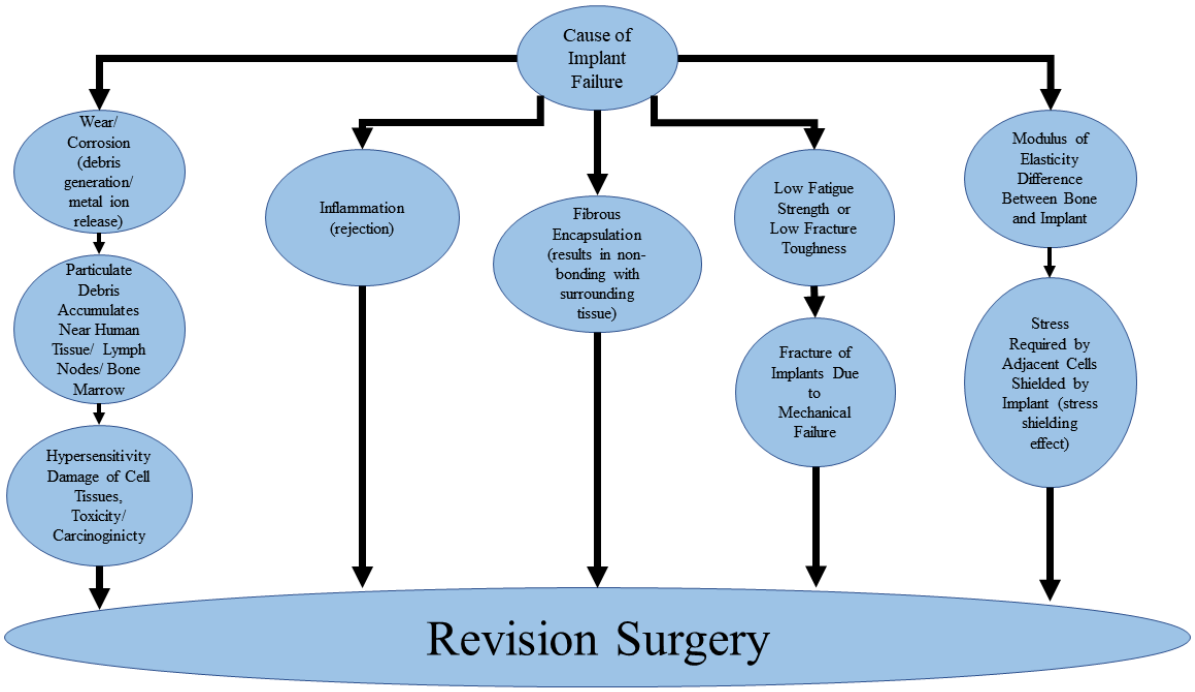

Figure 2.5: Flow Chart of Implant Failure Causes, Recreated Form Ref([31]).

Along with stress shielding, metallic devices have a higher incident rate of ionic corrosion, through gradual degradation by electrochemical or chemical attacks within the hostile electrolytic human environment[16,17,32]. Corrosion can also be affected by wear fatigue of the device and in many cases a synergistic combination of electrolytic attack and wear. After implantation, devices form an oxide surface (nm thickness) giving rise to osteoinduction creating close proximity of biological interfacing, however, connective tissue can grow to interfere with the osteoinduction and potentially cause implant loosening[17] (Figure 2.6).

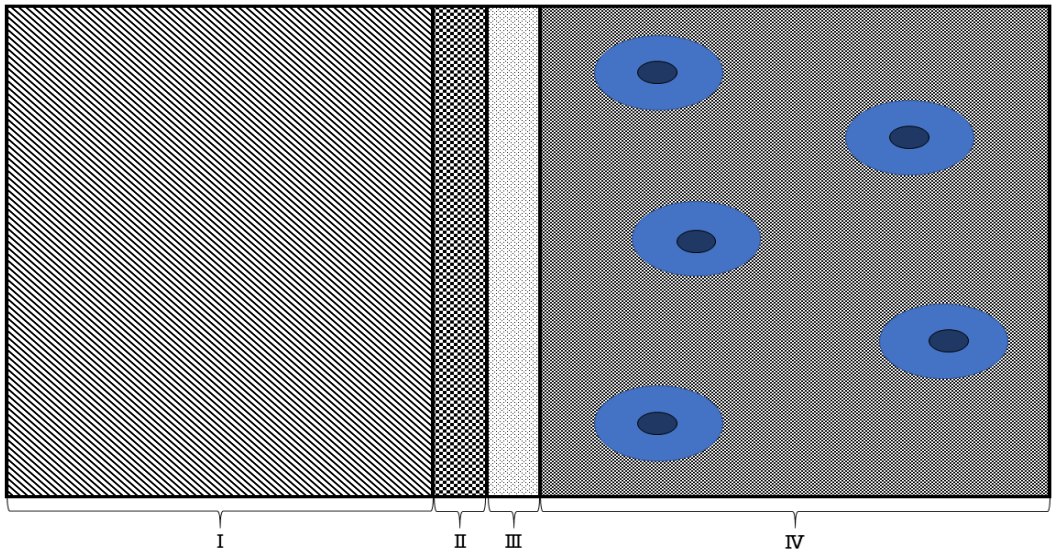

Figure 2.6: Metallic Interfacing With Biology; I: Bulk Material; II: Surface Layer of Materials; III: Adsorbed Layer of Water, Iron, and Proteins; IV: Cells in Biological Fluids([17]).

Corrosion, in general, can be described either as uniform surface corrosion or localized corrosion and can be derived their manufacturing defects, mechanical situations, or induced through environmental effects. Fabricated corrosions consist of crevice corrosion (affecting regions that are shielded from tissue fluids), pitting corrosion (sites corrosion on surfaces)[17], and intergranular corrosion (multiple grain regions, producing a heightened energy state with more active anodic regions)[34,35]. Mechanically induced corrosion can also occur depending on implant

location, these corrosions include stress cracking corrosion (occurrence of material under tension and environmental corrosion), fatigue corrosion (dynamic bending or loading interrupts passive film formation exposing underlying layers), fretting corrosion (movement from surrounding area removing and exposing new layer), and stress/galvanic corrosion (bending causes tensile side to be more anodic compared to compressive side, equilibrium upset causing accelerated corrosion from the more anodic side)[34,35]. Corrosion of devices in all forms can cause premature failure of devices mechanically and accelerate releases of metal particles and ions into the system, creating more toxic byproduct buildup and eliciting more immunological responses. In addition, metallic ions in the system can affect surrounding tissue through electrical currents altering the chemical environment, behavior of cells, and/or cellular metabolism[17].

Aseptic loosening of implants is a phenomenon that can occur from bone uptake and inflammatory responses, in which devices are loosened by defective bones[36]. Leading to device malfunctions and in some cases migration. Aseptic loosening can occur in a multitude of ways, from patient excessive activity, material fatigue, debonding at tissue-implant, stress shielding, inflammation, infection, and osteolysis[19]. In addition, wear causes macrophages to be attracted to

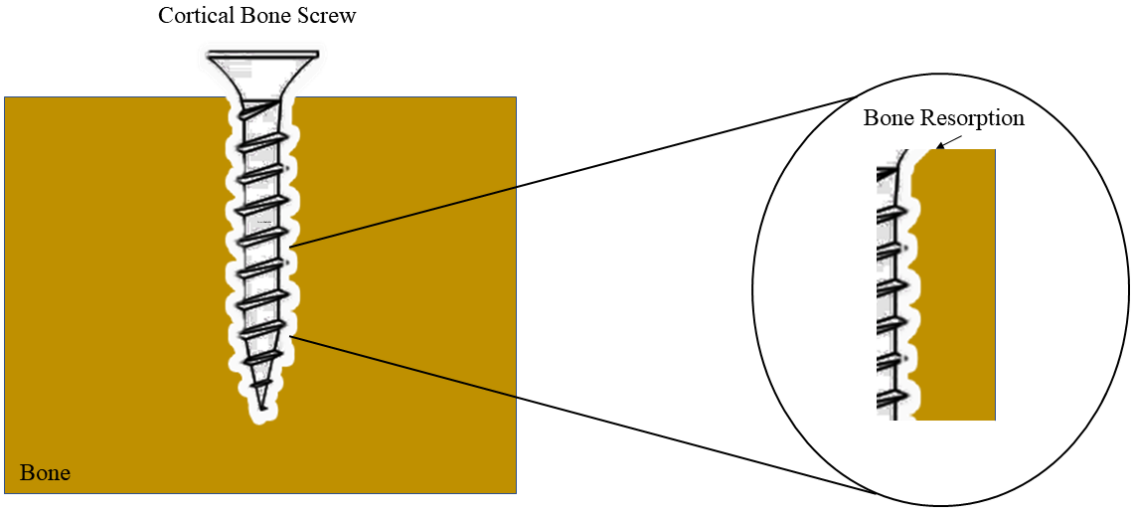

Figure 2.7: Example of Aseptic Loosening of a Cortical Screw.

the devices engulfing foreign objects[36], this can cause macrophages to die releasing enzymes and metabolites that can cause acidification in the immediate microenvironment[30]. The release of inflammatory mediators through this process results in chronic inflammation and tissue damage that negatively affects supporting bone in the area, causing adverse effects with the implanted devices[32,37,38]. In addition, wear particulates released from the devices have been shown to induce additional bone resorptive cytokines production, which increases further osteolysis[36,39].

2.2.2 Plastic

Polymers, primarily thermoplastics, have been used and researched for medical applications for many years. Thermoplastics such as Polylactic Acid (PLA), Polyglycolic Acid (PGA), their isomers Poly L-lactic acid (PLLA) is mostly crystalline, Poly D-lactic acid (PDLA) is mostly amorphous[40], copolymers of polylactic acid and polyglycolic acid (PLA-PGA), and polyether ether ketone (PEEK) are used for plastic orthopedic devices to date. Plastic devices are usually used in low load-bearing locations, this is due to their lower mechanical properties compared to metals[41]. Their mechanical properties when compared to cortical bone are starkly different as shown in figure 2.8, which depicts moduli of conventional bioresorbable plastics compared to an example of an idealistic bioabsorbable implant over time.

Plastics were introduced with the intention of being bioabsorbable, meaning they would be implanted, and over time be absorbed into the body and disposed of. This process would either entail the device being replaced by biological tissue upon its decomposition or biological tissue would in grow into the device and take over main loads. In the case of PEEK, these devices were developed to remain in place and be ambivalent to biology. This allows for potential revision surgeries to be performed post-operation if the need arises in the future. Thermoplastics, when

compared to metallic materials, exhibit more desirable mechanical properties in terms of bone analog stimulants, albeit thermoplastic applications in load-bearing procedures are limited.

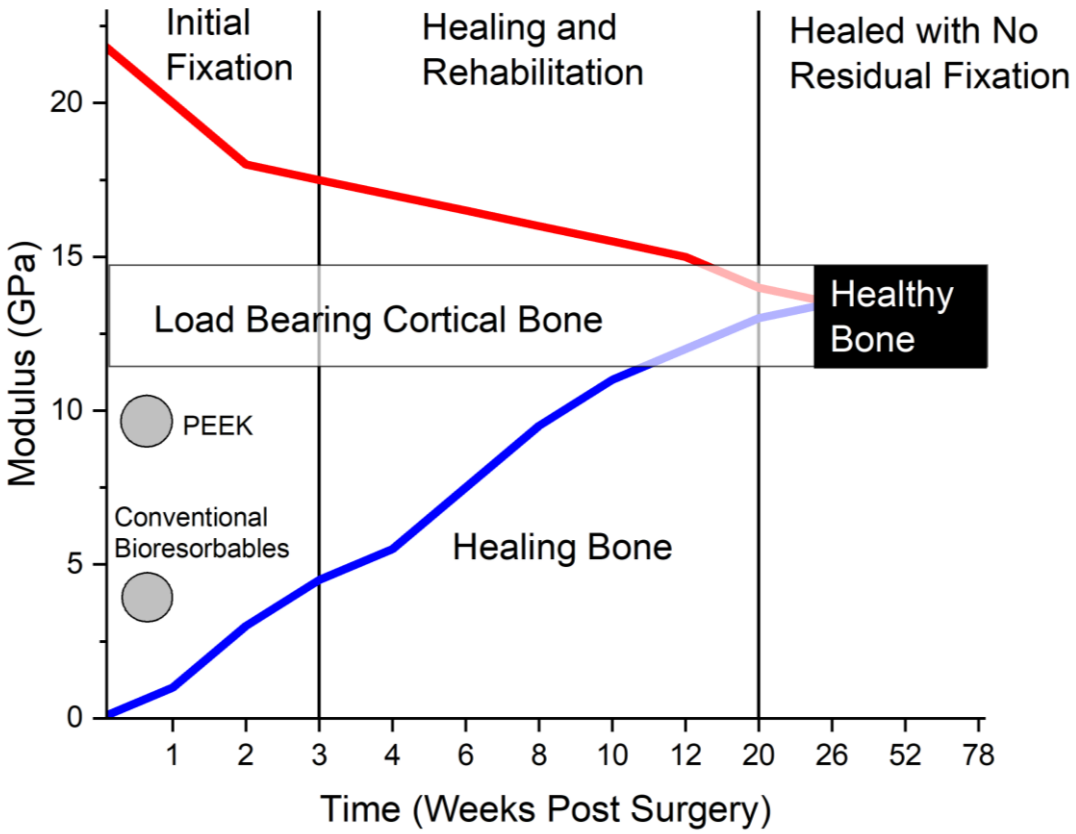

Figure 2.8: Ideal Residual Mechanical Properties of Absorbable Device (red), Bone Healing (blue), Example Moduli of Existing Plastics.

Thermoplastics, excluding PEEK, degrade through hydrolytic cleavage releasing either lactic acid or glycolic acid as a byproduct[42]. The time of mechanical decay for polymers is dependent on the type chosen, usually occurring over 5 to 8 weeks, with PGA decaying the fastest[21,43,44], while PLA decays slower, and PLLA degrading the slowest due to its higher resistance to hydrolysis than its isomer counter parts[40]. A comparison of thermoplastic modulus, strength loss, and mass loss can be seen in table 2.4[45,46].

Table 2.4: Thermoplastic Modulus, Loss of Strength, Loss of Mass

Polymer	Modulus (GPa)	Loss of Strength (Months)	Loss of Mass (Months)
PGA	12.8	1-2	6-12
PLA	3.5	~1	24-30
LPLA	4.8	6	>5 years
PLA-PGA	1.4-2.8	6-8 (weeks)	1-2 years
PEEK	4.0	NA	NA

Devices are degraded in two ways either by bulk degradation (middle out) or erosion/surface degradation (outside to middle)[45,47]. This process is facilitated by nonspecific hydrolytic scission of ester groups, being affected heavily by different physical and chemical properties such as chemical composition, structural configuration, processing, porosity, device size, molar mass, and morphology[21,29]. The porosity of devices plays a role in the expulsion of acidic byproducts which if not expelled property increase the rate of the hydrolysis[40]. This acidic environment exposes byproducts to carboxylic end groups which act as a catalyst (figure 2.9) to the internal hydrolytic process expediting the degradation rate[21,29,48]. If these acidic byproducts build up in the surrounding area the pH of the surrounding tissue is dropped, which in turn, can induce bone uptake that weakens the tissue[29,40,47–49] and/or causes negative immunological responses in the surrounding tissue[40,50–52].

Additionally, within the first two weeks after implantation, the physiological pH decreases to ~5.2 before reestablishing back to 7.4, this can cause early degradation of some polymers[17]. Although biodegradable plastics have improved post-operative monitoring due to their decrease in artifacts primarily in Magnetic Resonance Imaging (MRI)[53,54]. These devices can still suffer from

device implantation damage, debris migration, effusion, cyst formation, and specific bioabsorbable screws bone tunnel enlargement[51,55–60].

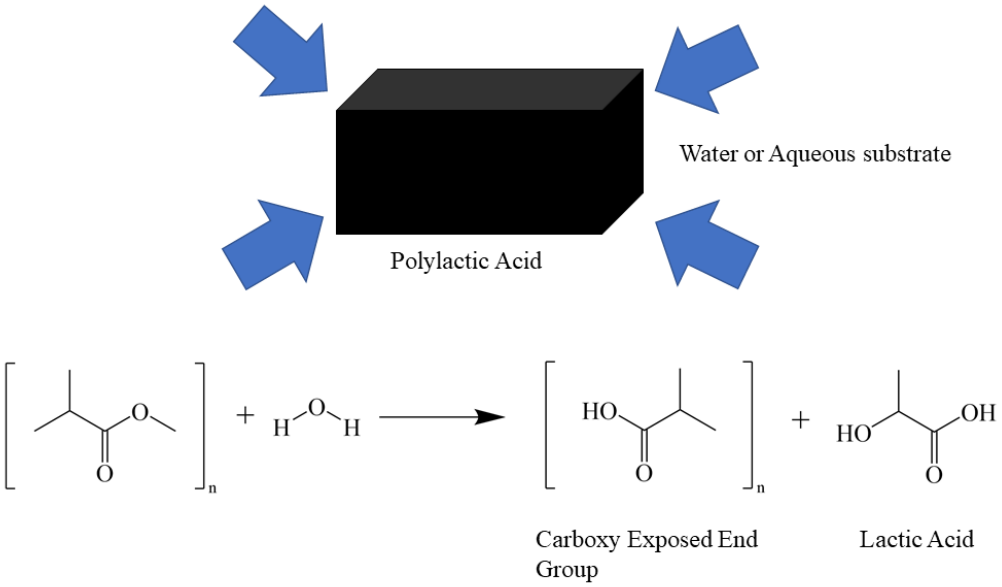

Figure 2.9: Example of Thermoplastic Hydrolytic Degradation and Byproduct Release, PLA Used as Example.

2.3 Targeted Potential Orthopedic Application

The field of orthopedics incorporates a large breadth of devices, with geometries and architecture varying dependent on location. Some examples of these devices are fixation plates, pins and screws, and suture anchors. Suture anchors themselves have revolutionized the orthopedic field for both open and arthroscopic surgeries, ensuring the secure positioning of tendons until physiological healing is achieved[61]. Typically these can be outpatient operations, one such prominent procedure is the repair of rotator cuffs[61]. An estimated 450,000 surgeries is performed annually in the United States for rotator cuff repair, which is expected to increase with the frequency of tendon tears within an aging population[62,63].

Arthroscopy rotator cuff surgeries are generally performed using the following surgical techniques, with specifics dependent upon operators' discretion. First, incisions are made around the shoulder (posteriorly and anteriorly), with the required number of portals dependent per operation. Fluid is then driven into the portals within cannulas and a camera is inserted. Arthroscopy diagnostic is then performed to establish the stability and integrity of surrounding tissues and bone, such as labrum and bicep tendons, and the superior and posterior portion of the humoral head. Soft tissue frays and debris are removed via an oscillating shaver until blooding surface is established to facilitate bone to capsule healing. A curved drill guide and flexible drill are used to drill a bone tunnel for the placement of the suture anchors. Suture anchors are then placed into the bone tunnel and seated with a mallet; the soft tissue is then placed under tension. A repair suture is then inserted, and the anchor is placed under tension as well. Once the soft tissue is sutured the excess suture is cut near the bone tunnel of the anchor. Sequential anchors are then placed in a similar fashion until the soft tissue is sufficiently sutured into place and is then probed extensively to ensure they are properly fastened[64].

Arthroscopic surgeries have been a positive addition to techniques for surgeries, being less invasive than other techniques previously used. While these techniques reduce the chances of infection there are other inherent complications that can arise, such as re-rupture, hardware complication, cyst formation, and tunnel expansion[65]. One concern intrinsically with procedures in which bone is drilled is a thermal increase within the bone during drilling. This thermic rise can cause osteonecrosis, leading to potential loosening of the devices within the bone tunnels as they expand[66–68]. Current materials of choice for orthopedic surgeons are primarily titania and PEEK, as both materials having positive clinical outcomes with their respective applications. There are however some limitations with these materials the most prominent being their resistance to change.

Both materials when conformed into a geometry are resistant to volumetric changes. Within certain applications, this attribute could be presented as non-desirable. With a material which could expand creating a constant device bone tunnel wall interface even in the event of bone tunnel expansion. One material of interest which has been making its way into the biomedical field is cellulose.

2.4 Cellulose

Cellulose nano-fibrils (CNF) are a relatively new bioplastic with applications ranging from hard ridged plastic replacement, hydrogels, and low-density lightweight plastics. With uses in filtration and separation membranes, oil separation from water, drug delivery, wound dressing, sensors[69], and numerous other biomedical applications[69–72]. CNF can be extracted from numerous sources of bast fibers (flax, hemp, jute, ramie, *etc.*), grasses (bagasse, bamboo, *etc*), seed fibers (cotton, coir, *etc*), wood (hardwood, and softwood), marine animals (tunicate, algae, fungi, invertebrates, and bacteria)[73]. CNF has been shown to have low cytotoxicity and high biocompatibility[70–72] leading to its potential use in soft-tissue implants and cartilage replacement, tissue engineering, antibacterial/antimicrobial activity, cardiovascular implants, cancer-targeting, cornea replacement, biological detection, and biology-device interfaces[70]. CNF is one of many potential collagen substitute materials investigated within the literature, such materials are compared and contrasted in table 2.5, along with a comparison of collagen to CNF morphology in figure 2.10.

Table 2.5: Materials Source, Structure, Positives & Negatives

Type	**Source**	**Structure**	**Pro**	**Con**
Collagen[74]	Natural	H-bonded Triple helix	Strong but flexible No inflammation Hydrophilic, compatible with biominerals	Costly except where it already exists
Acellular Collagen[75]	Biological Collagen	Triple helix Aggregation of fibers.	De-cellularized collagen Preferred material use	Time-consuming process of production demineralized
Alginate[76–78]	Brown algae Ionically linked or covalently linked	Copolymer cross-linked fibers	Abundant, cheap Easy to manipulate Can be crosslinked	Low mechanical properties Low dimensional stability Limited cell attachment
Chitin[79–81]	Arthropods Exoskeleton Cell wall of Fungi and Yeast	Linear polymer of amino sugar	Non-toxic Antibacterial Biodegradable Biocompatible Second abundant polymer	Inherently low mechanical properties Require mechanical improvement through materials (HA, Bioactive Glass)
CNF	Plant-based cellular walls	Mono polymer Cross-linked hydrogen fibers	Most abundant polymer Antibacterial Biodegradable Biocompatible	Not been studied for orthopedic applications Strength, time properties not known

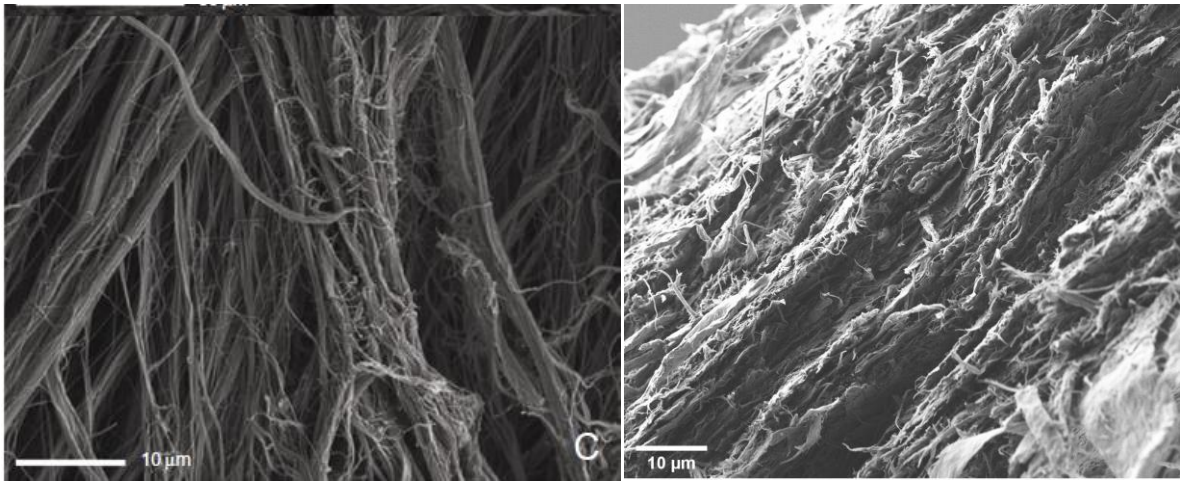

Figure 2.10: Comparison of Collagen (Left) and CNF (Right) (Collagen SEM From Ref([74])).

Cellulose is structured out of repeating cellobiose units, which are two repeating β-1,4-linked D-glucopyranose rings rotated oppositely to each other, with the monomer units arranged in a way that glycosidic oxygens occur in opposite directions. Equatorial-equatorial glycosidic linkage occurs as a result allowing adjacent rings to form hydrogen bonds between the rings oxygen atoms of one glucose unit and the hydrogen of the C-3 hydroxyl group of repeating rings. These hydroxyl groups along the chain create a network of intra- and intermolecular hydrogen bonds, along with van der Walls connections establish between the chain layers[82]. Cellulose structure can be seen below in figure 2.11) which emphasizes the hydrogen bonding network within the cellulose units. CNF is delignified cellulose that is then fibrillated through various means such as homogenization, grinding, refining, extrusion blending, ultrasonication, cryo-crushing, steam explosion, ball milling, and aqueous counter collision[73,83]. Homogenization is a more conventional method and the current method of CNF production at the University of Maine.

Previous work with cellulose in aqueous conditions has demonstrated its ability to increase volume overtime[84]. However, this is currently done rapidly when CNF is placed within aqueous

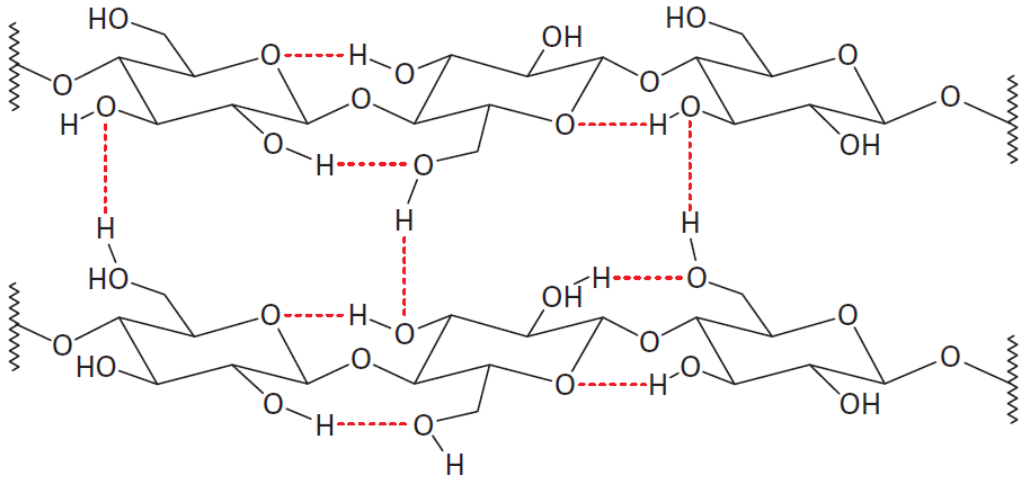

Figure 2.11: Schematic of Intra and Intermolecular Hydrogen Bonds From Ref ([82]).

solutions. Expanding to more than 50% of their original volume within 4 hours at biological temperatures (37°C). This increase in volume was additionally affected by the initial conditions of the samples, with samples that presented lower initial water content swelling less severely than samples that were at a higher initial water content, as shown below in figure 2.12.

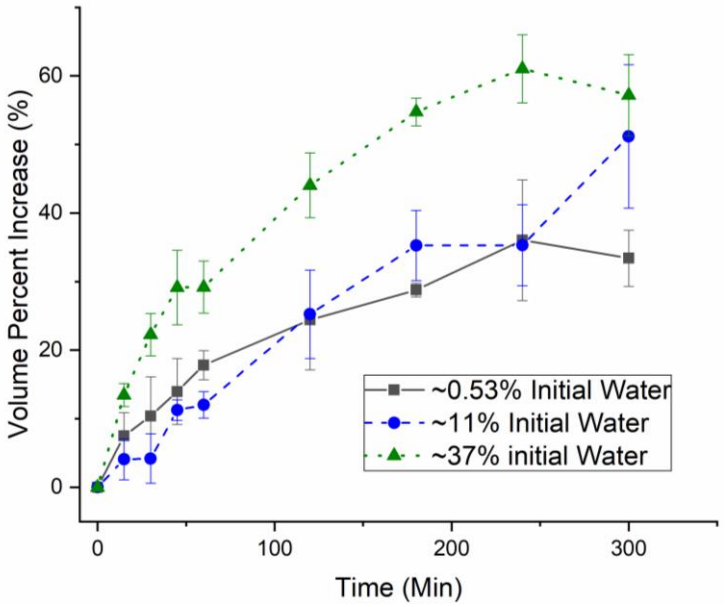

Figure 2.12: Volume Percent Increase of CNF Overtime Within Aqueous Conditions.

2.5 American Standard of Testing Methods and ISO

During device design materials physical and biological performances are determined and compiled to be accessible to manufacturers, thus decreasing the need to perform additional testing on materials. The U.S Food and Drug Administration (FDA) has catalogs of properties for materials called master files. These master files are reviewed heavily and under intensive scrutiny before they are accepted, and use distributed for use. This usually requires testing to be performed in specific ways and done within specialized facilities that are accredited for said testing. Though the testing required to formulate master files is intensive it also emphasizes the necessity of compiling the appropriate data on emerging materials such as CNF. Ensuring that materials are subjected to similar testing regimens before their potential use.

Understanding the physical properties of a material is imperative when designing new devices. With the capabilities of that materials being tested in a universal way similar to other facilities and their devices, as such, testing databases were created to provide a standardized pool of testing procedures, one such database is the American Standard of Testing Methods (ASTM). Figure 2.13 shows the path for a subset of basic physical properties to be tested, in this case, mechanical properties of materials. As CNF is still a relatively new material there are no specific ASTM standards that surround its testing. With this in consideration, standards were selected based on material similarities and similarities in the intended use of the material. Primarily these were based on the material property testing of plastics and their aqueous degradation. The ASTM standards selected were, ASTM D638-14: Standard Test Method for Tensile Properties of Plastics[85], ASTM D695-15: Standard Test Method for Compressive Properties of Rigid Plastics[86], ASTM D790-17: Standard Test Method for Flexural Properties of Unreinforced and Reinforced Plastics and Electrical Insulating Materials[87], ASTM D256-06: Standard Test Methods for

Determining the Izod Pendulum Impact Resistance of Plastics[88]. These standards describe specific testing rates, procedures, specimen size and geometry, commonly used resulting units, and equations.

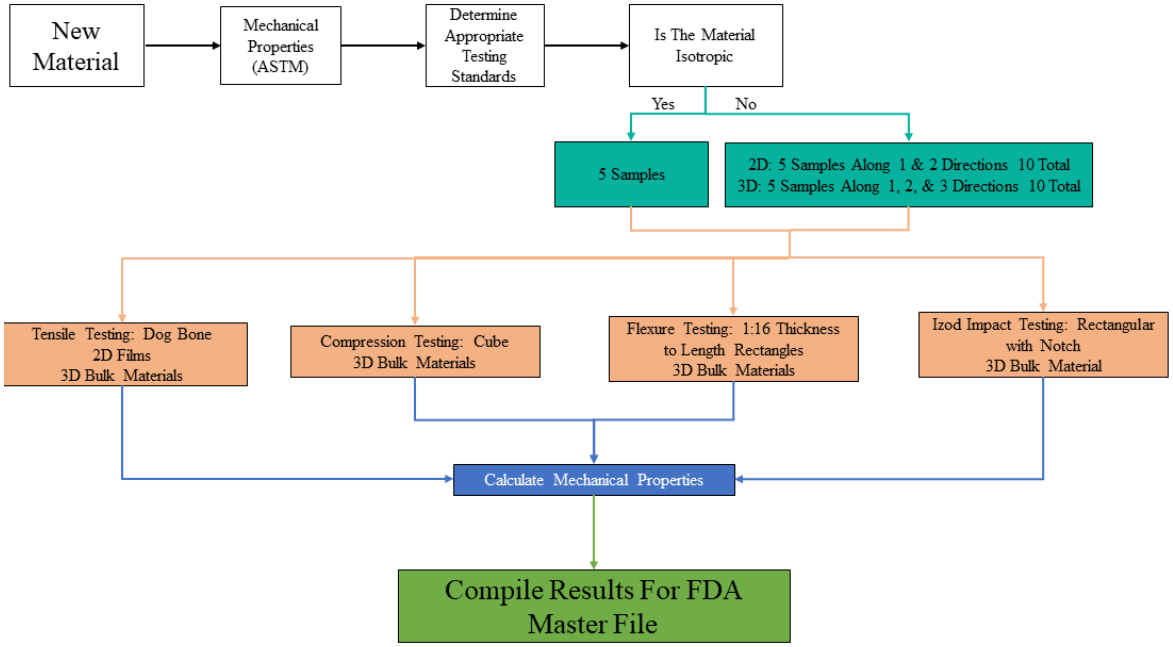

Figure 2.13: Flowchart of Mechanical Testing Considerations of Materials for FDA Master File.

To study the biological aspects of materials, mainly biocompatibility, the flowchart in figure 2.14 can be used to decide on adequate testing progress. While this involves a rigorous process from indicating whether or not the material is intended for direct contact, specifics of approved manufacturing and potential risk, to the previous testing provided on the material. Additionally, consideration of the materials composition is prudent during this process, as materials of known toxic substances should immediately be disregarded. In the case of CNF literature suggestions have been provided to give an affirmative result on its biocompatibility, however, standardized testing of this characteristic is sparse. As such it is recommended to characterize the materials using the International Organization of Standards, ISO 10993 Biological

Evaluation of Medical Devices. This consists of 23 parts, each describing a parameter and procedural guidance in testing decisions. As much of this pertains to devices in late-stage development, parts focusing on material characteristics were selected and tested at this time.

Investigated ISO's consisted of ISO 10993-5: Test for *In Vitro* Cytotoxicity[89], ISO 10993-12: Sample Preparation and Reference Materials[90], ISO 10993-13: Identification and Quantification of Degradation Products from Polymeric Medical Devices[91], ISO 10993-14: Identification and Quantification of Degradation products from Ceramics[92], ISO 10993-15: Identification and Quantification of Degradation Products from Metals and Alloys[93], ISO 10993-16: Toxicokinetic study design for Degradation Products and Leachables[94], ISO 10993-18: Chemical Characterization of Materials, and ISO 109993-19: Physio-Chemical, Morphological, and Topographical Characterization of Materials[95]. Part 5 incorporates looking at cytotoxicity from direct contact with cells, this is done by placing samples onto a monolayer of cells for a specified length of time, depending on the materials end purpose. Quantitative and qualitative analysis of the cultures is achieved by assessing cell death, inhibition of growth, and culture formation. Stains are used within the quantitative steps to determine cell viability and the degree of inhibition. Part 12 discusses and directs the testing specimens' dimensions and referencing materials to be used as positive and negative controls for a specific material subset. Parts 13-16 investigate leachable degradation products from polymeric, ceramic, metal, and alloy materials, these products are then tested for potential cytotoxic characteristics. Parts 18-19 investigate the physio-chemical and physical properties of materials used within devices.

This standard, while flexible on specific testing parameters, is highly effective and used throughout industry when materials are intended for biological use. Once these results are viewed by an acceptable source (I.e. FDA, etc.) the material is considered biocompatible and this data is

then compiled into the FDA master file, unless results are found unacceptable in which case additional biocompatibility data is required. While the flow chart in figure 2.13 involves copious steps, materials that have been previously instigated can bypass specific steps with referenced evidence. As CNF has had no previous existence within the FDA however, the long road of gathering all necessary data to prove biocompatibility is required.

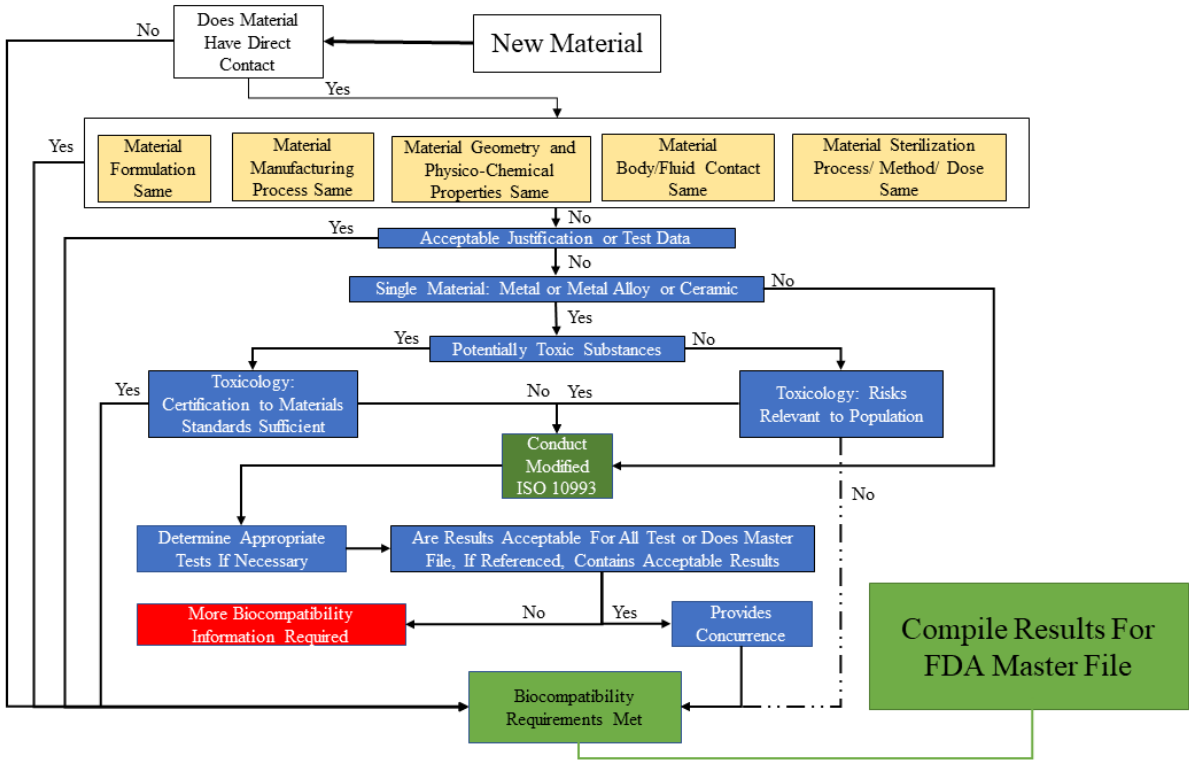

Figure 2.14: Flow Chart of Biological Testing Requirements for FDA Master File.

CHAPTER 3

PROPERTIES OF MANUFACTURED CNF

3.1 Introduction

Understanding the mechanical properties of materials is paramount when discovering the limitations and performance of new materials. For example, when working with fibrous materials discerning fiber alignment, i.e. if they are isotropic or anisotropic, helps direct the process for which they are manufactured. Isotropic refers to materials that have the same properties in all directions, while anisotropic properties vary in direction[35]. Notable isotropic materials include metals and glasses, while notable anisotropic materials include woods and a variety of composites[96,97]. Differences in properties between isotropic and anisotropic range from chemical, optical, and mechanical, to thermal[98,99].

Polymeric devices give great emphasis to the determination of polymer chain directions[35]. As polymers characteristically have optimum mechanical properties, such as tensile strength and compressional strength, along these polymer chains. Forces applied perpendicular to polymer chains cause these systems to fail at relatively low loads compared to forces applied parallel with the chains. Analysis of these directional properties is done using an axial approach, with a user-defined 1, 2, and 3 system, however, reporting of axial directions and values are necessary for consistency. Additionally, manufacturing techniques and processes can change the directionality of polymers, through heat and shear-thinning effects, as such precise reporting of device manufacturing is required. Through these heat and shear-thinning effects, many manufacturing processes can be tailored to produce devices with aligned polymer chains. Ensuring devices will have the desired properties for the specific device geometry and positioning.

CNF when processed as received forms a random entanglement of fibers, producing materials that are by nature anisotropic. As CNF is a 3 wt% slurry copious amounts of water must be removed to create a bulk source. This means a considerable amount of volume is lost and fibers within the system become randomly entangled. While within thin films and via a stretching method performed by Li *et al.*[100] fiber alignment can be achieved however when this is brought to scale it is difficult to create a system capable of creating this alignment. Thus analysis of properties derived from CNF dried using a modified method from Holomakoff *et al.*[101] was investigated. First within a 2D structure to see the effects of drying temperature, then within 3D structures to view bulk properties along with the axial directions.

3.2 2 Directional Films

3.2.1 Method

~200 ml of CNF was measured out and placed onto a porous ceramic brick, CNF slurry was then dispersed. A secondary porous ceramic brick was placed on top and pressed down until the force applied resulted in negligible removal of excess CNF. The two ceramic brick system was then placed into a dry air oven and heated at a temperature range from 50-100°C and dried to completion. Once dried films were cut along a designated 1 and 2 axis system into dog bone shaped specimens, with 5 specimens cut per sample. Due to the nature of thin films, ~100-200 micron in thickness, it was assumed that the 3rd direction or thickness direction would have little to negligible amounts of aligned fibrils. As such a 1 and 2 directions were chosen, where 1 is referring to the axis along the length and 2 is the axis along the width, as seen in figure 3.1.

Samples were dried post dog bone cut to ensure samples were sufficiently dry. They were then left in an environmentally controlled room at ~50% relative humidity (RH) for 48hr. Samples were then tensile tested sequentially using a single column Instron with two clamp apparatus and a 500 N load cell. Stress (Eq1.) and strain (Eq2.) were calculated from the raw data gathered, where

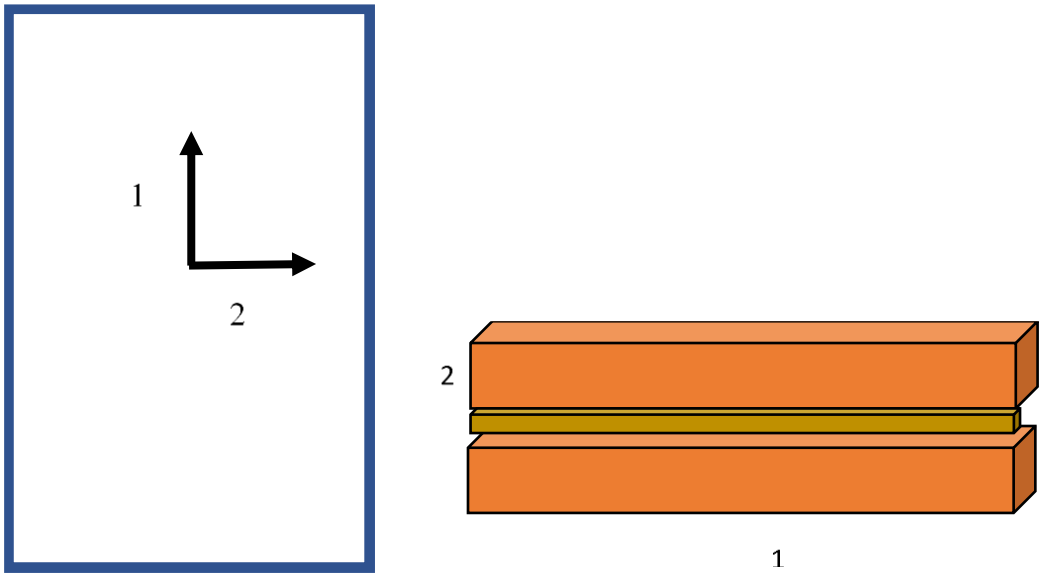

Figure 3.1: Axial Directions on Ceramic Interface (1 Along Length, 2 Along Width).

F is the force applied and A is the cross-sectional area in eq1, in Eq2. ε_l is the strain final and ε_i is the strain initial. Modulus and Ultimate load (Tensile strength) were calculated using Eq3 and Eq4 respectfully. Statistics were conducted by first performing a normalcy test (Shapiro-Wilk), then an ANOVA test (Appendix A), and finally a pairwise test in the form of a Tukey.

$$\sigma = \frac{F}{A} \qquad Eq.1$$

σ= Stress

F= Force Applied

A= Cross-sectional Area

$$\varepsilon = \frac{\varepsilon_l - \varepsilon_i}{\varepsilon_I} \qquad Eq2.$$

ε= Strain

ε_I= Initial Length

ε_l= Final Length

$$E = \frac{\Delta\sigma}{\Delta\varepsilon} \qquad Eq3.$$

E= Young's Modulus

$$S = \sigma_{Maximum\ Stress} \qquad Eq4.$$

S= Ultimate Strength

3.2.2 Results

After testing each specimen tensile strength, elastic modulus, and strain were recorded. Each trial at various temperature is plotted with the 1 direction shown in black and the 2-direction shown in red in Figure 3.2. As shown 60°C appeared to present higher moduli for both the 1 and 2 directions, with lower amounts of deviation between samples as other temperatures. Prior to statistics the two directions and individual subsets normality of modulus, strength, and strain were determined for each direction. This was performed by converting the raw data of a direction throughout all temperatures.

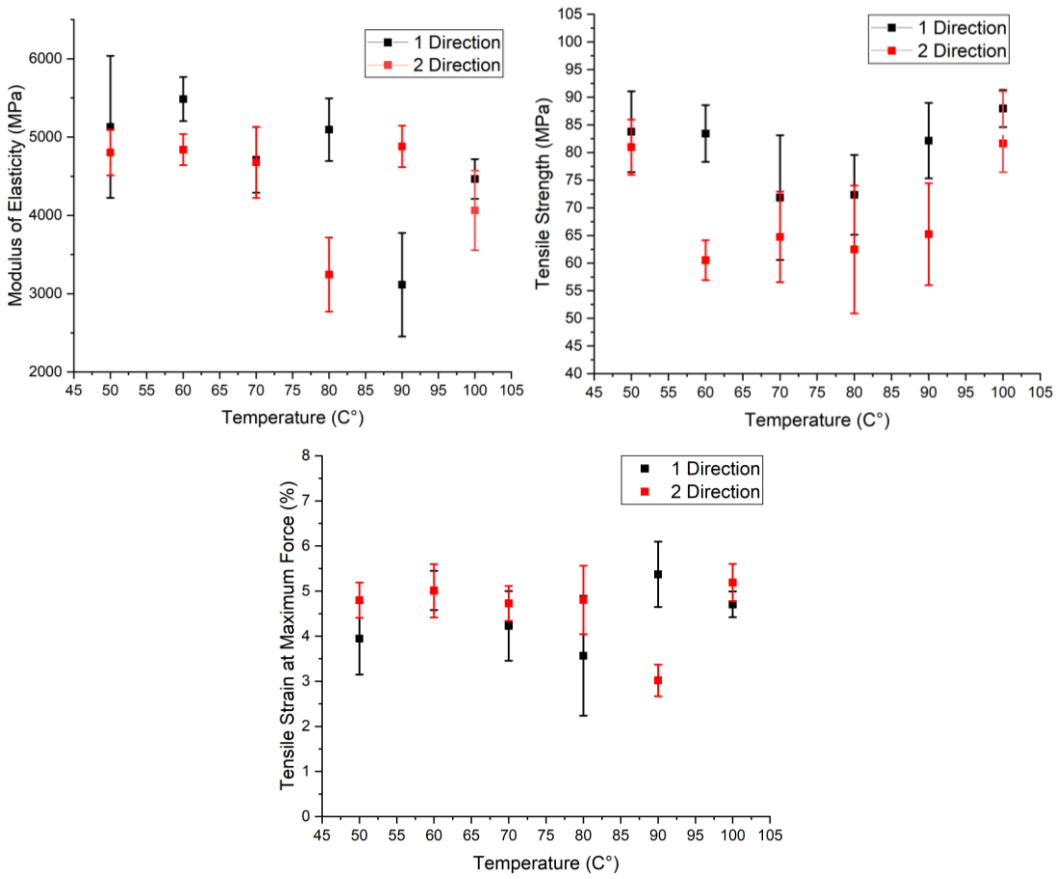

Figure 3.2: Thin Film Tensile Testing. Modulus of Elasticity (Top Left), Tensile Strength (Top Right), Tensile Strain (Bottom Middle).

These densities were then plotted, and bell curvature nature of the plots were viewed and shown in Figure 3.3. Statistics in the form of ANOVA Tests were done through an R script for all statistical analyses within the thesis. For analysis first, the two directions as a whole of temperature were compared, then the two directions at each temperature were compared. As shown the two-directional tension tests have no significance between them with the p-value above the $\alpha=0.05$.

However, once the two directions are examined between temperatures, ie. 1 Vs 2 at 60°C, some degree of significant differences is shown in the strength. While 80 and 90°C appear to be significantly different in modulus they were found not to be within the chosen alpha value. Meaning that looking at the variant temperature together show little significant variance between them, with very little effects being seen by drying temperature.

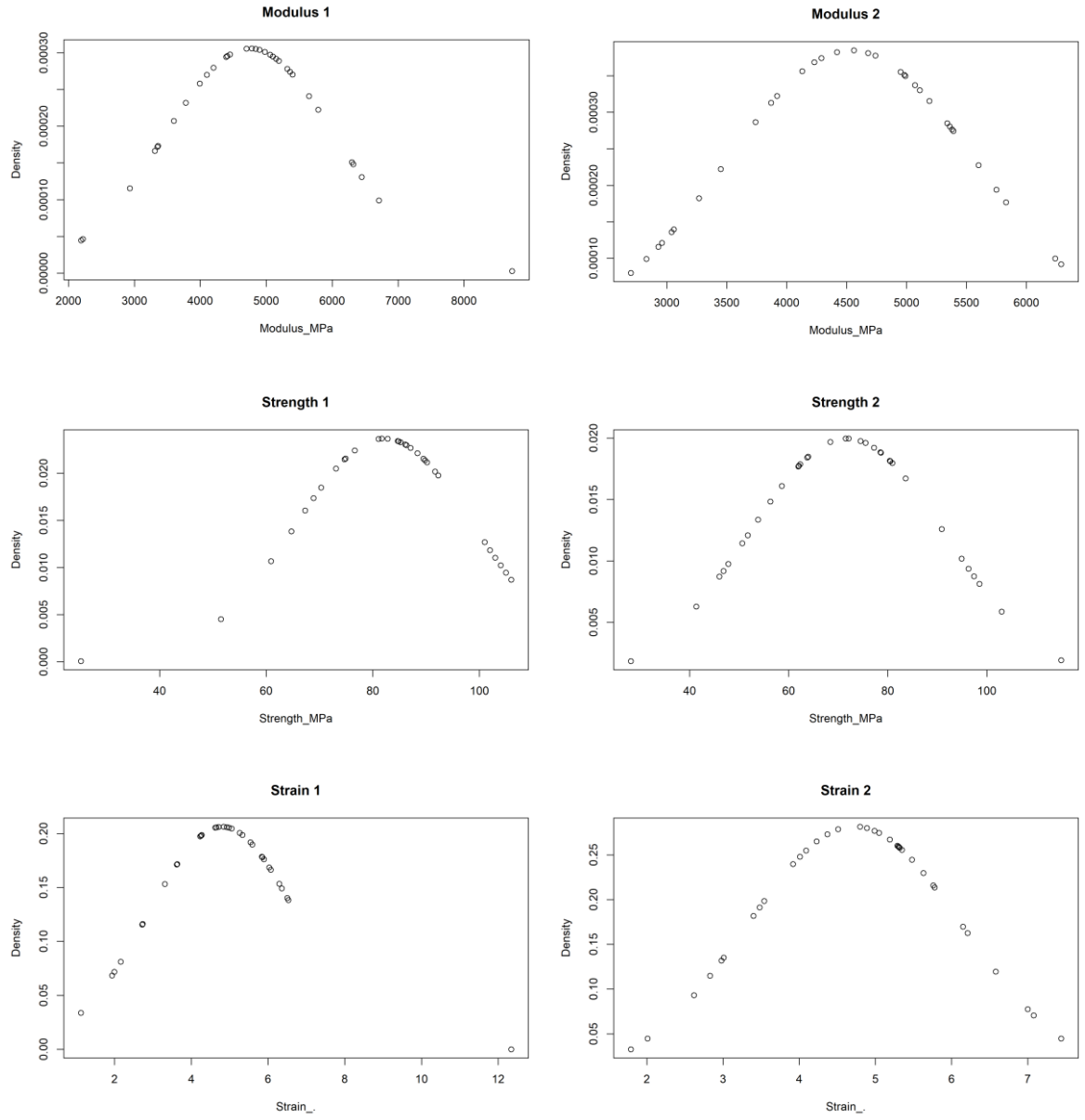

Figure 3.3: Normal Distribution of all Films Across All Temperatures.

Table 3.1: Temperature Variant Film ANOVAs. * Signifying P value Below Alpha= 0.05

ANOVA Categories	Modulus P Value	Strength P Values	Strain P Values
All Temperatures 1 Vs 2	0.451	0.02*	0.852
50°C 1 Vs 2	0.922	0.946	0.536
60°C 1 Vs 2	0.084	0.004*	0.903
70°C 1 Vs 2	0.989	0.43	0.987
80°C 1 Vs 2	0.081	0.625	0.983
90°C 1 Vs 2	0.088	0.24	0.053
100°C 1 Vs 2	0.621	0.376	0.318

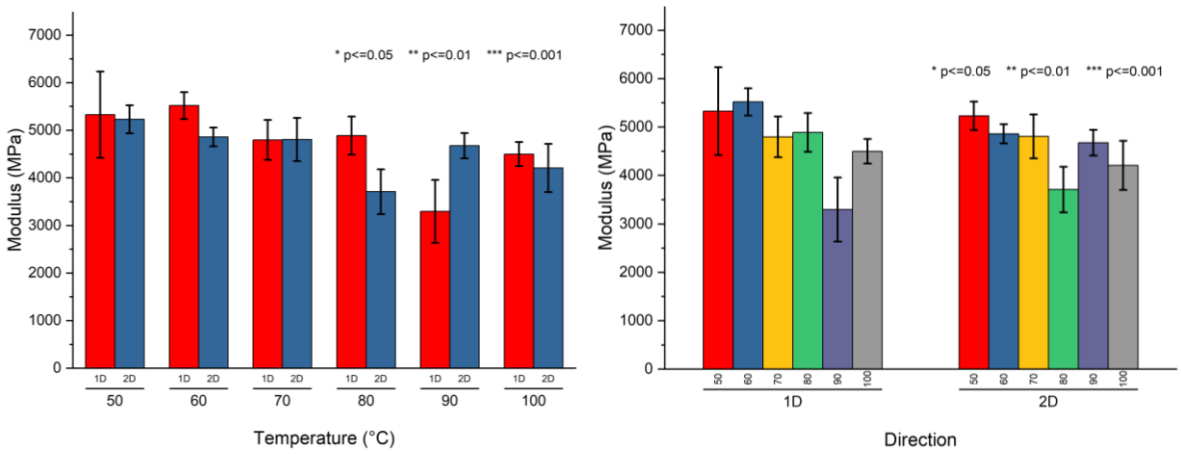

Figure 3.4: Tukey Box Plots of Film Directional Modulus (Left Grouped by Temperature, Right Grouped by Direction).

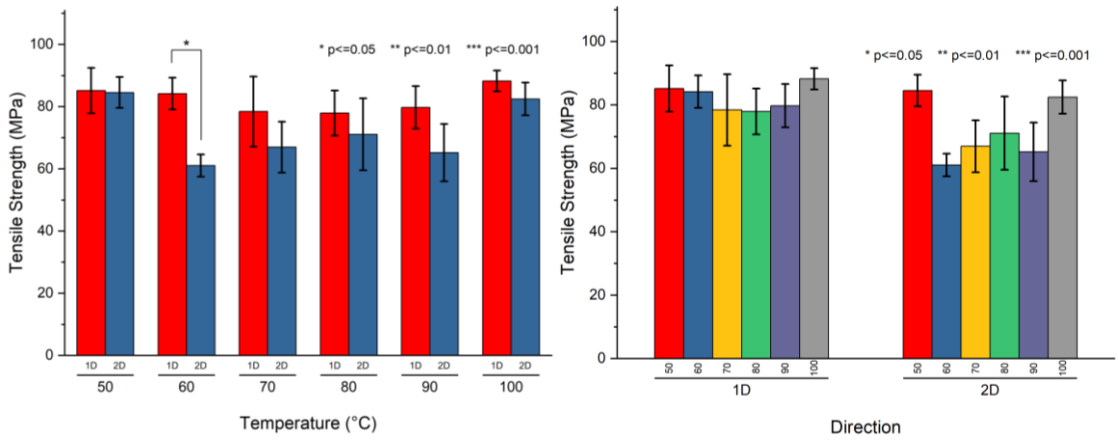

Figure 3.5: Tukey Box Plots of Film Directional Tensile Strength (Left Grouped by Temperature, Right Grouped by Direction).

3.2.3 Discussion

Through investigation, little variations were seen between the 1 and 2 directions of the 2-dimensional dried films at various temperatures. However, this may have been due to large sample set variations with each specimen demonstrating varying moduli and strengths. Factors that may have led to this are the variation in the location of samples being cut, heterogeneous pore distributed throughout the films leading to nano-micro voids within the films, and heterogeneous drying caused by capillary action closest to ceramic interfacing. Additionally, differing internal strains within the films lead to heterogenous wrinkle formation increasing variation between tensile specimens, creating different stress gradients and premature failure. Finally, human error can be contributed to the variation as well as the specimens were cut using generic scissors, creating weak points along the edges of the specimens causing premature and ill opportune results. Specimens created in a fashion with industrial material reduction methods will be investigated in bulk mechanical testing as discussed later within a 3D analysis.

3.3 3D Testing

3.3.1 Introduction

As mentioned above, anisotropic materials require testing in all directions. Bulk sources of CNF are desirable in terms of manufacturing, device design, and cost management. The addition of a 3-direction requires subsequent testing of mechanics in all directions. As bulk CNF provided more material other mechanical testing were possible such as compression, and flexure. A process previously used by the Mason lab was implemented. This process is similar to film drying in the fact that a porous ceramic interface is used to facilitate capillary action initially. For the preservation of material 70°C was used for drying bulk CNF. Two bulk forms of CNF were made per test. Testing was done with consideration to apparatus set up as specified in the ASTM's.

3.3.2 Method

5 gallons of CNF were placed into a mold with porous ceramic interfacing. The molds were then oven-dried at 70°C for 7 days. Once fully dried the CNF was then machined into a long rectangle through the use of a table saw and segmented into 3 smaller sections, one for each direction tested (1, 2, and 3). Each segment was then machined into appropriate subjects for tensile, compression, and flexure mechanical testing. The determination and procedural machining of test specimens for each mechanical test are shown below in Figure 3.6. The orange section depicts the ceramic mold that is used with the transparent section depicting the CNF inside of the mold. Due to limitations in the current drying process, each segment was cut into smaller slices. These slices were done perpendicular to the direction of the intended testing.

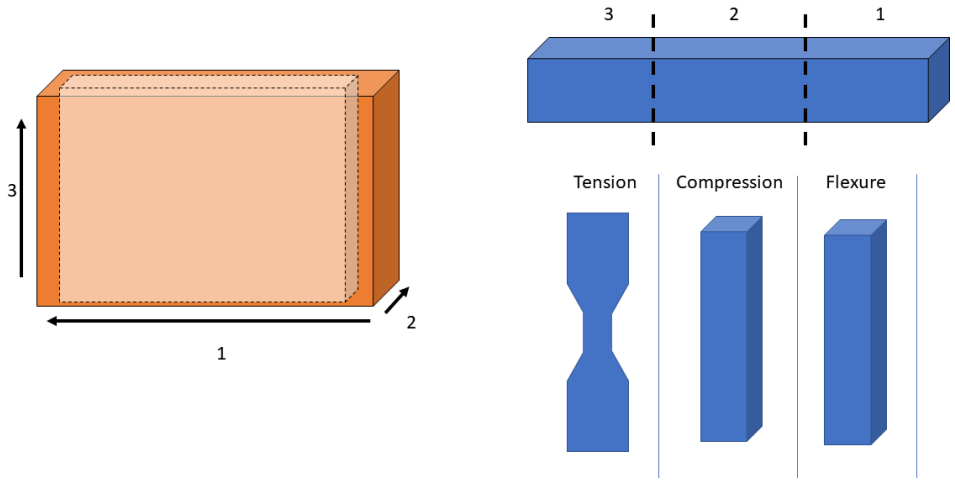

Figure 3.6: Bulk CNF Mold Procedure (right), Sectional Cutting and Prospective Specimen Shapes for Testing.

For each directional slicing figure 3.7 and figure 3.8 shows the appropriate slicing. After cutting the bulk CNF into its appropriate testing shapes, they were then placed into the environmental chamber (relative humidity 50% and 20°C) and left for 48hrs. They were then removed from the chamber and tested using an Instron 5900 or MTS citation model 43 double-column machine dependent on the load needed, with attachments specific for each testing style performed, I.e., a circular compression indenting head for compression testing. The samples were tested until mechanical failure, loads

and deformation were recorded and Young's modulus (Compression and Tension) at R^2=0.98 of initial stress strain slope, Flexure stress, Flexure modulus, Ultimate strength were calculated and shown in equations Eq5, Eq6, Eq7, and Eq8. Statistics were performed by first running a normalcy test with the Shapiro-Wilks test, then ANOVA, and finally a pair wise test in the form of a Tukey.

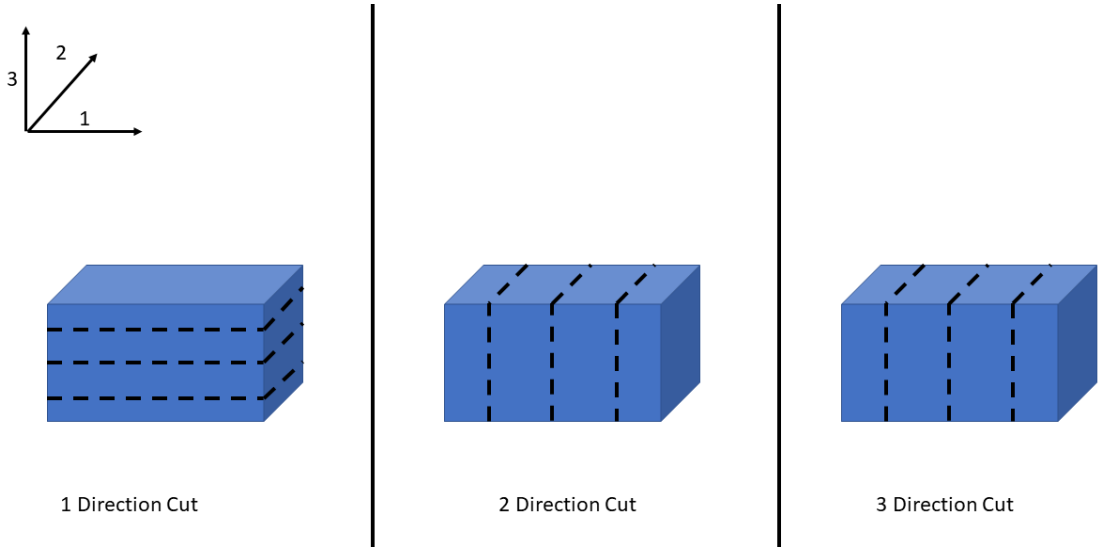

Figure 3.7: Directional Cutting into Sections for Testing Specimens, Tensile and Compression.

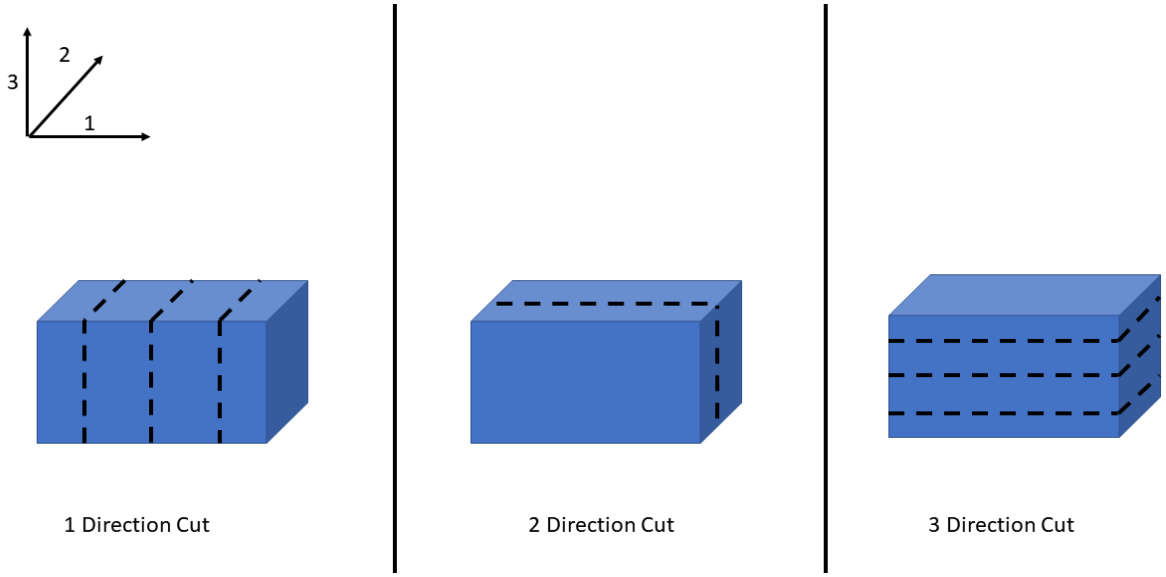

Figure 3.8: Directional Cutting into Sections for Testing Specimens, Flexure.

$$E_T = \frac{\Delta\sigma_T}{\Delta\varepsilon_T} \qquad Eq5.$$

E_T= Young's Modulus (Tensile)

$$E_C = \frac{\Delta\sigma_C}{\Delta\varepsilon_C} \qquad Eq6.$$

E_C= Young's Modulus (Compression)

$$\sigma_F = \frac{3FL}{2bd^2} \qquad Eq7.$$

σ_F= Flexure Stress

F = Force

L= Length of the Support Span

b= Width

d= Thickness

$$E_F = \frac{\Delta\sigma_F}{\Delta\varepsilon_F} \qquad Eq8.$$

3.4 Results

3.4.1 Compression

Solid CNF constructs were manufactured to ~25mm X ~12 mm X ~12 mm rectangles. These rectangles were compressed using a circular compressive head and base plate till failure or machine load limitation (48.93KN). Testing was performed at 1.3 mm/min and was initiated at a load of 5N. Load vs deformation was recorded and reformed into a stress-strain curve, modulus of elasticity and ultimate compression strength were then determined with an example curve being

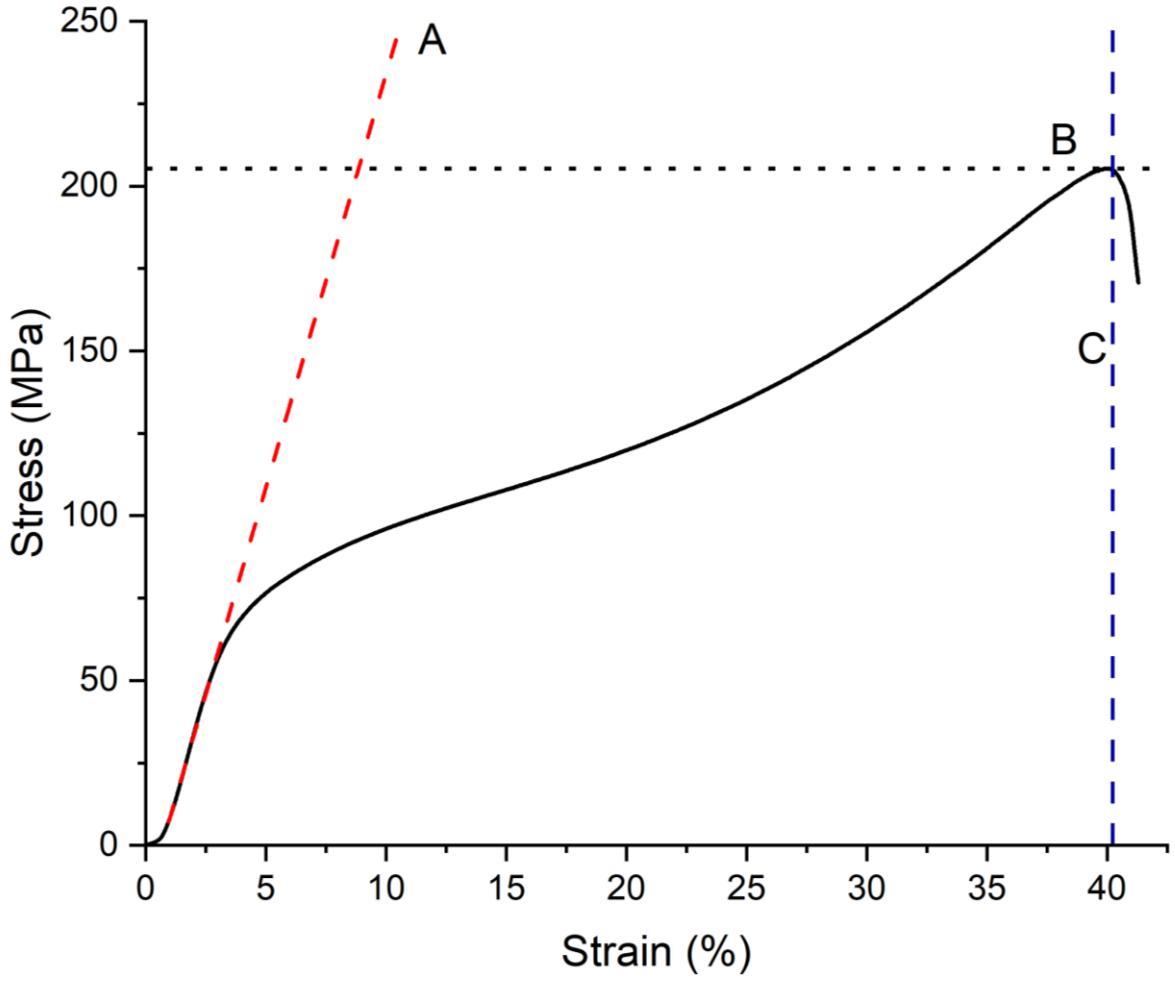

Figure 3.9: Example Compressive Stress Strain Curve (A: Modulus Slope, B: Ultimate Compressive Strength, C: Failure).

shown in figure 3.9. From this example curve, it is observed that there is a very short elastic deformation range of the material and a longer plastic deformation, A is shown as the slope used to calculate the modulus of elasticity, and B is the ultimate compressive strength which is the maximum stress experienced by the material before failure, and C is the moment of material failure. An additional sample figure is shown in figure 3.10 comparing the stress strain curves of CNF to that of known cortical and trabecular bone[2].

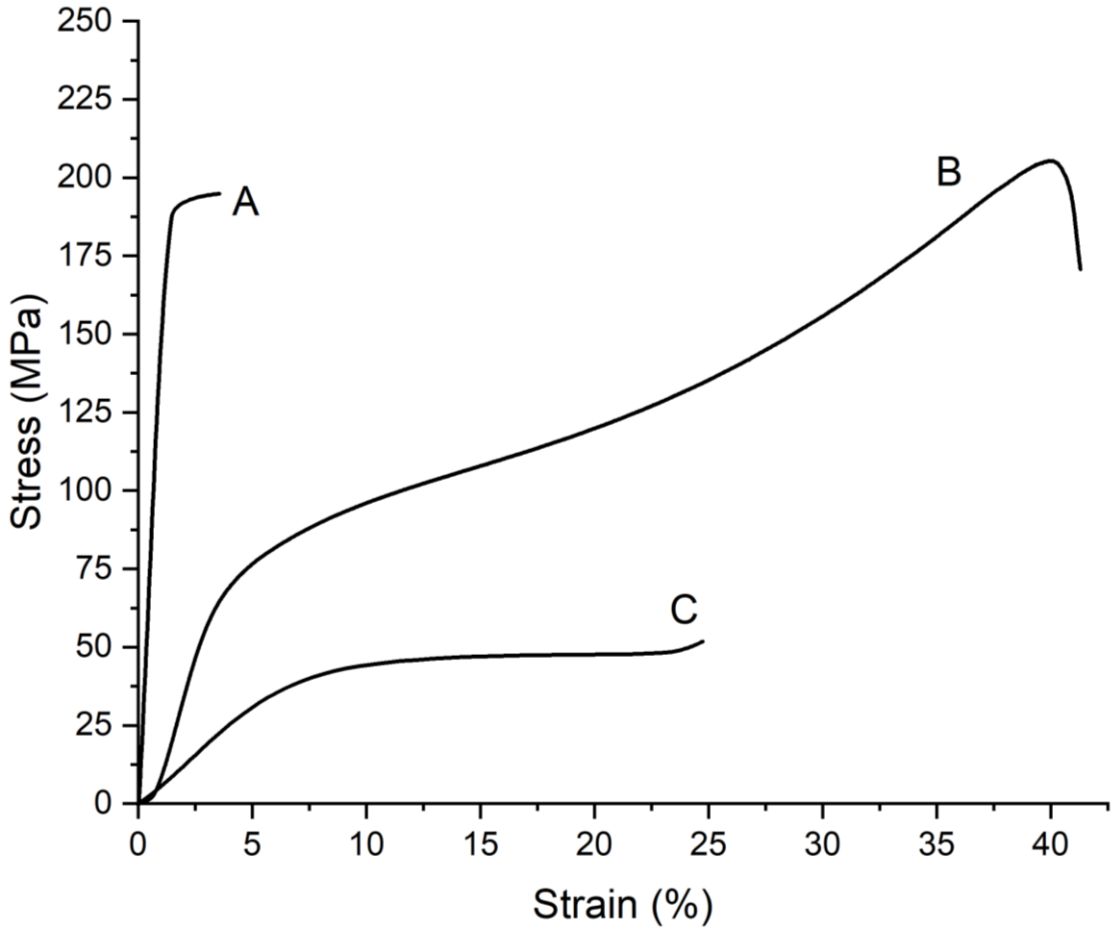

Figure 3.10: Example CNF Stress Strain Curve (B) Compared to Known Cortical (A) and Trabecular (C) Stress Strain Curves (Recreated From Ref[2])

Compressive strength and modulus of all directions can be seen in figure 3.11, with compressive strength on the left and moduli on the right. Compressive strength was seen to be highest within the 3-direction reaching on average 220 MPa, within our target of compressive strength analogous to natural bone, with some of the samples surpassing the set load limit of the testing rig at 48.93KN. While the 1 and 2 directions' compressive strengths were around 120 and 130 MPa respectively. Modulus was shown to be highest within the 1 direction around 2,300 MPa on average. This was caused by a sharper initial elastic deformation resulting in a linear portion from which the modulus was calculated.

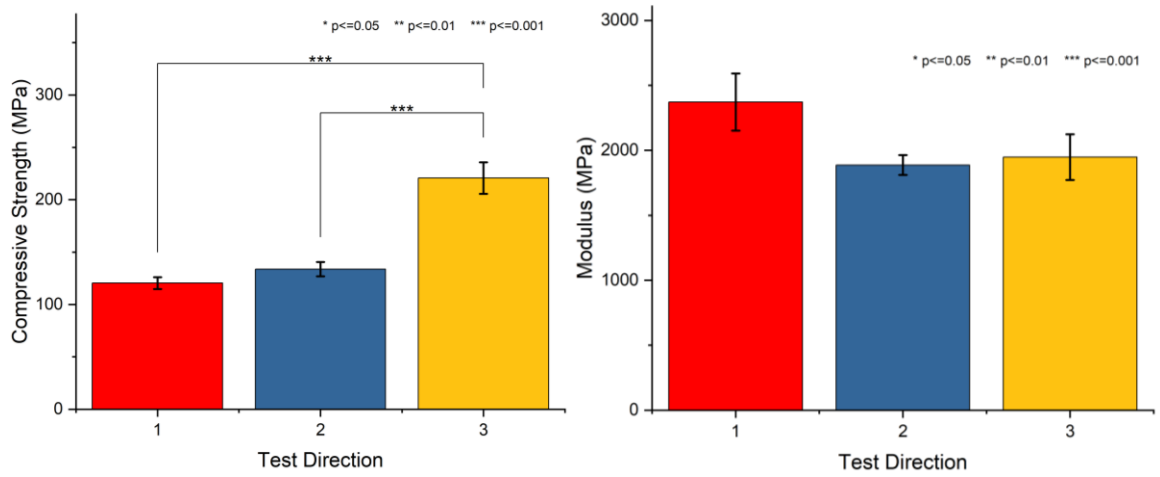

Figure 3.11: Average Compressive Strength (Left) and Average Modulus (Right) For Each Testing Direction.

Modality of compressive failure varied between sample directions, with the 1 and 2 directions failing linearly through the 2 directions with fiber gradient strain being seen along the rupture, and the 3-direction failing in a shear failure mode as the rupture was seen at a 45 angle across the 1 and 2 directions. Failure modality can be seen in figure 3.12, depicting the forces and line of failure for the samples with a supplementary image of samples. Emphasizing the linearity of the failure within the 1 and 2 directions and a shear failure within the 3 directions. The average

modulus and strength of all samples are displayed in table 3.2, with statistical p values and significance displayed in Appendix A1 table A1.

Modulus between samples showed no significant difference. However, in the compressional strength there was shown to be significance between direction 3 with direction 2 and 1, while there was seen to be no significance between compressional strengths between the 1 direction and 2 directions.

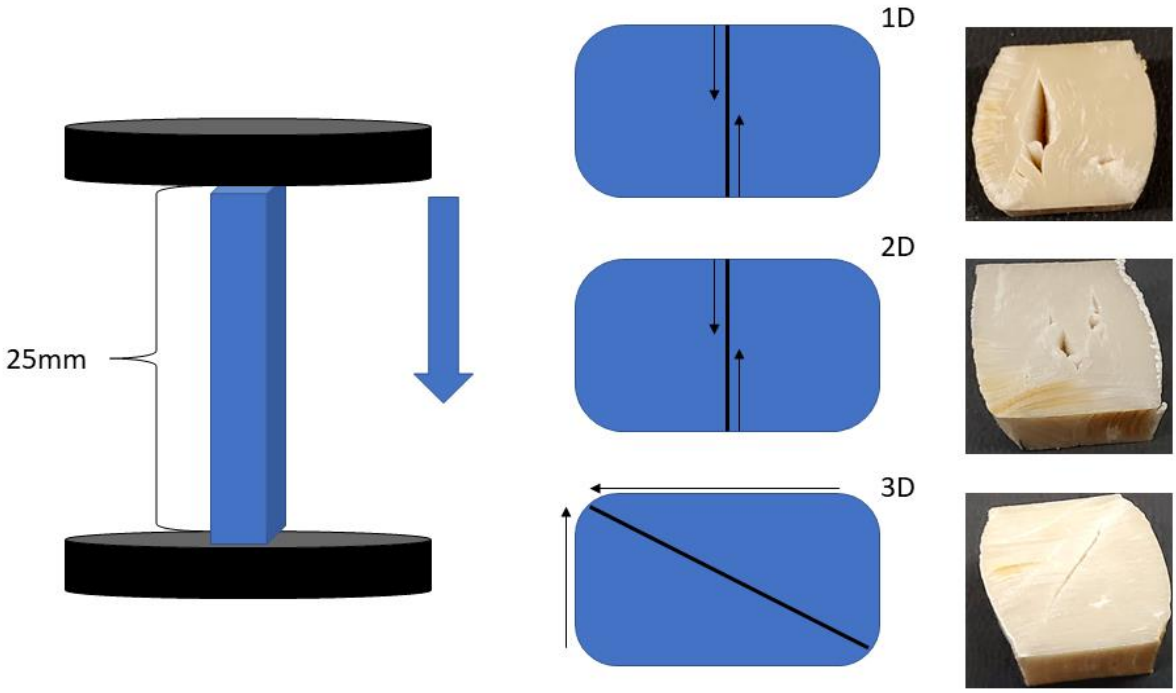

Figure 3.12: Failure of Directional CNF Under Compressive Loads.

Table 3.2: Compressive Mechanical Properties

Direction	Modulus (MPa)	Compressive Strength (MPa)
1 Direction	2295.26	119.65
2 Direction	1877.08	132.82
3 Direction	1894.55	217.60

3.4.2 Tensile

Bulk tensile samples were created by cutting CNF bulk into 25mm X 12mm X 2mm tab samples, as CNF is not an ideal material for conventual means of precision manufacturing i.e. water jet and laser cutting. As these procedures have the potential to change the chemical and physical properties of the material, an alternative simple reductive procedure was used. Additionally, as testing to this scale on CNF is relatively new previously a result of supply, trial and error were to be expected. Samples that were created into tabs showed difficulties being milled into specific dog bone testing specimens, holding small samples raised the risk of crushing and or stressing them before sample testing. As such they were tested as is, it should be noted that the failure point for many samples was within the grips, without a proper fillet loading the force into the gauge area, high forces were experienced in the grips. While this presented a flaw in the current testing it gave an approximation of the tensile properties of the samples.

Figure 3.13: Tensile Fixture Grip Used in Tensile Testing.

Tensile samples were tested using the MTS Criterion model 43 using a spring assisted tensile grip attachment shown in figure 3.13. Testing was performed at 1 mm/min, load vs extension was recorded and reformed into a stress strain curve, modulus of elasticity and ultimate tensile strength were then determined with Eq.5. Tensile samples strength and moduli are shown in figure 3.14, inversely to compressive testing it was shown that samples along the 1 direction had the highest mechanical strength while samples in the 3 directions had the smallest strength. Table 3.3 shows the average modulus and strength for each direction. Statistical analysis was performed and is shown in Appendix A1 table A2 and showed significant variance in all strengths of the direction and no significance when viewing modulus in any direction.

Table 3.3: Tensile Average Modulus and Tensile Strength

Direction	Modulus (MPa)	Tensile Strength (MPa)
1 Direction	1078.85	43.69
2 Direction	1086.77	28.43
3 Direction	889.53	7.17

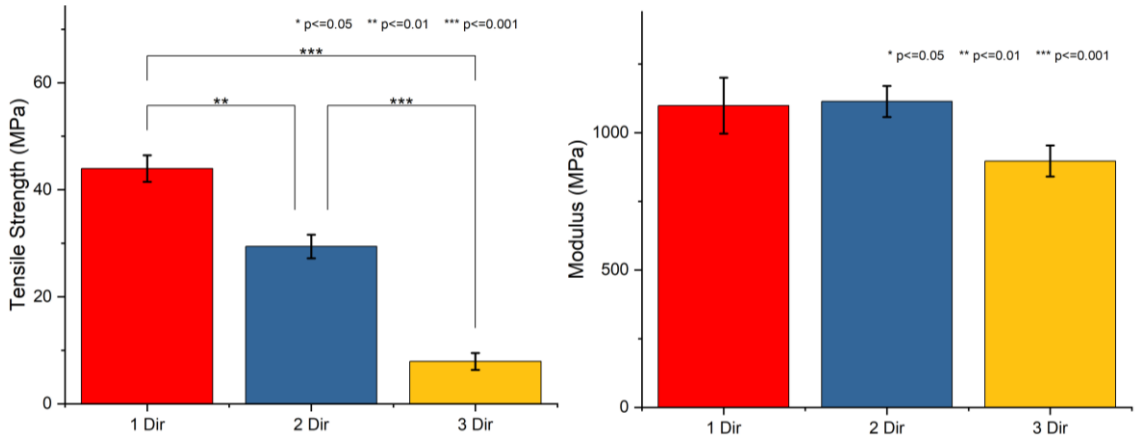

Figure 3.14: Average Tensile Strength (Left) and Average Modulus of Tensile Samples (Right).

3.4.3 Flexure

Flexure samples were produced using slices as mentioned in methods figure 3.15. Where the devices were sliced perpendicular to the axis of testing, as to allow forces to be applied along that axis. Samples were ~25mm X 12mm X 5mm and the support length was moved to 20 mm to allow full extension of the samples and to prevent devices from colliding with the support beams. The test was then run at 1 mm/ min until device failure or significant drop in load ~10N. A diagram of testing can be seen in figure 3.15 where the span with the sample is shown.

Once failure was reached, the test was concluded, and flexure modulus and flexure strength were calculated. It was noticed that the perpendicular force applied in the 1 direction resulted in strengths that were the lowest while again when applied in the 3 direction they had higher strength. Each of which is shown in figure 3.16, with the average modulus and strength shown in table 3.6. Statistical analysis was done and is shown in Appendix A1 tableA3. Again, there was shown to be significant for all strengths for every direction, there was also a significant variance when looking

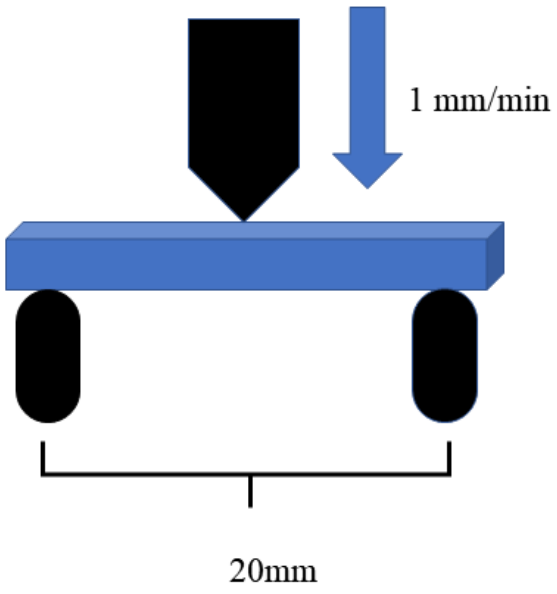

Figure 3.15: Diagram Showing Flexure Setup for Testing.

at modulus values, with the 1 direction compared to the 3-direction comprising the most variance in the sample set.

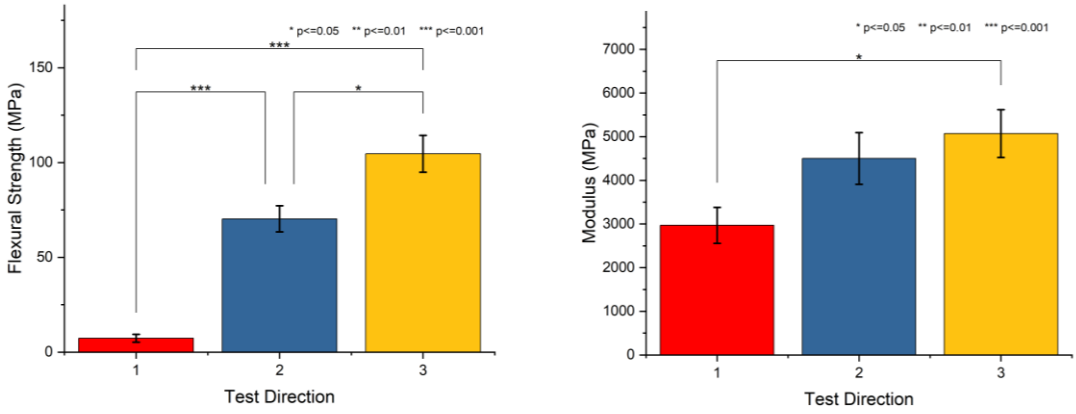

Figure 3.16: Flexure Modulus (Right) and Flexural Strength (Left) of 3D Beams.

Table 3.4: Table of Flexure Moduli and Flexure Strength

Direction	Flexure Modulus (MPa)	Flexure Strength (MPa)
1 Direction	2970.04	7.33
2 Direction	4501.08	70.28
3 Direction	5070.25	104.64

3.5 Discussion

The methodology of drying CNF holds a noticeable effect on fiber orientation, mechanical performance, and failing modalities. As such care should be taken when designing bulk CNF, taking into account drying interfacing, and the size of the material to be dried. As moduli and strengths differ dependent on the direction in which a force is applied, devices should be created in the direction in which they should resist forces. With devices intended to have high rigidity by compressive means being created along with the 3 directions or height of the CNF ingots.

However, with the procedure for which these large scales bulk were made, there were some discrepancies in geometry, with the length of the ingots dwarfing the other two directions significantly.

This also posed some limitations with keeping testing to specific ASTM standards as there was a lack of material for which sample dimensions could be kept. This was the case for all tensile and flexure samples. While all samples within these tests were uniform in dimensions, additional tests should be conducted where samples are more analogous to dimensions within the ASTM. For this, the molds in which the CNF is dried should be modified to ensure a square geometric shape is produced. This in itself can pose an issue as well, as the required CNF to create such a bulk dry would be 2 to 3 times more than the CNF currently used to produce the samples used within these experiments. Reproducible machining techniques should be designed and implemented when making samples in the future, as variations between sample shape and thickness swayed the results of the mechanical testing considerably. Samples should also be made to load forces on desired locations without concern of premature failure or device limitations as seen from tensile and flexure testing. CNF bulk is a relatively new material within the mechanical testing world, with little data to compare results confidently.

CHAPTER 4

CYTOTOXICITY ANALYSIS OF CNF

4.1 Introduction

The investigation of biological interfacing with intended device materials is essential when designing medical devices out of newer materials. Multiple factors of biological interactions should be considered when selecting materials. Factors include biocompatibility, low cytotoxicity, cellular integration, etc. Standard testing of medical devices can be found within the international organization of standards (ISO), specifically, ISO 10993 offers multiple standers to fully understand the biological effects materials and devices can have. While the standard is dense in terms of full device testing parts can be done in a stepwise action. With an emphasis on cellular cytotoxicity being at the forefront and housed within ISO 10993-5: Biological Evaluation of Medical Devices[89]. Within this standard testing is broken into two experiments depending on the device's intended use and implantation. For devices that are intended to break down expediently, extract from degradable materials is extracted and tested with a cell monolayer. For devices intended for long-term implantation, materials are exposed to the cellular monolayer for an extended period and tested.

While medical devices are constantly evolving incorporating new novel materials and manufacturing variants, the testing format is essential to ensure consistent results and reproducible testing environments. One such emerging biopolymer cellulose nano-fibrils (CNF) has been investigated heavily within the biomedical field with applications ranging from *in situ* softening cortical implants, soft-tissue implants and cartilage replacements, drug delivery systems, and wound healing[70]. As CNF's inter and intra hydrogen bonding within the base chain provides the

material with unique mechanical, and physiochemical properties, all of which allow the material to be tailorable for a multitude of means[70,71,102–105].

While preparation procedures for the standard testing are universal, methods of cell viability and standing are numerous. With methods ranging from metabolic activity, targeted membrane stains, membrane inhibited nuclei dead stains and metabolically cleaved staining. One such stain is MTT, a stain that has been used for years to discern the indirect viability of cells, through the use of dye reduction[106]. The purpose of this study is to view the effectiveness of MTT method of cell viability with 3D constructs of CNF. Which will further the understanding of large-scale CNF constructs within the field of biomedicine.

4.3 Methods

CNF was obtained at 3wt.% solids from the Product Development Center (PDC) located in Jenness Hall at the University of Maine. 5 gallons of CNF were fully dried at 70°C in a dry oven while inside of a porous ceramic mold. The resulting bulk CNF was then reduced and manufactured into intended sample sizes. Substantial amounts of CNF were produced to simulate potential large-scale adaptations.

Cell strain used within the culture was MC3T3-e1 (mice pre-osteoblast cells) with Alpha Minimum Essential Medium (α-MEM) + 10% by vol. fetal bovine serum (FBS) culture media. α-MEM with ascorbic acid was used due to limitations on the supply chain and supporting evidence from Izumiya *et al*[107], who found no significant difference in proliferation of MC3T3-e1 cells between the two culture media. Five 35mm 6 well plates each well seeded with 10,000 cells at 2mL of culture media were used for assays. ISO 10993-5 was then followed adapting to a 6 well plate format. Cultures were left until 80% sub confluency was obtained in each well, once 80% sub confluency was obtained culture media was removed and new culture media was added (3mL)

before specimens were placed into each well. Specimens were placed into the plates by hand carefully near the center of the wells as shown in Figure 4.1. Specimens consisted of a blank (just cells), a positive extract (10% bleach), a positive control (Polyurethane), a negative control (Polyethylene), and CNF specimens. All specimens were 25mm X 5mm in dimensions and were pretreated with a soaking of 10mL DI for 10 minutes before sterilization to prevent thermal decomposition. They were then sterilized using a wet autoclave (Autoclave model HV-85) at 121°C for 60 minutes.

MTT (3-[4,5-dimethylthiazol-2-yl]-2,5-diphenyltetrazolium bromide) assay was used following a protocol from molecular probes and was scaled to conform to 6 well plates instead of

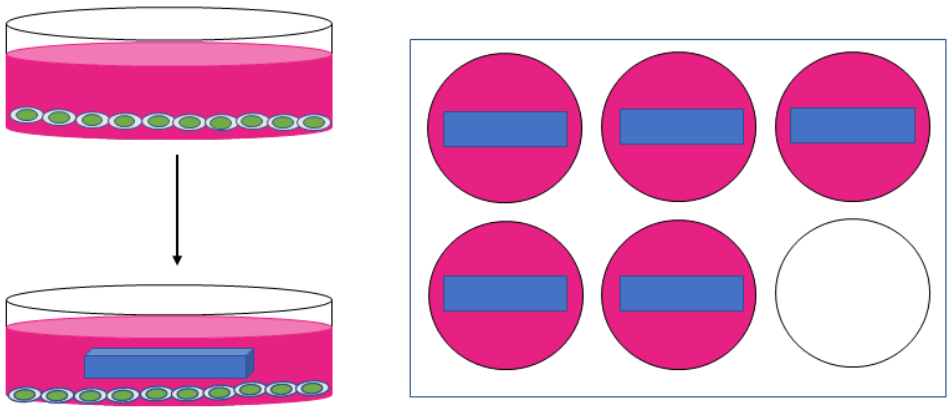

Figure 4.1: Cell Monolayer Growth, Placement of Samples in Well Plates.

96 well plates using recommended allotments of media per well 2 mL. The procedure was as follows, for imaging 4 6 well plate patches 0.01g of MTT was mixed and sonicated with 2 mL PBS making a 12 mM stock solution. Media was then removed from each well and 1 mL of culture media was added. Then 100µL of 12mM MTT solution was added, and wells were agitated. 850µL was then removed leaving 250µL left within the wells, 500µL of Dimethyl sulfoxide (DMSO) was added and plates were left in an incubator for 10 minutes. A BioTek Cytation 5 experimental procedure was programmed to observe both optical plate reading, scan reading absorbance at

540nm, and bright-field images of the individual wells, this was done in a 5 X 5 array of the well area through the Cytation 5. Corresponding absorbances were displayed as a heat map table with corresponding sample location as high absorbance, which is compared with bright field imaging sample location.

4.4 Results

All samples were analyzed in a 5 by 5 array within the Cytation 5, and triplicates of absorbance were measured and displayed. These arrays of absorbances and images of wells were

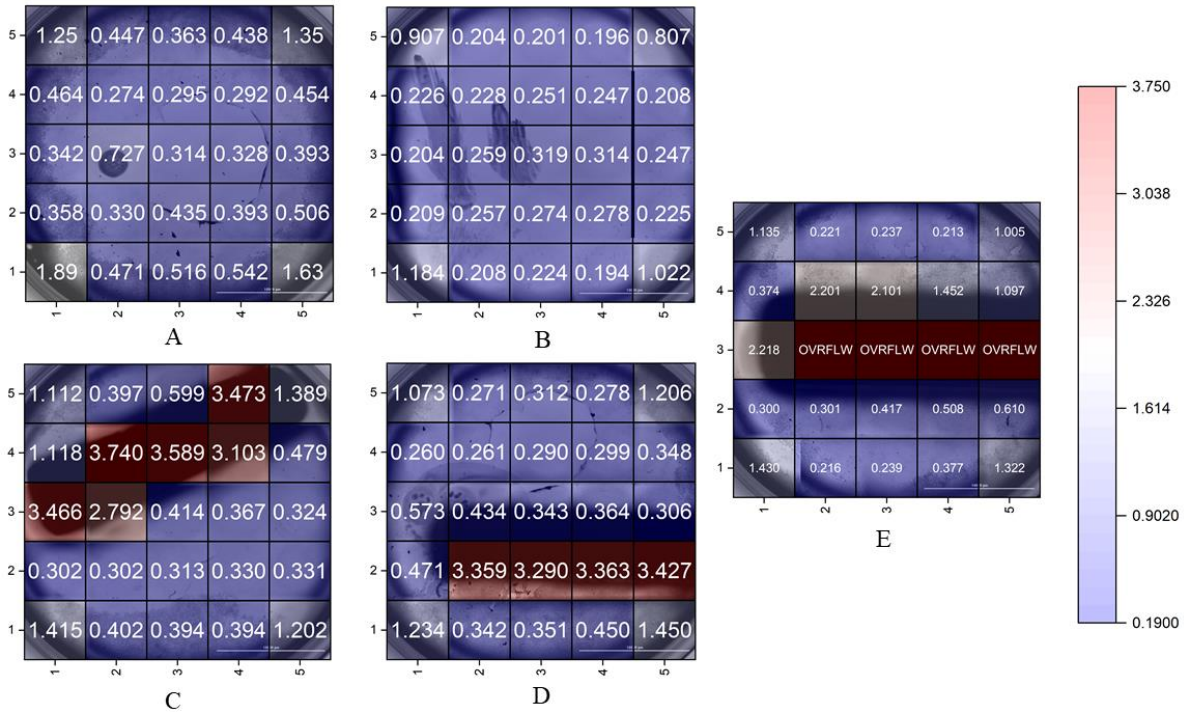

Figure 4.2: Heatmap of Absorbances Taken From 5X5 Array (Blue Low & Red High). (1000µm Scale). A. Blank, B. Bleach, C. Positive, D. Negative, E. CNF.

recorded, and a heat map was made overlayed well A1 as displayed in figure 4.2. Heatmaps were overlayed on top of a brightfield image of a well, displaying the edge effects and the high OD on top of and near the samples. From the blank control, edge effects were noticed and omitted from the average optical density (OD). All OD from the blank control was averaged and a standard

deviation was created, from this standard deviation OD above were omitted from the test samples. The average optical density was determined per plate and used in Eq 9. to calculate cell viability.

$$V_{MTT=\frac{OD_S}{OD_B}} \qquad Eq.9$$

Where V_{MTT} is the cell viability of the MTT method, OD_s is the average optical density of the sample, and OD_B is the average optical density of the blank control. Cell viability, OD, and thresholding values are shown in table 4.2.

Table 4.2: Cell Viability and Optical Density of All Sample Sets

Sample	Optical Density Average	Viability (%)
Blank	0.361 (+0.441 Threshold Value)	100
Bleach	0.239743	66.34
Negative	0.329	91.26
Positive	0.332	91.88
CNF	0.302	83.69

Thresholding of OD was necessary to obtain values within the parameters of Eq 9. as displayed in figure 4.3 with a comparison of the means and outliers within these sample sets both raw and threshold. As wells with samples had considerably higher OD in well this would give more than 100% viability which is not feasibly possible.

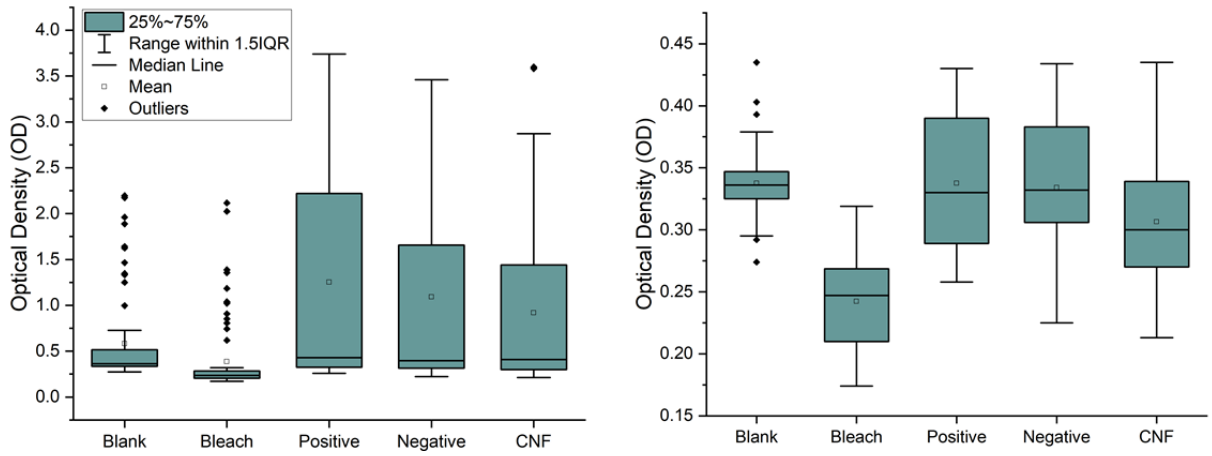

Figure 4.3: Box and Whisker Plot of OD From Raw Data (Left) and Threshold Data (Right).

4.5 Discussion

Using MTT assay format metabolic staining with OD measurements it was found that CNF had a reduction in viability >70% from that of the blank control, meaning it is nontoxic. While these are promising results for the material as its intended purpose, several concerns can be found with the use of MTT as a format to discern cytotoxicity. First placement and movement isolation of the samples is difficult and can cause skewed results in the OD average. As samples are placed gently by hand there is no means for all placements to be universally placed. Additionally, during movement of the well's samples can move which can cause potential disruption and trauma of the monolayer of cells, which could additionally kill cells. CNF within this format as well as some concerns due to its hydrophilicity, once placed within the wells the CNF absorbs culture media creating a complication with cells within proximity of the specimens. With this absorption of fluids specimens also swell, this could also pose complications as the samples swelling could scrape cells underneath causing a cascade of death as well.

While our negative control within this testing series worked well our positive control which was supposed to elect a decrease in cell viability did not react in the fashion which we expected.

This may be a result of treatments from the purchaser, as many of the positive cytotoxic materials used within the experiments are blacklisted and difficult to obtain. In conclusion, MTT assay is effective to view cell viability, however, within this specific experiment it may be more beneficial to use a different staining technique that is not limited to obstruction from the devices placed. This usually is not an issue with the use of MTT because most experiments with this stain are usually to assess drugs and/or extracts, and therefore do not suffer from potential issues such as our bulk material experiments.

CHAPTER 5

PRODUCTION METHODS OF HIGH MINERAL COMPOSITES

5.1 Introduction

Composite materials have become a paramount resource for modern society. Leading to the research and development of countless new composite materials. Composites are classified as containing at least two chemically identifiable phases separated by interfaces[108]. Composite properties are strongly influenced by several factors such as filler shape, size and distribution, properties and volume percentage of filler, matrix properties, dispersion of filler particles in the matrix, and state of filler/matrix interface[109]. In this paper, we will be addressing specifically the dispersion of filler particles in the polymer matrix. One common industrial solution is mixing under high aqueous conditions. Creating an environment in which particulates of minerals are highly dispersed, increasing their likelihood of interacting with the polymer without the solids falling out of the solution[110]. As polymer composites create lightweight robust materials their uses have a wide range of applications. From sensors, aerospace, automobile, construction, and concrete, to biomedical applications[111–114]. Biocomposite is a term given to composite materials with biomedical applications and biological interfacing. Thermoplastics such as Poly(Lactic Acid) (PLA) and Poly(Glycolic Acid) (PGA) are the common biomedical device that is commonly composited with titania or bioceramics[108,115]. Thermoplastics have been researched and used within biomedical applications for decades, however with the emergence of biopolymers a shift has occurred for more sustainable sources. One such biopolymer is Cellulose nano-fibrils (CNF).

Over the last couple of decades, the research and development of novel biomaterials and biocomposites have been astounding. Cellulose nanofiber (CNF) composites have been a

promising material as it is easily made from an abundant renewable resource with excellent biocompatibility and mechanical properties. These properties are contributed to intra and inter-hydrogen bonding throughout and in between CNF chains. However, despite these properties, there are always steps that can be used to improve them. One such way is through the addition of additive minerals creating composites. The ideal mixing of CNF with additives would have the additives coating individual fibers. Studies by Li *et al.*[116] have shown that water pretreatment steps with adequate mixing have been found to increase the flexural modulus and flexural strength of hydrophilic composites which is desirable.

As adhesion between filler and polymer phases have a drastic effect on mechanical properties, it is important to ensure there is bonding of the materials usually done with a wetting method[115]. This wetting method is dependent on the hydrophilicity properties of the filler and the polar groups associated with the intended polymer matrix. The objective of this research is to determine the effects of mechanical mixing on the properties of produced films and determination of water pretreatment steps to CNF slurries at weight percentages of 3% and 1% effects on the properties of high composite films produced. While the CNF slurries are at their varying weight percentages titanium dioxide will be added as the composite and mixed thoroughly. The goal is to determine the level of homogeneity achieved with the different percentages of CNF by weight and assess the mechanical properties of the composite film created.

6.3.2 Materials

CNF was obtained from the Product Development Center (PDC) at the University of Maine at 3 wt.% solids. Titanium Dioxide was obtained through (Dupont) with a diameter of (~20nm). Distilled water (DI) was used through the University of Maine in-house distilled water system

(16MOhm). A commercially available Kitchen Aid Mixer (Pro 5) was obtained to perform small-scale mixing. A vacuum filtration system with a (Thomas Model 917CAB12 917) pump.

5.3 Experimental Procedure

Three mixing styles were implemented to investigate particle dispersion in low and high viscosity conditions (Method 1-3). All suspensions were mixed for a time period of 1, 2 ½, and 5 minutes. Control films were made with ~200g of 3wt% CNF. In all mixing conditions, 4 titania composites were made, the weight of 3wt% CNF and Titania are shown below (Table 5.1).

Table 5.1: Weights and Weight % of All Composites

CNF 3wt% Solids Addition (g)	CNF Dry (g)	Titania Addition (g)	Wt.% Dried Titania Composite (wt.%)
200	6	0.67	10
200	6	2	25
200	6	6	50
200	6	18	75

Films intended for poor mixing (Method 1) were mixed by hand with a spatula in a beaker. High viscous mixing (Method 2) was performed with a commercially available tabletop mixer (Kitchen Aid). This was done at a speed of 2 (95 rpm), due to material dispersion by mixing paddles; this was done in a 30-second interval, for material to be pushed back into the mixing path. Low viscous mixing (Method 3) was performed with a dilution of CNF at 1 wt% solid, titania was added, and suspensions were titrated to a pH of 2 with ~2mL of 2M nitric acid and all mixed at

speed 2(95rpm). This was done to positively charge the titania particles to add attraction to the negatively charged CNF fibrils[117,118]. Types of Mixing styles and times are shown in (Table 5.2)

Table 5.2: Mixing Styles and Times

Specimens	Mixing Style	CNF solution (wt%)	Mixing Times (minutes)
Control	Hand Mixing	3 %	1, 2.5, 5
10 % Titania	Mixer	3 %	1, 2.5, 5
25% Titania	Dilution	1 %	1, 2.5, 5
50% Titania			
75% Titania			

Post mixing diluted suspensions then underwent vacuum filtering to remove additional DI, vacuum filtration shown in Figure 4.1. Following filtration, suspensions were laid out onto a porous ceramic interface with an additional ceramic interface covering the slurries. The films were then oven-dried at 60°C (Fisher Scientific Thermotemp Model:737F) for 48 hours (hr.). Films were then removed and cut into “dog-bone” tensile specimens and square specimens for scanning electron microscopy. Specimens were then placed into an environmentally controlled room at 50% relative humidity (RH) and 23°C. Tensile specimens were tested on an Instron 5942 with manually adjusted tensile grips and a load cell of 500 N. Tensile testing was performed at a rate of 1 mm/min. Figure 4.2 depicts a flowchart that describes the process of the different mixing methods and final testing. Additionally, scanning electron microscopy (SEM) was performed with an Amray 1820 SEM Microscope.

Figure 5.1: Vacuum Filtration Setup for Dilute Mixed CNF.

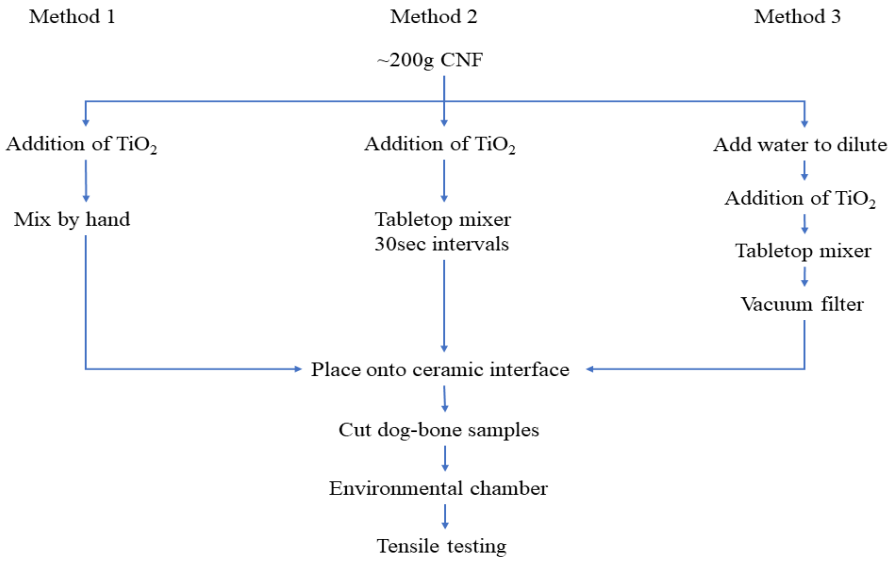

Figure 5.2: Flowchart of 3 Mixing Methods and Testing Performed.

5.4 Results

5.4.1 Post Vacuum Filtration Particulate

Filtrate extracted from the vacuum filtration step was dried and weighed for excess titania, weight loss and percent loss of titania were calculated. These values are shown in figure 5.3 with

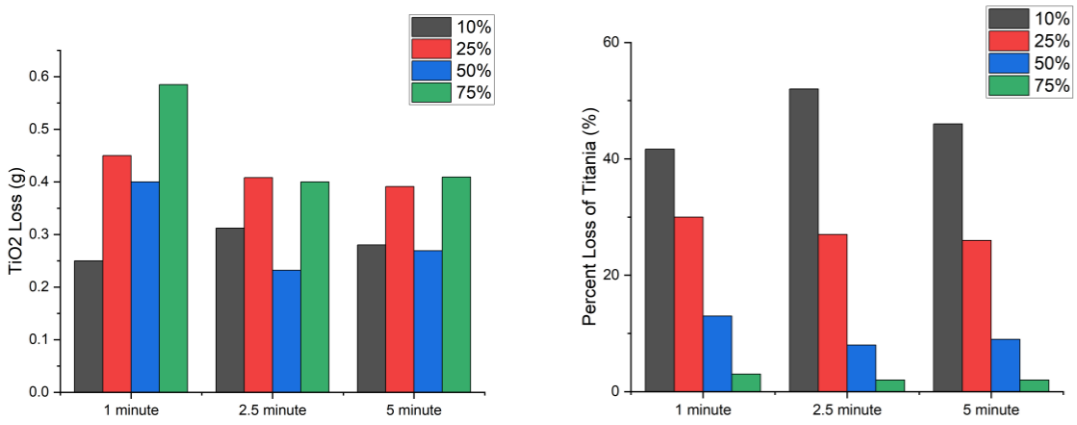

Figure 5.3: Titania Loss Gram (Left) and Titania Loss Percent (Right).

each percent. It was found that as composites wt% of titania increased there was a relatively low percent loss of titania at the higher the wt%, establishing optimum conditions for which titania stays suspended within the slightly negatively charged CNF.

5.4.2 Mechanical Analysis

A 3D printed stencil was made to create the dog-bone shapes and to mark the grip lengths of 25mm. Following 24 hours within the environmentally controlled room samples were taken out and placed into sample containers with desiccant packets additionally conditioned within the environmentally controlled room. All samples were mechanically tested until failure using a single column 500N load cell Instron 5942, ultimate tensile load, and Young's modulus were recorded for each sample set through an average of 5 specimens. Tensile strength for all individual sample

sets was measured at maximum stress before the break with the average displayed for hand-mixed, tabletop mixed, and dilution mixed in figure 5.4, figure 5.5, and figure 5.6 respectively. Commonly seen throughout all mixing styles 50 and 75% composites had considerably lower mechanical properties than the initial CNF and other composites. Emphasizing a capping effect brought about by large nanoparticle interaction with intramolecular hydroxyl groups, essentially interrupting the hydroxyl group hydrogen bonding and decreasing the mechanics of the films produced. Additionally, 25% composite had a noticeable effect as well on strength of the produced films. Showing a decrease during numerous mixing methods and times. Statistic was performed across CNF, 10% composites, and 25% composites, the categories were across hand mixing vs table mixing, mixer times, and finally mixer vs dilutions of films found in Appendix B table A4.

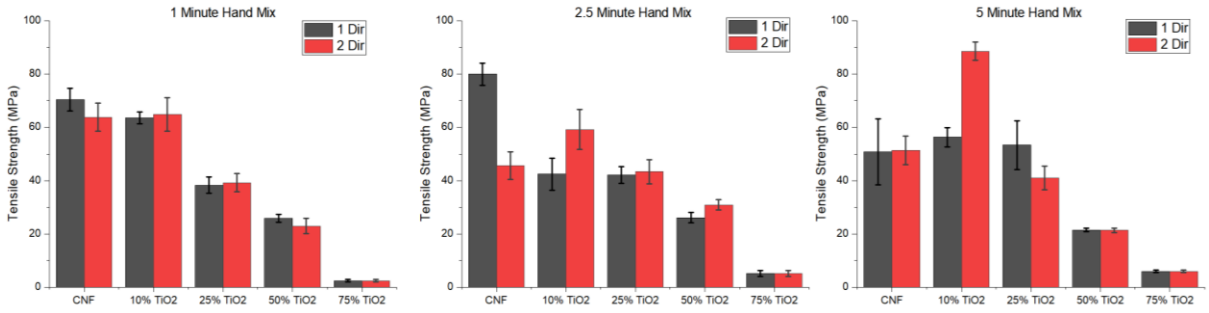

Figure 5.4: Tensile Strength of Hand Mixed Films at All Time Points (1 Direction Top, 2 Direction Bottom).

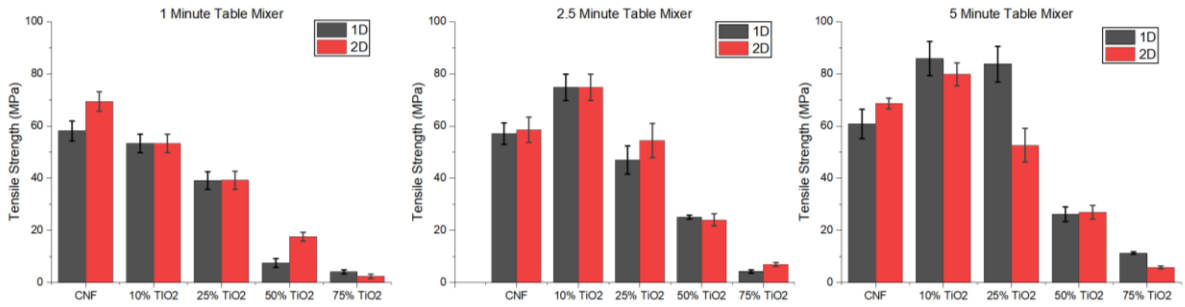

Figure 5.5: Tensile Strength of Table Mixer Films at All Time Points (1 Direction Top, 2 Direction Bottom).

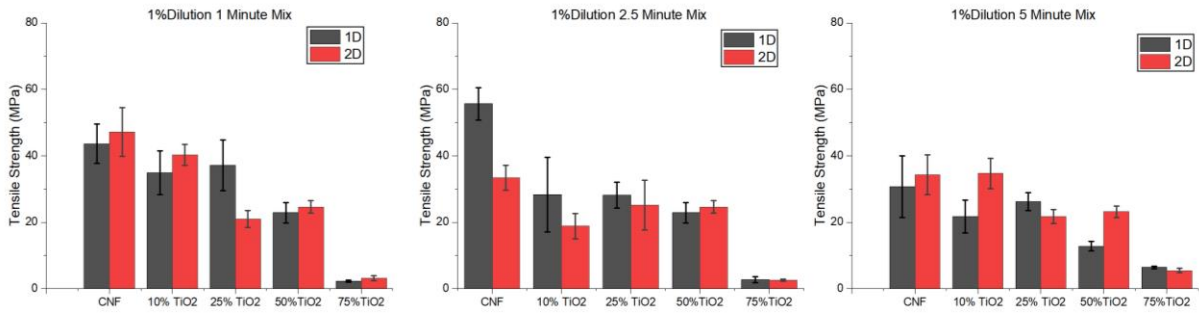

Figure 5.6: Tensile Strength of Dilution Mixed at All Time Points (1 Direction Top, 2 Direction Bottom).

Young's modulus of all mixing methods and times was calculated using the initial linear portion of the stress-strain curve with Eq. 3 with an R^2 value above 0.98. All moduli across all directions, mixing style, and time are shown in figure 5.7, figure 5.8, and figure 5.9. As previously seen with tensile strength, films suffer similar effects to modulus with increasing composite content, decreasing the hydrogen bonding, and creating a brittle material. Statistical analysis was performed on the modulus of all mixing styles, time, and direction and is displayed in Appendix B table A4.

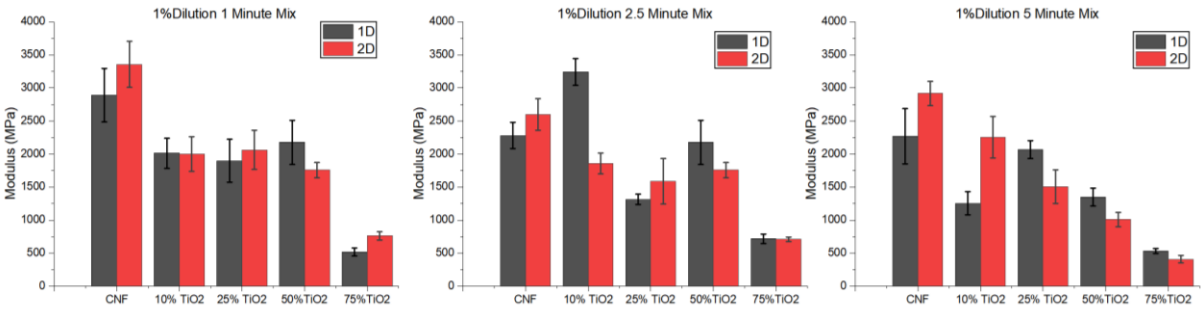

Figure 5.9: Young's Modulus of All Dilution Mixed Films at All Time Points (1 Direction Top, 2 Direction Bottom).

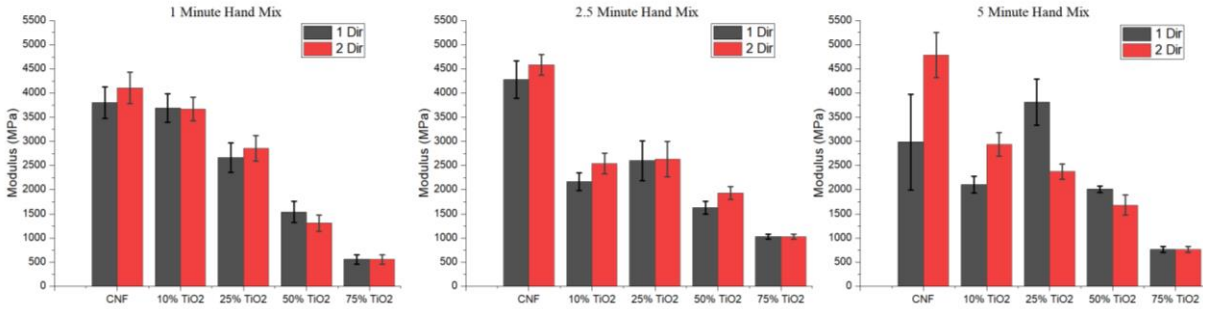

Figure 5.7: Youngs Modulus of All Hand Mixed Films at All Time Points (1 Direction Top, 2 Direction Bottom).

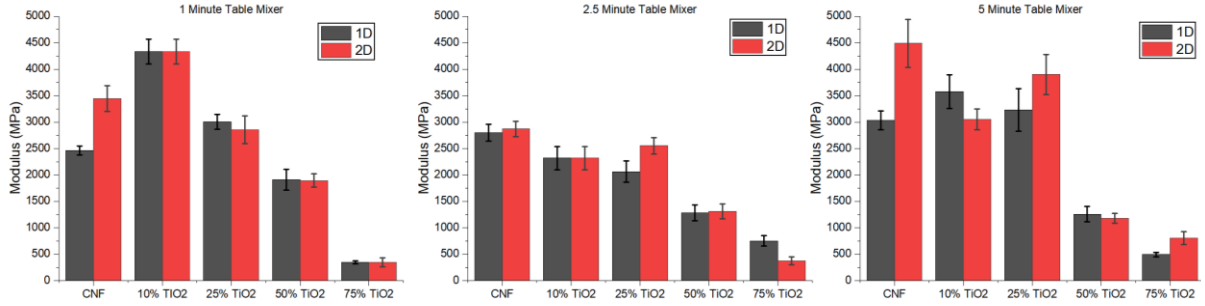

Figure 5.8: Youngs Modulus of All Table Mixed Films at All Time Points (1 Direction Top, 2 Direction Bottom).

Only 10% and 25% composites were compared for statistical analysis, as there was too much variability within the 50% and 75% composites. Also, when performing tests, they were noticeably more brittle being able to be broken with the small loads. It was found that when mixing with a tabletop mixer there was no significant difference between mixing of 1 minute. While there was a significant difference is between hand mixing in the 5-minute category determined by increased strength and moduli. As hand mixing induces potential human error the use of a table mixing machine should take this issue away from the mixing process. When comparing the table mixer times, it was a significant difference with all times to 5 minutes additionally 5-minute films performed the best under mixing conditions within the 10% and 25% composites. Strengths reached 90 MPa, however, there was shown to be a slight decrease in modulus for the 10 films.

When comparing table mixed samples and dilute mixed samples it was shown that for both directions there was a considerable significant difference. With all sample times in the mixer category outperforming dilution. This may have been a result of the two heterogeneous drying methods a filtration process coupled with a ceramic brick interface.

5.4.4 Statistical Analysis

Statistical analysis was performed only on samples control (CNF) through 25% titania additive. first determining the normalcy with a Shapiro-Wilk test for all categories were conducted and shown in Appendix A2. While there was shown to be one subset of data from both the modulus and strength testing to be rejected from normalcy this was assumed to be brought about through randomness within the samples and could be resolved with a higher N in the future. Next pairwise statistics were run in the form of Tukey and shown in figures 5.10 for strengths pairwise statistics and figure 5.11 for Modulus pairwise statistics. There was shown to be a statistical difference thought the hand mixed samples when compared as a whole, while there was less variation within the mixer and diluted samples for both modulus and strengths of the sample. However, when looking at sample types there was shown to be variations between the mixer and diluted samples of many titania composites. Additionally, it should be pointed out that dilution samples on average did poorly when compared to both hand mixed and mixed.

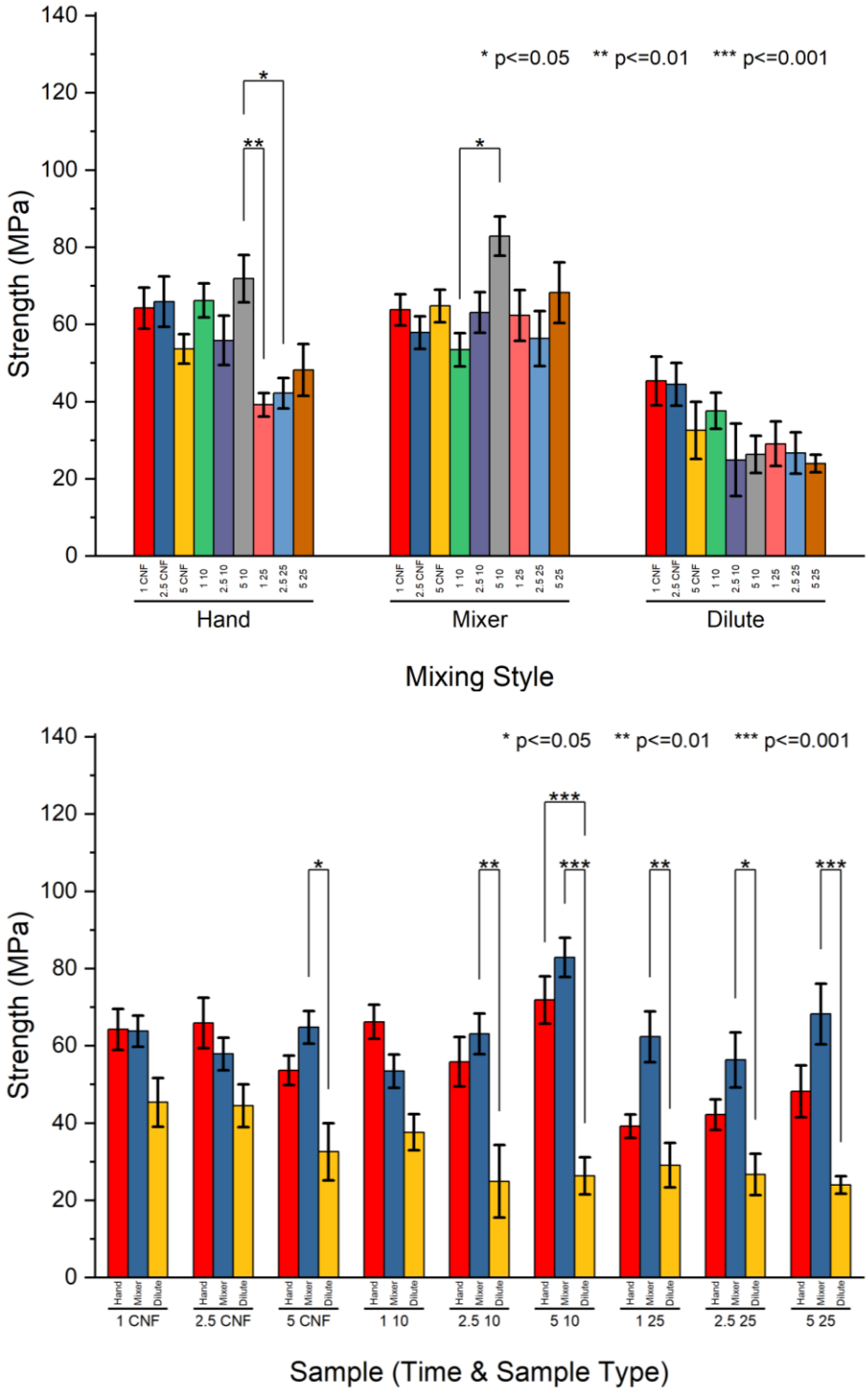

Figure 5.10: Tukey Box Plots of Modulus from Titania Mixing Tests (Top Grouped by Mixing Style, Bottom Grouped by Sample Type).

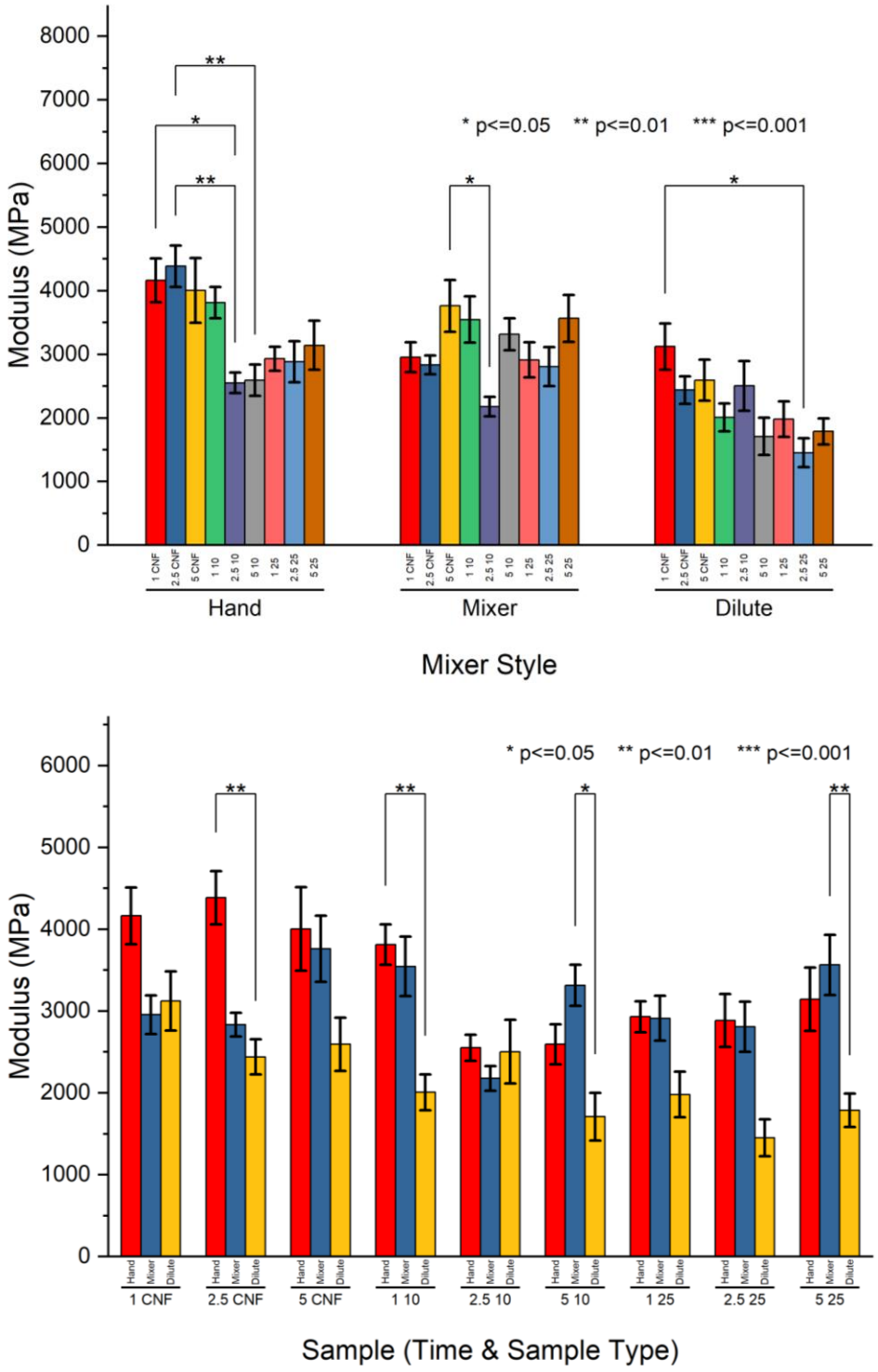

Figure 5.11: Tukey Box Plots of Modulus from Titania Mixing Tests (Top Grouped by Mixing Style, Bottom Grouped by Sample Type).

5.4.5 Scanning Electron Microscopy

Scanning electron microscopy (SEM) was then obtained for control, 25%, and 75% films. This was done by looking at a matted image of each sample, with an additional cross-sectional image at 25%. Images of control samples can be seen in figure 5.12, it was shown to have trace amounts of mineral scattering across the surface. This could be a result of impurities left by the porous ceramic interface material or residuals of titania on the surface of the interfaces that were not effectively cleared when cleaned. Regardless most of the film is shown to be primarily CNF fibrils, as shown by the amount of contrast needed to adjust images.

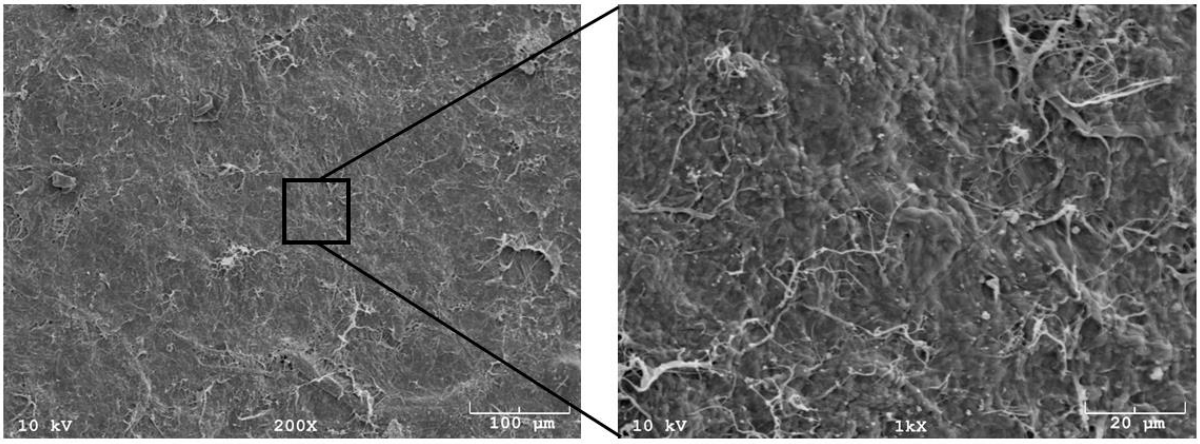

Figure 5.12: Control SEM of CNF (100µm Left, 20µm Right).

25% composites are shown in figure 5.13 with a matted image on the top middle and an image of a cross-sectional area at 100µm zoomed in to 20µm. From the matted image, it is shown that there is a high dispersity of particulates as compared to the control image with a granular appearance being present. Cross-sectional images were obtained by freeze-fracture to try and preserve the fibrous morphology of the film. While this was maintained to some extent being seen on the edges and top of the films some distortion of the matrix can be seen, also within the cross-sectional image laminate formations can be seen within the CNF composite as it is dried.

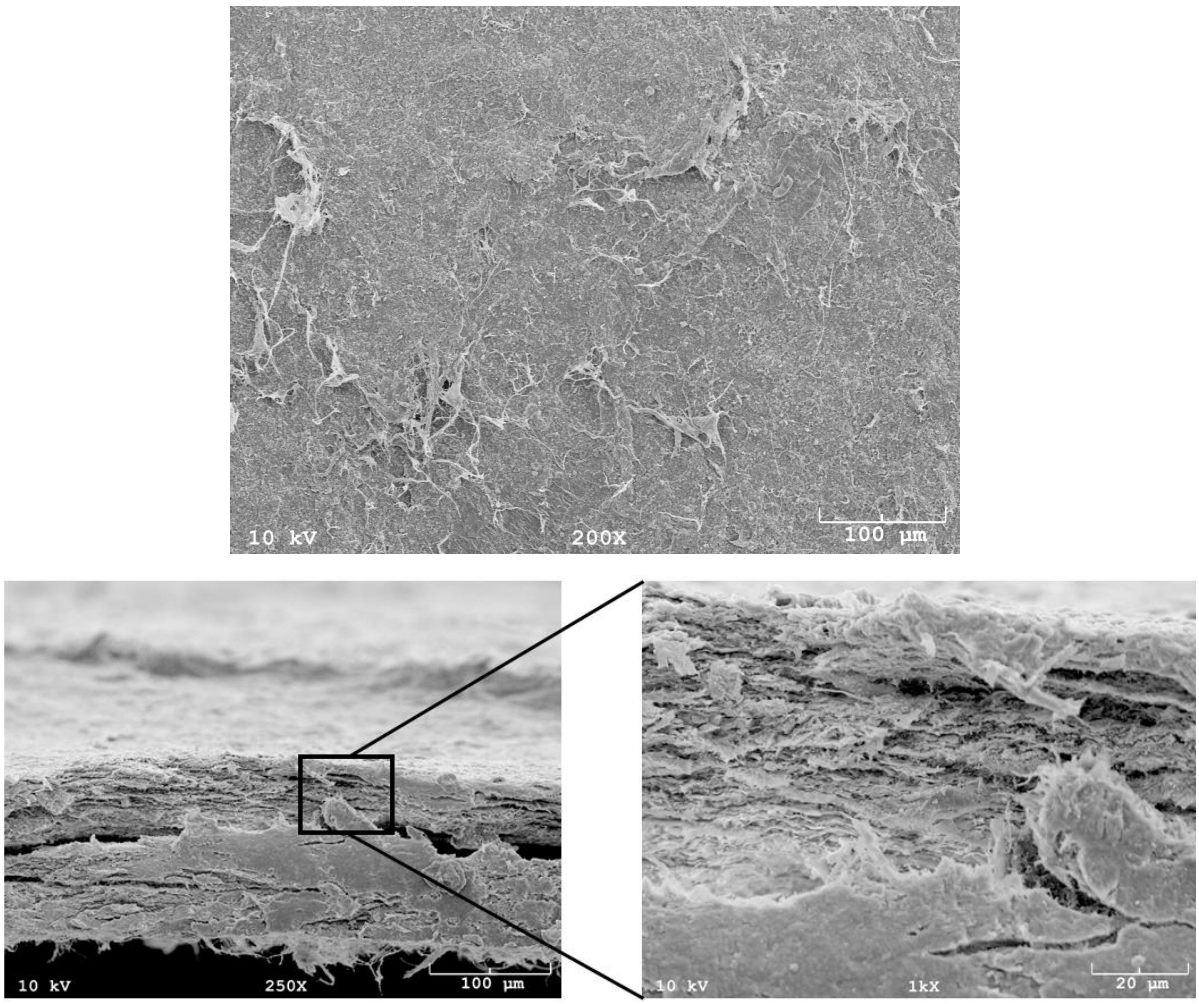

Figure 5.13: 25% Titania Composite SEM of Cross-section (100µm Top Middle, 100µm Left, 20µm Right).

Finally, 75% titania can be seen in figure 5.14, demonstrating a film composite where the filler and matrix switch rolls, being a matrix of titania with fille amounts of fibers. This extreme coating of the fibrils explains the severe degree of bonding interruption and brittleness of films tested. With the majority of the film being heterogeneous distributions of aggregated titania particulates. Within the 75% films, there was shown to be residual titania nanoparticles which can be seen aggregating together and creating pockets of titania.

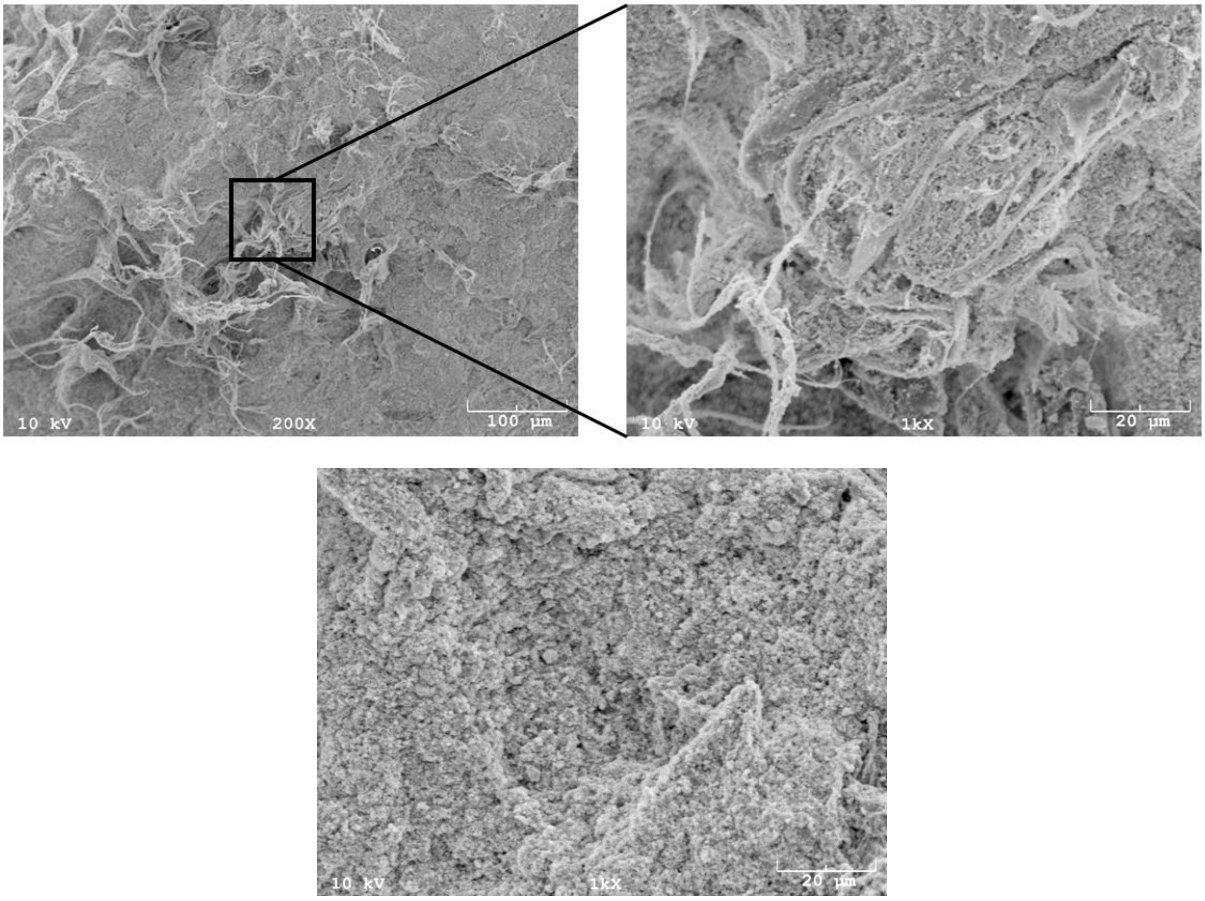

Figure 5.14: 75% Titania Composite SEM Image (100µm Upper Left, 20µm Upper Right, Bottom Middle 20µm).

5.5 Discussion

While the mixing method affects the visual mixing of CNF composites, loading amounts posed an issue for the mechanical properties of the films. Which had a noticeable decrease of modulus and strength over time with increasing additions of filler. With a catastrophic decrease in mechanical properties as the filler reaches a point in which it becomes the matrix. This is thought to be due to interfaces with the intramolecular hydrogen bonding of the CNF. With an increasing interruption as higher wt% of hydrophilic filler is present. As composites between 50 and 75% showed very poor mechanical properties and a very brittle nature to them. Additionally, samples

that were diluted and mixed before vacuum filtration showed difficulties upon removal from the filter paper. Creating a heterogeneous layered suspension with the top retaining water and the bottom-most layer closest to the filter paper becoming a stiff dehydrated film. It was found that the use of a table mixer improved mechanical properties with a 5-minute mixing time, while compared to hand mixing and a dilute mixing style.

This created films that were flawed, with different heating and drying throughout the films. Another issue with the mechanical testing of the film is sample consistency and sample flaws. As samples were stiff in nature creating a gauge filleted was difficult and usually resulted in micro-tears in samples leading to premature failure. Additionally, for some films the use of cutting tools also presented issues creating similar micro tears throughout the sample. Human error also plays a role in sample discrepancies as well, with each specimen being created slightly differently and, in some cases, drastically different depending on how they are prepped and created. Residues from the drying interface and previous testing may also be of concern when proceeding with composite manufacturing in the future.

However, despite the complications of this initial experimentation with CNF composites via ceramic brick interfacing, there is still a need to continue with CNF/mineral composites, as minerals such as hydroxyapatite and other calcium phosphates sources are common with increases and improvements in osteointegration and conductive/inductive properties *in vivo*. Within the orthopedic field fillers typically reach no higher than 25%, moving forward this should be the target filler amount, and optimizations should be taken to increase CNF interactions and minimize capping of the fibrils.

As this was a small-scale preliminary test a small sample size was used, this may have influenced statistics and average results obtained. A more comprehensive study should be used in

the future which can consistently produce samples without the possibility of randomness through the drying process. Once a larger N is established a more comprehensive understanding of the interactions of nanoscale composites within the nanofibril system can be analyzed and potentially utilized within the system in the future.

CHAPTER 6

CROSSLINKED CELLULOSE NANO-FIBRILS

6.3.1 Introduction

While CNF has promising applications within the biomedical field, its hydrophilicity presents complications when placed in aqueous locations, i.e biological systems. Primarily these complications include, swelling, premature mechanical decay and failure, and if applied in dynamic (high shear) systems migration of material. Previous work has shown that substantial mechanical decay of 3D structured CNF in biologically analogous heated DI water occurs within as little as 30 minutes[84]. Water gain and percent swelling of structured CNF devices were seen within this timeframe as well. As this is not optimal for any form of implantable device alternatives to the structure and networking of CNF are needed.

As such is it proposed to crosslink CNF, this would allow for sustained mechanical and structural integrity within prolonged aqueous conditions. Some crosslinking processes however can be extremely chemically harsh and not suitable for use within biological applications, greatly limiting crosslinkers available for use within CNF matrixes. One advantage to CNF is the abundance of hydroxyl groups which are commonly used as the terminal grouping of most bio-friendly crosslinking agents. Examples of these agents are Poly(Acrylic Acid), Citric Acid, and Epichlorohydrin[119–123]. They have been shown to possess good biocompatibility, relatively easy processing, and compatibility with CNF. These agents commonly use a process of esterification binding within the hydroxyl groups of polymers and maintaining their preexisting networks prior to aqueous introduction.

One such polymer of interest is Polycup™(Polycup), specifically Polycup™ 9130, which is a polyamide epichlorohydrin. This is an excellent choice of crosslinker within the CNF samples intended for medical applications as Polycup has been through the FDA analysis previously for oral applications. Meaning it would be an easily compatible polymer resin to crosslink CNF, additionally, it has been shown to work relevantly well within polymer systems with hydroxyl terminal groups and within a set temperature similar to that currently used to process CNF. As such the investigation into the loading amount of the polymer resin within CNF and specific temperature and degradation effects were conducted.

6.2 Procedure

CNF was obtained as-is from the Product Development Center at 3wt%. Polycup was added to 200g of CNF at loading amounts of 0.25%, 1%, 2.5%, and 5% by weight. Suspensions were then calibrated to an operation pH between 7-9 ensured by pH test strips, this was done within the specifications described by the products company. Suspensions were then mixed for 5 minutes and placed onto porous ceramic interfaces and dried at 70°C. Once dried (~24hr) samples were cut into dog-bone tensile testing samples and tested to failure and contact angle was measured. Additional films with control were made, cut into strips (10mm X30 mm), and submerged in biological temperature (37°C) DI. Films were then taken out at time periods of 30s, 1, 2.5, 5, 7.5, and 10 minutes, 5mm of the end of the strip was held in place with a 63g hydrophobic surfaced weight while the other end was freely hanged off an edge. The deflection of the films was measured and recorded as a percent deflection from the dry strip conditions, mass before and after were taken and recorded as a mass gain percent.

6.3 Results

6.3.1 Mechanical Analysis

Tensile dog bone specimens were made for each percent of Polycup with a control sample. Dogbone specimens were then tested until failure or drop in mechanical load, load over time, and extension was recorded and used to calculate the modulus and tensile strength. Figure 6.1 and figure 6.2 respectively. Across all Polycup wt% for the 1 and 2 direction samples, there was found

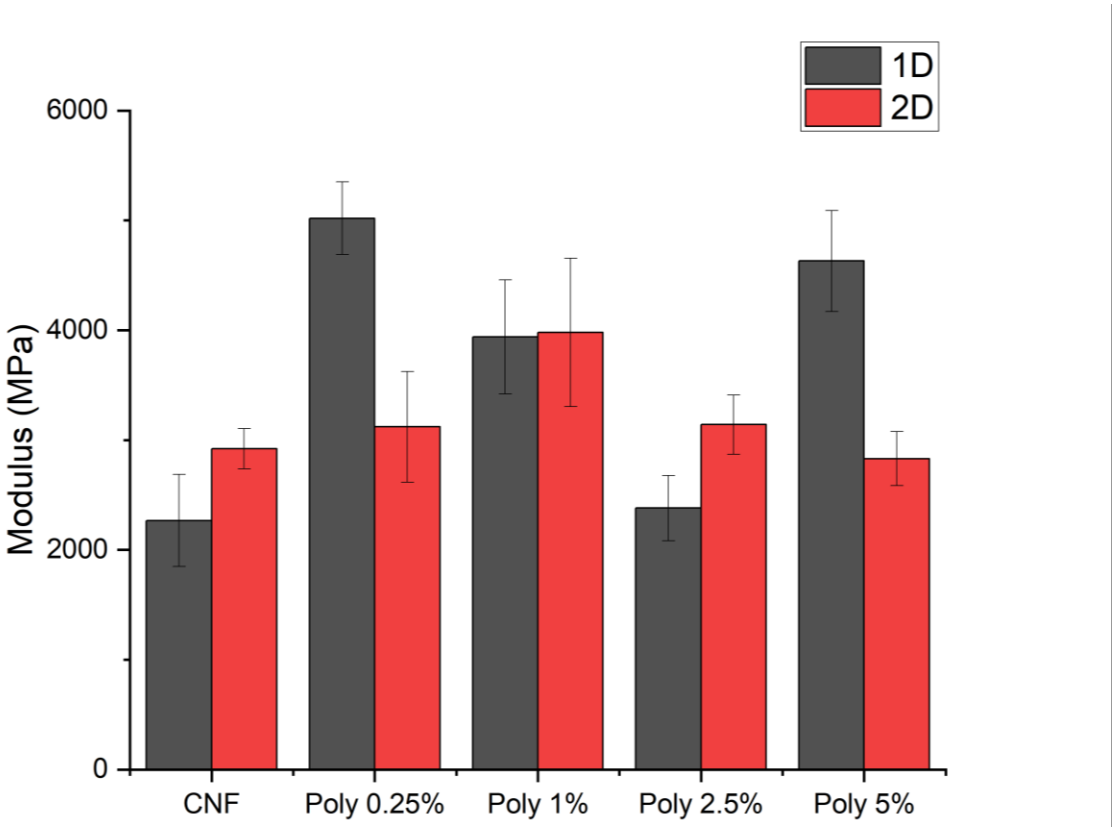

Figure 6.1: Modulus of Tensile Tested Polycup Films.

to be variant results. With a decrease in Young,s modulus for Polycup 2.5% and an increase in modulus at Polycup 5%. This difference in modulus could suggest some effects of the polymeric chain being introduced into the system. However, as samples were created in films residual

mechanical properties post submersion to view polymer effects were difficult to obtain, as such future work should create larger testing specimens.

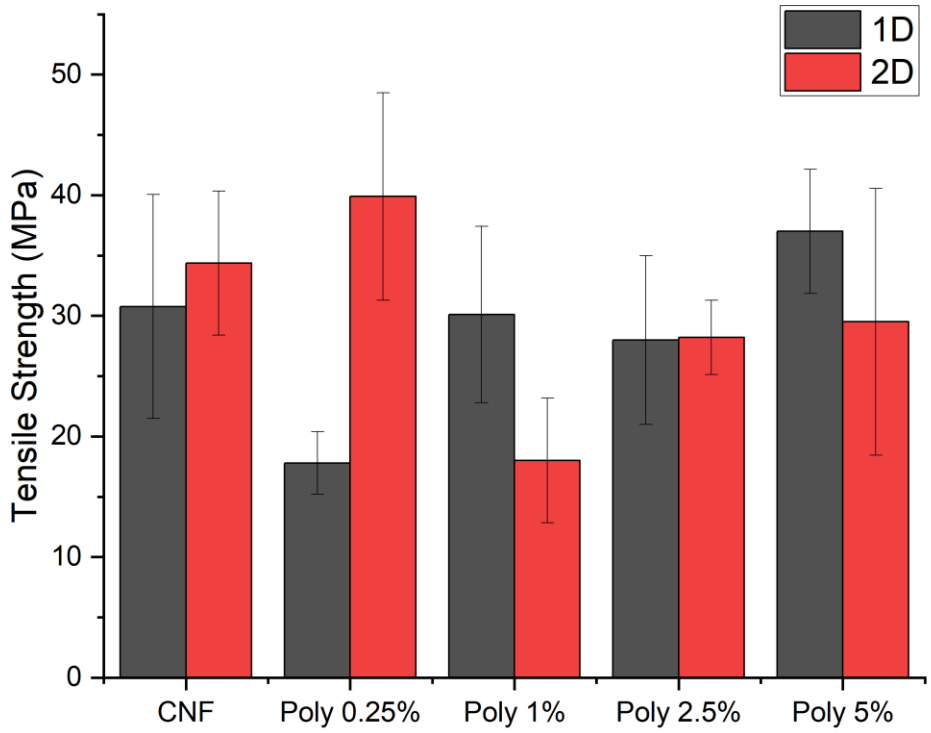

Figure 6.2: Strength of Tensile Tested Polycup Films.

6.3.2 Aqueous Stability

As samples were produced in thin films an innovative method to test mechanical stability was devised. This was done by placing a ~5mm edge of prepared samples onto a hydrophobic surface and placing a weight on top of it. All masses and current position of films were recorded. Next films were placed into contained with biological temperature DI for 30 sec, 1, 2.5, 5, 7.5, and 10 minutes. Consistency of placement was kept by placing numbers on one side of samples and ensuring numbers were facing the same way as initial measurements. At each time point the

samples were removed, slightly pressed to a paper towel to remove excess water, weighed, and were placed into our edge system and tested for deflection.

Water gain percent are displayed in figure 6.3, however deflection of films from the force of gravity was variable due to drying effects, mainly on the strain and curling of the films within short time periods, it was found that many of the films would curl up while being measured as, negative flexing resulted as such measurements were not used and different methods of film mechanical stability should be investigated.

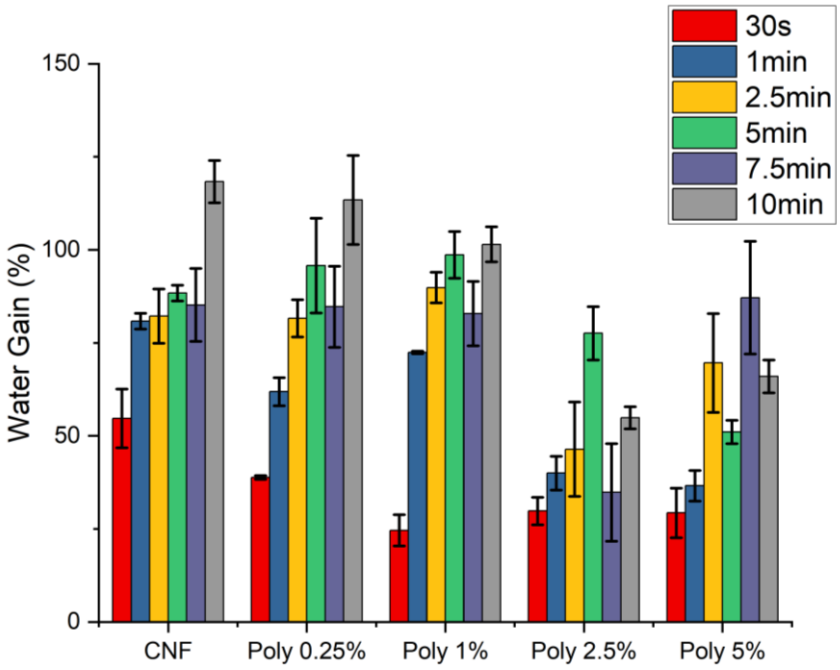

Figure 6.3: Water Gain Percent of All Polycup Wt% Films.

Water gain percent was noticed to decrease with higher loading of Polycup, with Polycup 2.5% and Polycup 5% performing well with 10 minutes showing minimum water gain out of all samples with no significance between them. Comparability there was found to be a significant difference between samples at 10 minutes submersion of the 2.5% and 5% Polycup films.

The water contact angle was taken at the 0.25% and 2.5% to determine the wettability of the films and understand the hydrophilicity of the composites, as shown in figure 6.4. While

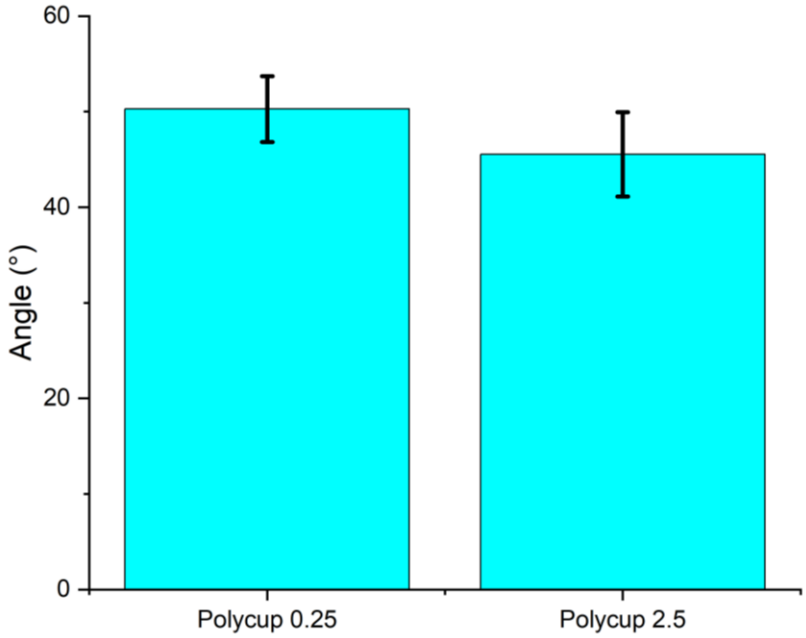

Figure 6.4: Contact Angle of 0.25% and 2.5% Polycup Films.

contact angle indicates if materials are hydrophilic under an angle of 90°, it can also tell you the wettability of a surface. 6 replicates of droplets were done per film and recorded; it was noticed that the 0.25% film had a slightly higher angle when compared to 2.5% multiple factors can be contributed to variants when looking at contact angle. Such factors consist of surface morphology[124], porosity[125], and device accuracy(0.8°). With water as a droplet format on porous material, it is strongly absorbed within giving a smaller apparent angle. With rougher surfaces for hydrophilic material also displaying smaller contact angles. Additionally, water was used within this experiment, to detect significance between the two contacts other liquids should be investigated as well such as Diiodomethane.

6.3.3 Statistical Analysis

Statistical analysis of Polycup crosslinked CNF was performed, first with a normalcy test through a Shapiro-Wilks, shown in Appendix A3. Then an ANOVA was performed (Appendix C) followed by a pairwise Tukey test. Modulus of Polycup samples can be seen in figure 6.5, where there is significance with the 1 direction between multiple samples of Polycup crosslinked specimens, whereas with the 2 directions between specimens there was shown to be no variation, potentially indicating that along the 2 directions samples had a more consistent strain and

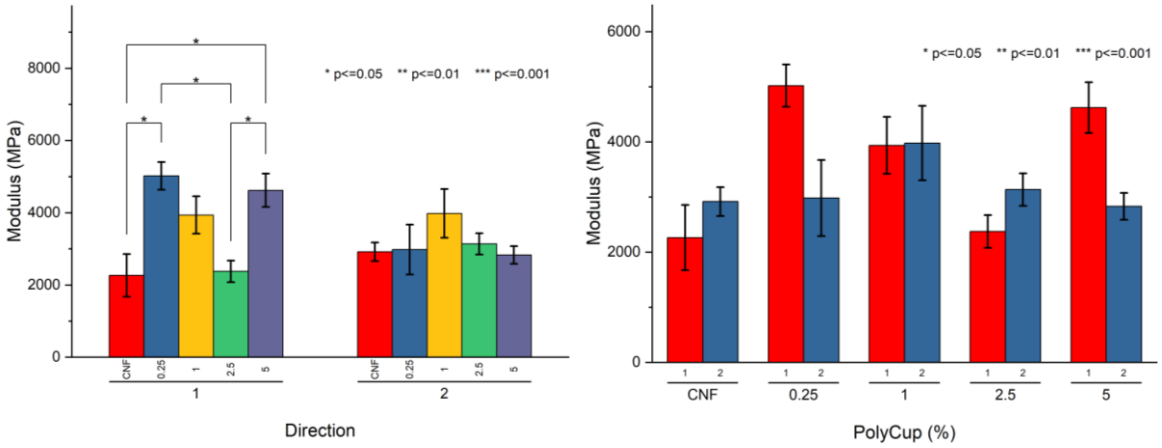

Figure 6.5: Modulus of Polycup Specimens Grouped as Directions (Left), Modulus of Polycup Specimens Grouped as Sample Type (Right).

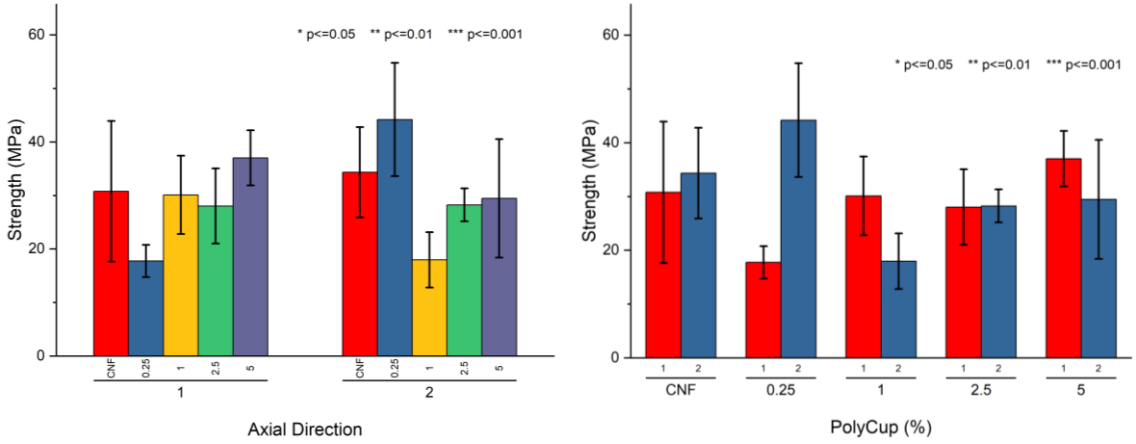

Figure 6.6: Strength of Polycup Specimens Grouped as Directions (Left), Strength of Polycup Specimens Grouped as Sample Type (Right).

alignment of fibers. When looked at a comparison of each specimen for each direction there was shown to be no significance between them. Strength statistical analysis is shown in figure 6.6, where there was shown to be no significance between any of the directions when compared to Polycup percent or when comparing all Polycup percent within a direction.

Water gain statistics were performed in a similar method as described above, with Shapiro-Wilks table being shown within Appendix C, followed by ANOVA (table A5 and A6), and finally a pair wise comparison through Tukey. An overall analysis was made for each Polycup percent

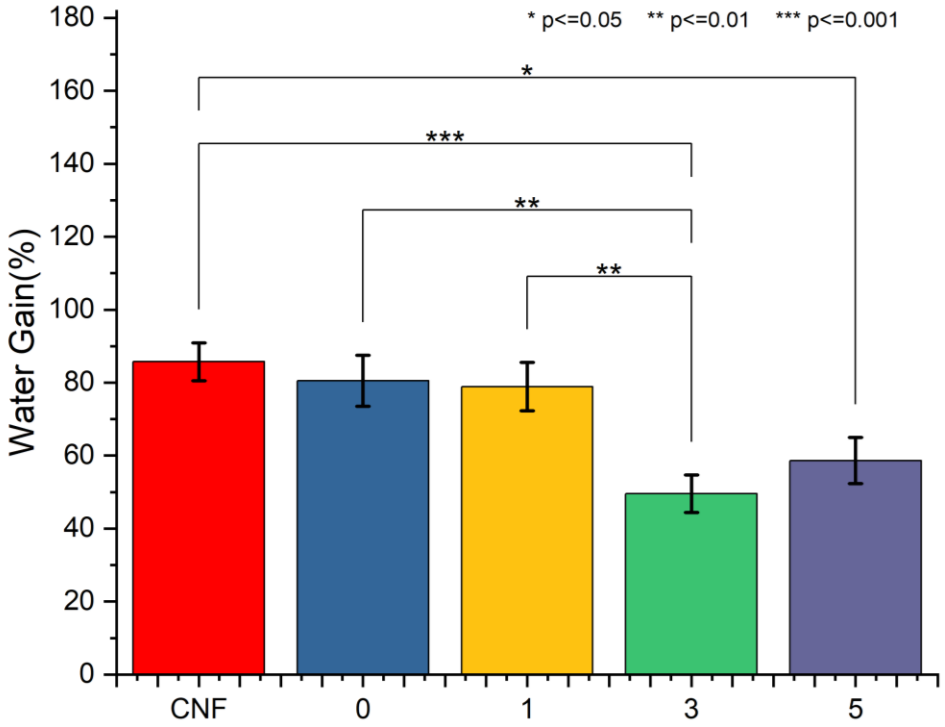

Figure 6.7: Water Gain Percent Across All Polycup Samples and Times.

specimen over all times and is shown in figure 6.7. It was found that overall, there was a significance between 2.5% Polycup and all other wt% below it. Which showed encouraging signs for the specimens at a wt% of 2.5%. Next time points for each sample were compared between themselves and is shown in figure 6.8.

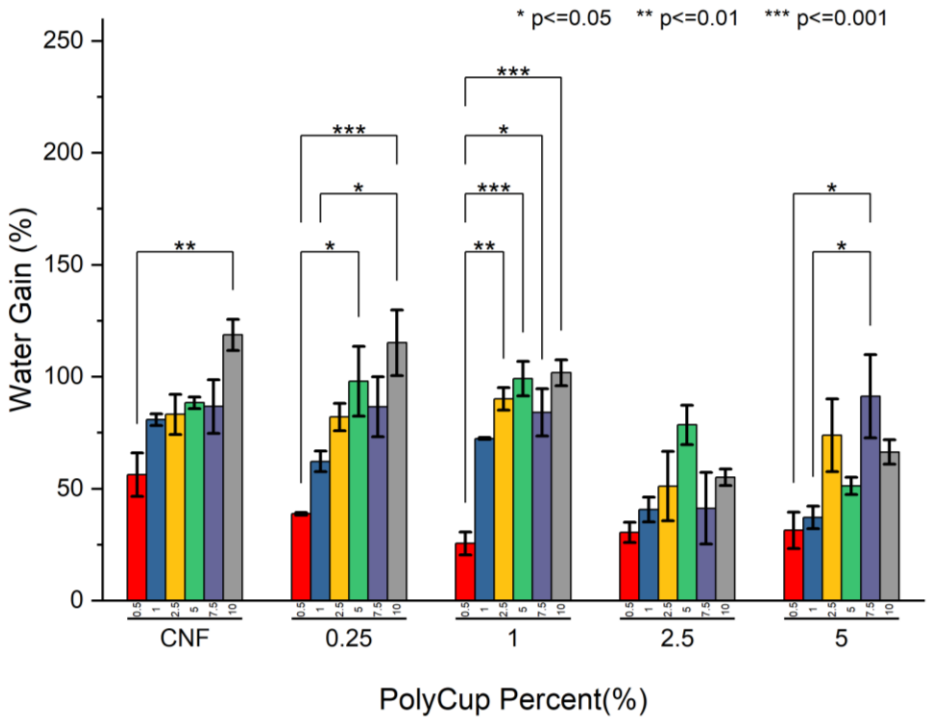

Figure 6.8: Water Gain of Time Points for Each Polycup Wt%.

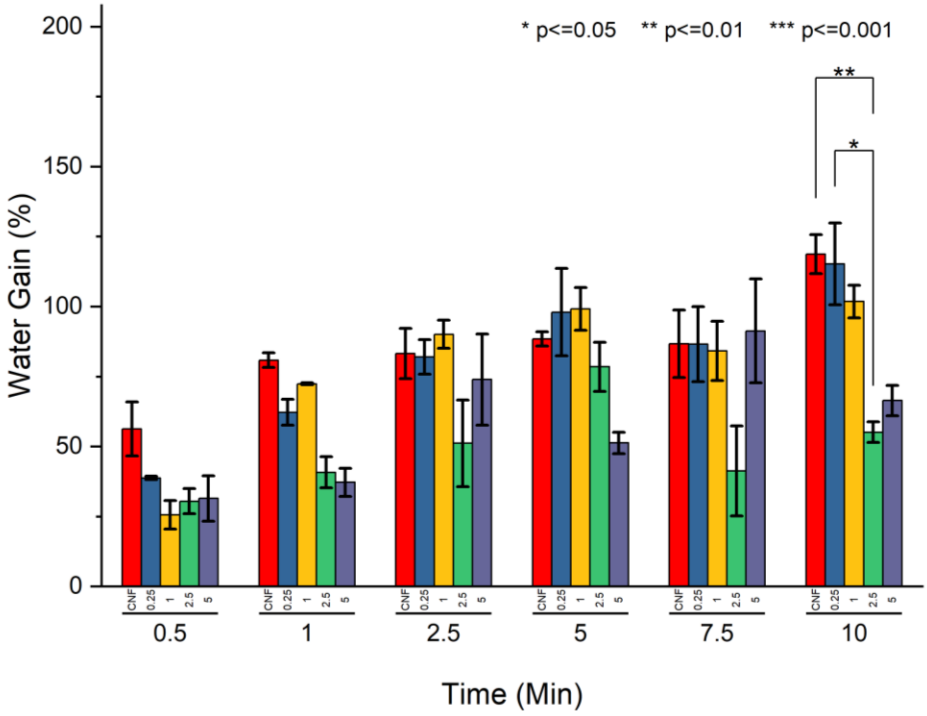

Figure 6.9: Water Gain of Specimens Grouped as Time Points.

Which showed that in the 2.5% Polycup specimens over the 10 minutes there was no significance between their average water gain, unlike other specimens which showed significance at end time points. This is encouraging as samples had little variation between them at 2.5% demonstrating some ability to resist water uptake. Finally, each time point was investigated, and the statistical analysis is shown in figure 6.9, when comparing all crosslinked samples of CNF at each time it was shown that there was no significance for time points up to 7.5 minutes. However, at 10 minutes there was shown to be significance between pure CNF and 0.25% when compared to 2.5% Polycup. More trials using larger sample sizes should be used to prevent randomness of samples and obtain a normal data set, as one sample set was shown to be rejected from the normalcy test. Additionally, a sample set of 3 does not provide a powerful set for statistics. Further experimentation is needed to fully understand the results from aqueous submersion testing.

6.4 Discussion

The use of a crosslinker is essential for the potential application of CNF within the human body. While Polycup provided a crosslinker with passively adaptable chemistry utilizing the abundant hydroxyl groups, work is needed to optimize its loading and drying. Mechanical strength was shown to stay the same for all films produced while the moduli of films was shown to improve in with the addition of polymer crosslinker. There was shown to be significantly less water absorption within films that have higher crosslinker as well, indicating a potential for sustainability within aqueous solutions and environments. Large-scale production should be looked at next to be able to fully characterize the mechanical stability of the samples. Using a small gravity-driven bending test, in theory, is a viable means to characterize thin films, however, using a more robust method would be beneficial. The use of thin films can pose a problem for long-term aqueous studies as film removal from containers will become increasingly more difficult without potential

specimen destruction. This is expectably true with the control samples of CNF which have been shown to break down rapidly in DI.

Time points used within this experiment additionally may have been too acute for an accurate depiction of deflection and Polycups potential mechanical stability of samples. As such additional experiments should be carried out with a more chronic timeline for extraction points. One problem noted with finding deflection percent is the curling of some samples when introduced into aqueous condition and left out before measurements could be taken. Water uptake into the films were substantial for non-crosslinked films compared to films treated with Polycup. With optimizations of loading amounts being required, as within the medical world, less of something additional is better. From the data collected it is suggested that between 1% and 2.5% there is a potential to effectively crosslink the films. Additional trials should be conducted using larger bulk sources changing their morphology and porous structures more conducive to materials intended for manufacturing. Effective crosslink should also be determined to investigate the percent of fibers with the material being effectively crosslinked. Additionally, surface crosslinking should be investigated to determine if materials could benefit from similar properties while only having the surface being treated.

CHAPTER 7

POTENTIAL MARKET ENTRY DEVICE AND MODELING OF CNF ANCHOR DEFORMATION

7.1 Introduction

Currently, the medical field is overflowed with devices, as such identifying and designing specific devices to enter this competitive market space is challenging. One problem in particular to platform material devices is the amount of time and funding it takes to bring the devices to a functioning capacity. This becomes an even more daunting issue with materials intended for multiple device applications and the degree of hazard regarding each of the devices. Hazards pertaining to devices are decided depending on devices classification, to which there are 3 types of classifications provided by the FDA[126]. Class 1 devices are relatively easy in design and require less regulation and controls due to their decreased hazard of harm, as they are not intended for sustained usage and have limited biological contact. Nanomaterials in particular have had difficulties while going through the FDA 510K process, it was found that in the years from 1960-2017 only 36 medical devices had gone through the process[127].

Examples of Class 1 devices are hospital beds, arm slings, and oxygen masks. Class 2 devices are more complex devices for which more sustained usage and contact is intended, as such more rigorous FDA regulation is needed to ensure safety from hazards and effectiveness. Examples of Class 2 devices are X-ray machines, contact lenses, and suture anchors. Class 3 devices are devices intended for sustaining or supporting human life, as such these devices are much more heavily controlled and require scrupulous FDA regulation to ensure device efficiency

and potential risk factors related to them. Examples of Class 3 medical devices are heart valves and defibrillators[128].

Most medical devices within orthopedics are classified as Class 2[129] due to potential hazards associated with the intended sustained use. As such device reviews, along with networking device discovery were used to determine a device suitable for entry for CNF. One device that was identified as a potential entry device was a suture anchor. Suture anchors are devices used to fix ligaments and tendons to bone. While devising specific samples and testing for the efficacy of CNF for use as suture anchors is a lengthy process taking many years and funding for its development, simple simulations via an example Solidworks can provide a compelling view of the environmental situations CNF would experience as suture anchors device material. Using previously evaluated experimental values for modulus and strengths a 3D model of a screw can be placed under forces that have been established as failure forces for other suture anchors within the space. This allows for a timely and cost-effective view of the CNFs capabilities as a material before going through a long and financially burdening process that might not yield expected values and ultimately fail.

7.2 Solidwork Simulation Setup

A simulation was created in Solidworks using a free sourced cortical screw by Hari Krishnan. As the dimensions of suture anchors used are protected by their respective brands, a similar screw shape was found and used. The dimensions of the outer diameter and length were similar to those expressed for suture anchors. For suture anchors in particular it is important to understand the pullout strength of the material. CAD model of screw procured had a 4 mm diameter, 9.6mm length, and a 0.7 mm threading. Each direction 1, 2, and 3 were tested separately to understand manufacturing variants possible from the resulting CNF ingot. Experimental values

obtained within previous chapters were used and yield strength (the point at which elastic deformation ends and plastic deformation begins) was obtained. For this study, all screw thread surfaces were fixed, and an axial pull-out force was placed at the top of the screw in Solidworks. The forces used were 256N, 465N, and 564N, which corresponded to failure loads of single-loaded, double-loaded, and triple-loaded suture anchors respectively, Barber *et al*[130]. A diagram of the screw with load directions and arrows indicating fixed geometries can be seen in figure 7.1. After the end of the simulation an image of the corresponding stress indicator with heat mapping on the model were captured and reported.

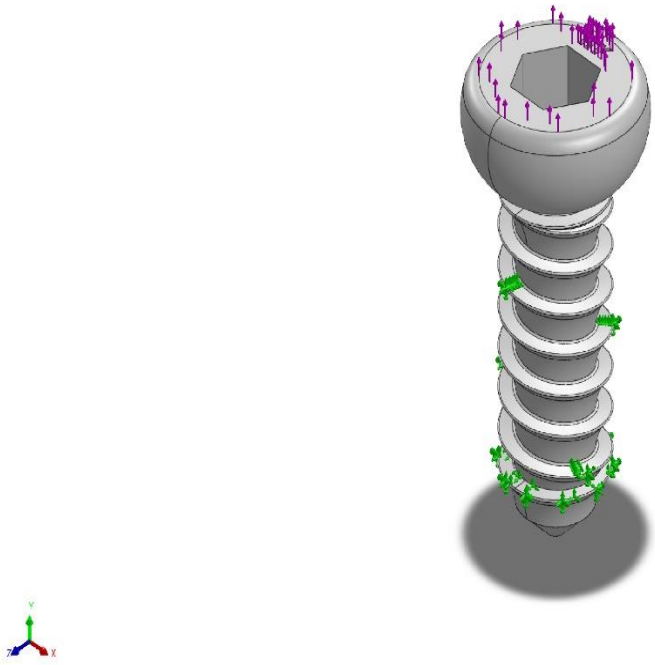

Figure 7.1: 3D Screw Model, Force (Purple) and Fixed Geometries (Green).

7.3 Simulation Results

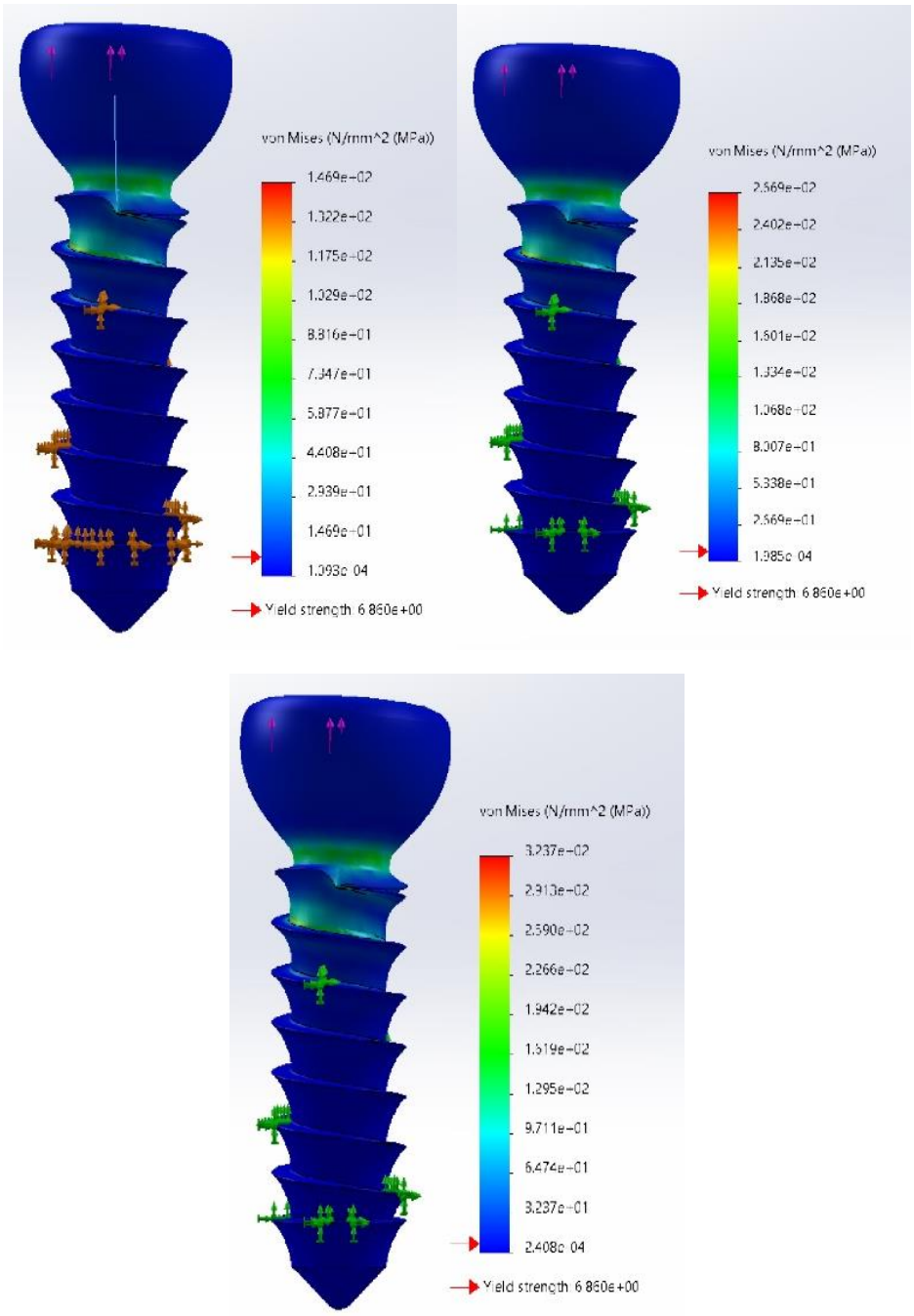

Figure 7.2: Simulation Using 1 Directional Tensile and Compressive Properties. (Top Left. Single Loaded, Top Right. Double Loaded, Bottom Middle. Triple Loaded).

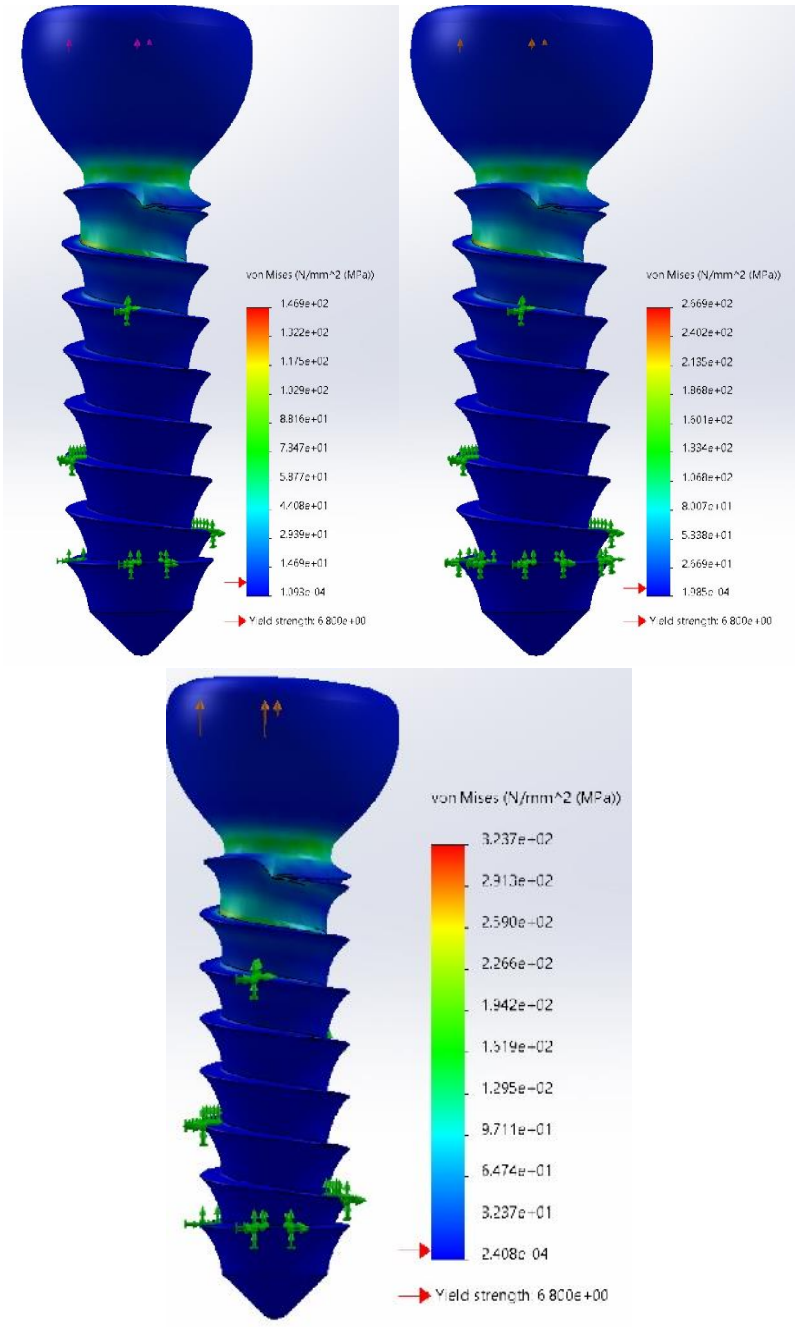

Figure 7.3: Simulation Using 2 Directional Tensile and Compressive Properties. (Top Left. Single Loaded, Top Right, Double Loaded, Bottom Middle. Triple Loaded).

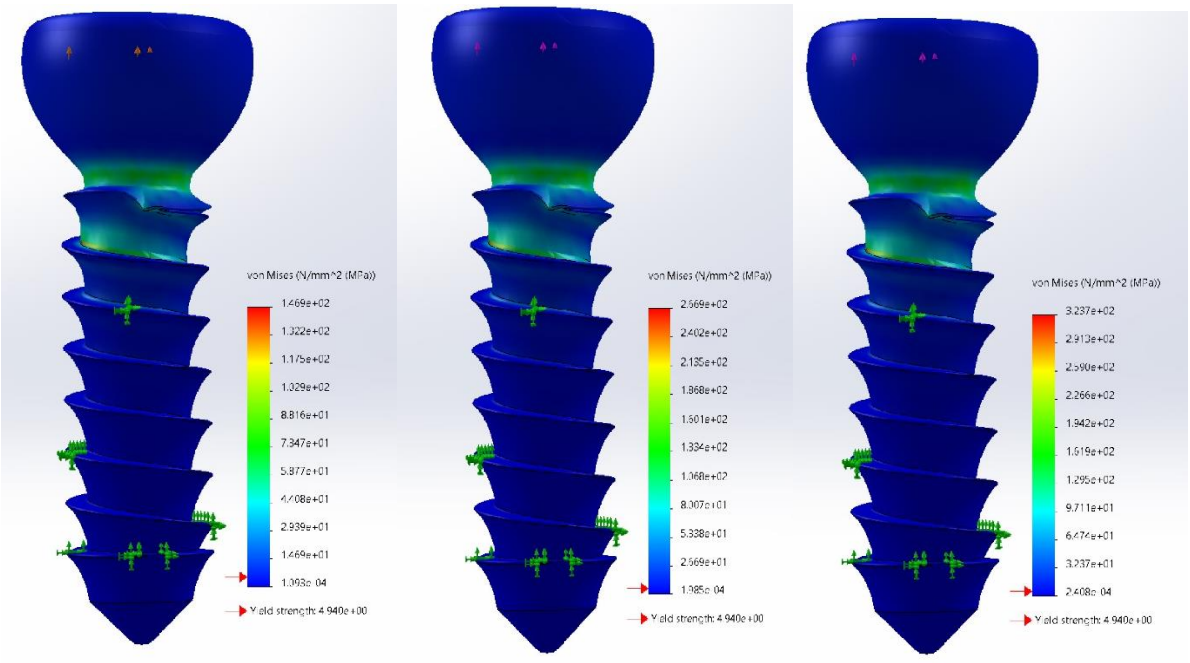

Figure 7.4: Simulation Using 3 Directional Tensile and Compressive Properties. (Left. Single Loaded, Middle. Double Loaded, Right. Triple Loaded).

It was shown that for all increasing loads screws with the properties of CNF would perform within a positive regime. While the neck of the screw and the screw head itself display distortions brought about by the loads. Through all simulations using known failure loads, there was no discovered failure within the screws. There were distortions to the threads closest to the neck of the screw and this should be noted, additionally, it was found to be higher stresses within the area near the top screw threads as well. Displaying some amount of risk with the threads closest to the applied force, which was viewed in all the screws. Direction 2 screws were shown to have the highest yield strength when compared to the other two tested directions.

7.4 Discussion

It was shown through simulation modeling of a screw during pullout would not result in device failure, and above would yield of all screws would be reached near the screw head. Meaning that plastic deformation would be accruing and permanently deform the samples. While simulations performed within this experiment were minimal, locking all thread spaces, future endeavors should be taken to have larger headspace. This can create a more dynamic analysis and simulation of axial pull-out of screws. Tensile data from bulk should be reviewed and attempted again with different specimen dimensions, reaching dimensions similar to ASTM standards.

It should be noted that models were conducted under a limited number of variables. As they were used to conduct the initial check on whether or not materials could perform under basic modeling. Prototypes should be made and tested to ensure the results of the modeling and to optimize material inputs and dimensions. Through experimental values, better modeling could be performed and could accurately predict the performance of prototypes before taking the next step to *in vivo* studies.

One major downside to the use of simulations is that mechanical flaws within samples are not represented, such as porosity of samples and or reductive manufacturing pitting or fracture tears through the sample. Which could shield loads and offload areas and cause devices to prematurely create small prototypes before modeling would validate the simulation and give it the freedom to accurately predict future device loading and potential failure, without the need to go through potentially expensive and wasteful process destroying prototypes without a sensible idea of characterization. As complex devices will need the use of precision milling through computer numerical control (CNC) cutting, which depending on complexity becomes a costly procedure.

CHAPTER 8

CONCLUSION

8.1 Summary

The number of medical devices increases each year, with optimized devices for new and emerging procedures. While current devices are proficient in their own rights, they are not without their flaws. As such the investigation of a relatively new biopolymer, CNF, has been studied throughout this thesis for the sole purpose of determining its potential within the field of orthopedics. Mechanically, bulk CNF has the potential to perform well, displaying strengths through compression similar and above that of cortical bone. Through 2d film experiments, it was shown that temperature between 50 and 100°C had little effect on the directionality of films. This may be a limitation when going from a 2D model to a bulk 3D model, as there is a significant change in the volume of CNF produced and models used, specifically in the height direction introduced with 3D. This introduced a 3rd dimension for which fibers could align themselves. Temperature is important when going to bulk as it has been observed that increased energy into the system has the potential to affect internal stresses, which increase and cause warping of the CNF bulk. As such a low temperature approach should be used to allow fibers to have time to arrange and fall in a passive way. While three direction materials showed impressive mechanical properties, sample preparation for mechanical trials should be investigated and drying molds for which the CNF is made should be optimized to obtain enough material to be reduced into adequately sized samples. Directionality of CNF is important, with CNF being a random entanglement of fibers. Carefully studying each direction to determine fiber alignment within the systems is crucial and should be considered within the final manufacturing process.

CNF has been shown to be within effective ranges to not be categorized as cytotoxic, which provides evidence for its potential use within biology. However, this is just a first step within the long road towards determine a material's cytotoxicity and getting it approved for potential use. While the base material of CNF was shown to have encouraging results, all other subsets and composites will need to go through equal scrupulous testing to determine their potential toxicity. As mineral addition is intended within the CNF matrix it should be tested for any potential cell death it could elect. Additional tests should be conducted with more robust positive material, which due to its potential toxicity poses a challenge to obtain.

Longer mixing and use of a mixing device shows improvements with mechanical properties. As hand mixing introduces human error, the use of tabletop mixing encourages homogeneous mixing throughout the films. With longer mixing periods showing improved mechanical properties. Dilutions while in theory could be an effective way of mixing, current means introduce variability upon drying. As filtering can produce heterogamous layering with large amounts of cellulose. Creating a dry packed layer of material within contact to the filter paper and a loosely packed more aqueous layer near the top of the filter funnel. When placed upon the ceramic heating molds these heterogeneous zoned, wet and dryer areas of cellulose, can cause fibers to be arranged in a multitude of ways. As they are not allowed to align themselves effectively during drying. Low percent of additives showed encouraging results, however larger percent showed conflicting results. Higher minerals overloaded the system which can interrupt the interactions between fibers and create a mat of minerals with a filler of fibers in the matrix. The addition of composites and different formations is desirable for devices, mixing of mineral oxides, BMP, and crosslinking agents. Viewing the multiple methods of mixing will give an

approximation to mixing conditions within common industrial settings and give informed discission making when going to large scale production of CNF.

Crosslinking is a desirable process performed on many hydrophilic materials, as aqueous mechanical properties can be sustained and modified for controlled breakdown. There is an abundant amount of crosslinkers, but one within the FDA system is desirable. As such Polycup presented itself as an acceptedly crosslinking polymer. It was shown that with a small pH treatment between 7-9 and implementation of Polycup, water uptake of samples was decreased. With 2.5% Polycup addition improving its water uptake over the acute trial. Water contact can be a useful tool when looking at the wettability and hydrophilicity of a material. However, it is susceptible to variability due to morphological properties. With roughness and porosity of hydrophilic materials decreasing contact angle and increasing the wettability of the material. Additionally depending on pore size and distribution within the materials absorbance of aqueous fluids would increase as well.

Modeling and simulations of materials is a commonly practiced in many areas of engineering. While this can give a base understanding of potential performances of constructs made from specific materials. It should not be the only evidence given for its application. That said, the preliminary performance of CNF screws showed promise for the materials uses within the field. With known forces that create failure being applied, CNF screws demonstrated sufficient mechanics to not fail. While yield is surpassed and devices would be deformed, absolute failure would not be achieved.

8.2 Future Work and Recommendations

CNF from the work displayed in the presented thesis suggests its potential use within the medical field. However, as medical devices take years to finalize testing and produce, much to is

needed to understand the current CNF system better. In particular material loading and aqueous degradation properties and optimizations. Many devices within the medical field that are plastic are loaded with osteo-inductive and -conductive materials to improve their osteointegration within the body. This will require optimizing the mixing of CNF with other minerals and limiting their effects on the fiber's native hydrogen bonding interactions which give it its unique properties or maintaining fiber bond interactions through other chemical means. As many devices do not surpass more than 25% filler a limitation of filler should be introduced with testing.

Tabletop testing is a desired aspect of laboratory work and making samples and specimens that can be rapidly produced and tested allow many scientists to expediently provide results. This was the driving force for using films as a means to model larger scale systems. However, films present flaws within them that cannot accurately portray the results within larger samples. Mainly they create a layered drying through the use of two interfaces and create pours that can prematurely cause failure when mechanically tested. Additionally, the films produced are brittle across all variants, meaning that reductive means to make samples cause tears in the films which again could cause premature failure when testing. As such work should be done to create a small mold capable of creating uniform shapes with adequate material for sample preparations.

Bulk properties should be introduced in shear, torque, and impact as well, with these properties being important for a basic understanding of materials performance. Due to limitations in equipment as a result of backlogged work following the pandemic, materials could not be tested as such. Material studies on these specific properties should be investigated and recorded. Testing of specimens within the dimensions of ASTM standards should be done and upon positive results, samples should be sent to an external facility for an accredited test. This also applies to cytotoxicity testing as well requiring external means of testing for accreditation. As MTT provided positive

results, difficulties with the material should be addressed using other stains to optimize results. Different controls should be obtained with a positive control being found with substantial cell death. Devices should also be restrained within the wells so as not to disturb the monolayer below and cause a cascade of cell death signaling. Different sanitation methods should be reviewed, as dry autoclave showed signs of thermal decomposition for CNF samples, Gamma ray sterilization could provide a more suitable sterilization method.

Crosslinking of CNF was done at an acute time scale, while showing promising results future experiments should be done to determine the longevity of the specimen's size and mechanical properties. Specimens should also be created at a bulk scale to ensure degradation and mechanical properties can be tested. Work should also be done to find optimum loading of crosslinker, as suggested there is potential for loadings between 1 and 2.5% to be effective at maintaining low water uptake. Work should also be done as chronic testing instead of acute testing. Being performed over months to determine sustained properties of crosslinking with the CNF. Determination of effective means to expediently get results from long term aqueous degradation trials, this entails using a higher temperature for a shorter time, potentially cutting down the required time of experimentation by months. Other means of crosslinking should be investigated to instead of bulk crosslinking, one such method would be surface crosslinking. Introducing the crosslinker via dunking CNF into solutions of it then drying at the specified setting times.

Composites of minerals and crosslinkers should be investigated to understand the potential end product that would be manufactured into devices. These prototype devices should also be made and tested within specific environments and situations to which they are intended to be implanted. Careful analysis should be done on the prototypes, including mechanical testing and degradation properties. Once sufficient data is collected, and the results are encouraging, *in vivo*

trials should be conducted to view the devices within a biological model. Small models such as mice are usually performed first, then larger animals such as pigs are used prior to conducting human trials for devices and materials. Once positive trial results are collected from large animal models, clinical trials should be conducted. Finally, the process of bringing end product CNF devices to the FDA should be considered.

REFERENCES

1. Clarke B. Normal Bone Anatomy and Physiology. *Clin J Am Soc Nephrol*. 2008:131-139. doi:10.2215/CJN.04151206

2. Lin C-Y, Kang J. Mechanical Properties of Compact Bone Defined by the Stress-Strain Curve Measured Using Uniaxial Tensile Test : A Concise Review and Practical Guide. *Materials (Basel)*. 2021;(14):4224.

3. Nobakhti S, Shefelbine SJ. On the Relation of Bone Mineral Density and the Elastic Modulus in Healthy and Pathologic Bone. *Curr Osteoporos Rep*. 2018;16(4):404-410. doi:10.1007/s11914-018-0449-5

4. Murphy W, Black J, Hastings G. Cancellous Bone. *Handb Biomater Prop Second Ed*. 2016:v-vi. doi:10.1007/978-1-4939-3305-1

5. Barrère F, Blitterswijk CA Van. Bone regeneration : molecular and cellular interactions with calcium phosphate ceramics. 2006;1(3):317-332.

6. Chaudhry AA, Knowles JC, Rehman I, Darr JA. Rapid hydrothermal flow synthesis and characterization of carbonate- and silicate-substituted calcium phosphates. *J biometerials Appl*. 2012;28(3):448-461. doi:10.1177/0885328212460289

7. Fathi MH, Hanifi A, Mortazavi V. Preparation and bioactivity evaluation of bone-like hydroxyapatite nanopowder. *J Mater Process Thechnology*. 2007;2:536-542. doi:10.1016/j.jmatprotec.2007.10.004

8. Shepherd JH, Shepherd D V, Best SM. Substituted hydroxyapatites for bone repair. *J Mater Sci Mater Med*. 2012;23:2335-2347. doi:10.1007/s10856-012-4598-2

9. Liu Q, Huang S, Matinlinna JP, Chen Z, Pan H. Insight into Biological Apatite : Physiochemical Properties and Preparation Approaches. *Biomed Res Int*. 2013;2013:13.

10. Köse N. Biological Response to Orthopedic Implants and Biomaterials. *Musculoskelet Res Basic Sci*. 2016:3-14. doi:10.1007/978-3-319-20777-3

11. Hart NH, Nimphius S, Rantalainen T, Ireland A, Siafarikas A, Newton RU. Mechanical basis of bone strength : influence of bone material, bone structure and muscle action. *J Musculoskelet Neuronal Interact*. 2017;17(3):114-139.

12. Bacabac RG, Mullender MG. Mechanobiology of bone tissue Mecanobiologie du tissu osseux. 2005;53:576-580. doi:10.1016/j.patbio.2004.12.005

13. Gusmão CVB de, Belangero WD. How Do Bone Cells Sense Mechanical Loading? *Rev Bras Ortop (English Ed*. 2015;44(4):299-305. doi:10.1016/s2255-4971(15)30157-9

14. Xiao Y, Xiang L, Shao J. Bone morphogenetic protein. 2007;362:550-553. doi:10.1016/j.bbrc.2007.08.045

15. Iain H. Kalfas, M.D. FAC. Principles of bone healing. *Nurosurg Focus 10*. 2001;10(4):1-4. doi:10.3171/foc.2001.10.4.2

16. Manivasagam G, Dhinasekaran D, Rajamanickam A. Biomedical Implants : Corrosion and its Prevention - A Review. *Recent Patents Corros Sci*. 2010;2(2):40-54.

17. Balamurugan A, Rajeswari S, Balossier G. Corrosion aspects of metallic implants — An overview. *Mater Corros*. 2008;59(October 2018). doi:10.1002/maco.200804173

18. Mavrogenis AF, Dimitriou R, Parvizi J, Babis GC. Biology of implant osseointegration. 2009;9(2):61-71.

19. Long PH. Medical Devices in Orthopedic Applications. *Toxicol Pathol*. 2008:85-91. doi:10.1177/0192623307310951

20. Sukegawa S, Kanno T, Kawai H, Shibata A. Clinical Report Long-Term Bioresorption of Bone Fixation Devices Made from Composites of Unsintered Hydroxyapatite Particles and Poly-L-Lactide. *J Hard Tissue Biol*. 2015;24(August 2009):219-224.

21. Rezwan K, Chen QZ, Blaker JJ, Roberto A. Biodegradable and bioactive porous polymer / inorganic composite scaffolds for bone tissue engineering. 2006;27:3413-3431. doi:10.1016/j.biomaterials.2006.01.039

22. Vergnol G, Ginsac N, Rivory P, et al. In vitro and in vivo evaluation of a polylactic acid-bioactive glass composite for bone fixation devices. *J Biomed Mater Res - Part B Appl Biomater*. 2016;104(1):180-191. doi:10.1002/jbm.b.33364

23. Sathiyakumar V, Jahangir AA, Mir HR, et al. Patterns of Cost and Spending Among Orthopedic Surgeons Across the United States: A National Survey. *Am J Orthop*. 2014;(January):7-13.

24. Weber M, Renkawitz T, Voellner F, et al. Revision Surgery in Total Joint Replacement Is Cost-Intensive. *Biomed Res Int*. 2018;2018:8. doi:10.1155/2018/8987104

25. Herzog MM, Marshall SW, Lund JL, et al. Cost of Outpatient Arthroscopic Anterior Cruciate Ligament Reconstruction Among Commercially Insured Patients in the United. *Oropeadic J Sport Med*. 2017;(Cdc):1-8. doi:10.1177/2325967116684776

26. Ambrose CG, Clanton TO. Bioabsorbable Implants : Review of Clinical Experience in Orthopedic Surgery. *Ann Biomed Eng*. 2004;32(1):171-177.

27. Peterson J, Sodhi N, Khlopas A, et al. A Comparison of Relative Value Units in Primary Versus Revision Total Knee Arthroplasty. *J Arthroplasty*. 2018;33(7):S39-S42. doi:10.1016/j.arth.2017.11.070

28. Kremers HM, Visscher SL, Moriarty JP, et al. Determinants of Direct Medical Costs in Primary and Revision Total Knee Arthroplasty. *Cinical Orthop Relat Res*. 2013;(471):206-214. doi:10.1007/s11999-012-2508-z

29. Navarro M, Michiardi A, Castan O, Planell JA. Biomaterials in orthopaedics. 2008;(July):1137-1158. doi:10.1098/rsif.2008.0151

30. Chen Q, Thouas GA. Metallic implant biomaterials. *Mater Sci Eng R*. 2015;87:1-57. doi:10.1016/j.mser.2014.10.001

31. Gepreel MA, Niinomi M. Biocompatibility of Ti-alloys for long-term implantation. *J Mech Behav Biomed Mater*. 2013;20:407-415. doi:10.1016/j.jmbbm.2012.11.014

32. Hallab NJ, Jacobs JJ. Biologic effects of implant debris. *Bull NYU Hosp Jt Dis*. 2009;67(2):182-188. http://www.ncbi.nlm.nih.gov/pubmed/19583551.

33. Shayesteh N, Mohsen M, Andani T, et al. Metals for bone implants: safety, design, and efficacy. *Biomanufacturing Rev*. 2016;1(1):1-16. doi:10.1007/s40898-016-0001-2

34. Temenoff JS, Milkos AG. *Biomaterials: The Intersection of Biology and Material Science*. 1st ed. (Horton MJ, Stark H, Lonschein J, et al., eds.). Upper Saddle River: Pearson Prentice Hall; 2008.

35. Ranter BD, Hoffman AS, Schoen FJ, Lemons JE. *Biomaterial Science: An Introduction to Materials in Medicine*. 2nd ed. (Ranter BD, Hoffman AS, Schoen FJ, Lemons JE, eds.). San Diego: Elsevier Academic Press; 2004.

36. Greenfield EM, Bi Y, Ragab AA, Goldberg VM, Van De Motter R. The role of osteoclast differentiation in aseptic loosening. *J Orthop Res*. 2002;20:1-8.

37. Wooley PH, Schwarz EM. Aseptic loosening. *Gene Theropy*. 2004;11(February 2015):402-407. doi:10.1038/sj.gt.3302202

38. Keegan GM, Learmonth ID, Case CP. Orthopaedic metals and their potential toxicity in the arthroplasty patient: A REVIEW OF CURRENT KNOWLEDGE AND FUTURE STRATEGIES. *J Bone Jt Surg*. 2007;89(5):567-573. doi:10.1302/0301-620X.89B5.18903

39. Sansone V. The effects on bone cells of metal ions released from orthopaedic implants. A review. 2013;10(1):34-40.

40. Maurus PB, Kaeding CC. Bioabsorbable Implant Material Review. *Oper Tech Sports Med*. 2004:158-160. doi:10.1053/j.otsm.2004.07.015

41. Directions F. An Overview of Mechanical Properties and Material Modeling of Polylactide (PLA) for Medical Applications. 2016;44(2):330-340. doi:10.1007/s10439-015-1455-8

42. Piemonte V, Gironi F. Kinetics of Hydrolytic Degradation of PLA. *J Environ Polym Degrad · January 2013*. 2014;21(July):313-318. doi:10.1007/s10924-012-0547-x

43. Suming Li. Hydrolytic degradation characteristics of aliphatic polyesters derived from lactic and glycolic acids Article. 1998;(april). doi:10.1002/(SICI)1097-4636(1999)48

44. Ontakis GMK, Agkalos JEP, Osounidis TIT, Elissas JM, Atonis PK. Bioabsorbable materials in orthopaedics. 2007;73:159-169.

45. Eglin D, Alini M. DEGRADABLE POLYMERIC MATERIALS FOR OSTEOSYNTHESIS : TUTORIAL. 2008;16:80-91. doi:10.22203/eCM.v016a09

46. Vaid R, Yildirim E, Pasquinelli MA, King MW. Hydrolytic Degradation of Polylactic Acid Fibers as a Function of pH and Exposure Time. *Molecules*. 2021;26(7554).

47. Vieira AC, Vieira JC, Ferra JM, Magalhães FD, Guedes RM, Marques AT. Mechanical Study of PLA-PCL Fibers during In Vitro Degradation.

48. Vert M, Mauduit J, Li S. Biodegradation of PLA / GA polymers : increasing complexity. 1994;15(15):1209-1213.

49. Athanasiou KA, Niederauer GG, Agrawal CM. Sterilization, toxicity, biocompatibility and clinical applications of polylactic acid / polyglycolic acid copolymers. *Biomaterials*. 1996;17(2).

50. Agrawal CM, Athanasiou KA. Technique to Control pH in Vicinity of Biodegrading PLA-PGA Implants. *John Wiley Sons*. 1996:105-114.

51. Chevallier R, Klouche S, Gerometta A, Bohu Y, Herman S, Lefevre N. Bioabsorbable screws, whatever the composition, can result in symptomatic intra-osseous tibial tunnel cysts after ACL reconstruction. *Knee Surgery, Sport Traumatol Arthrosc*. 2019;27(1):76-85. doi:10.1007/s00167-018-5037-9

52. Debieux P, Ces F, Lenza M, et al. Bioabsorbable versus metallic interference screws for graft fixation in anterior cruciate ligament reconstruction (Review). *Cochrane Database of Systematic Rev*. 2016;(7). doi:10.1002/14651858.CD009772.pub2.www.cochranelibrary.com

53. Sadat-Ali M, Azzam Q, Bluwi M, Al-Umran AS. Case Report Fibroxanthoma A Complication of a Biodegradable Screw. *Assoc Bone Surg*. 2009:2284-2287. doi:10.1007/s11999-009-1170-6

54. Drogset JO, Grøntvedt T, Myhr G. Magnetic Resonance Imaging Analysis of Bioabsorbable Interference Screws Used for Fixation of Bone – Patellar Tendon – Bone Autografts in Endoscopic Reconstruction of the Anterior Cruciate Ligament. *Am J Sports Med*. 2006;34(7):1164-1169. doi:10.1177/0363546505285384

55. de Padua V, Vilela J, Espindola WA, Godoy R. BONE TUNNEL ENLARGEMENT WITH NON-METALLIC INTERFERENCE SCREWS IN ACL RECONSTRUCTION ALARGAMENTO DOS TÚNEIS ÓSSEOS NA RECONSTRUÇÃO DO. *Acta Ortop Bras*. 2018;26(5):305-308.

56. Marinescu R, Antoniac I, Laptoiu DAN, Antoniac A, Grecu DAN. Complications Related to Biocomposite Screw Fixation in ACL Reconstruction Based on Clinical Experience and Retrieval Analysis. *Mater Plast*. 2015;(September).

57. Cox CL, Spindler KP, Leonard JP, Morris BJ, Dunn WR, Reinke EK. Do Newer-Generation Bioabsorbable Screws Become Incorporated into Bone at Two Years After ACL Reconstruction with Patellar Tendon Graft ? A Cohort Study. *J Bone Jt Surgery, iIcorporated*. 2014:244-250.

58. Watson JN, Mcqueen P, Kim W, Hutchinson MR. Bioabsorbable interference screw failure in anterior cruciate ligament reconstruction : A case series and review of the literature. *Knee*. 2015;22(3):256-261. doi:10.1016/j.knee.2015.02.015

59. Sprowson AP, Aldridge SE, Noakes J, Read JW, Wood DG. Bio-interference screw cyst formation in anterior cruciate ligament reconstruction — 10-year follow up. *Knee*. 2012;19(5):644-647. doi:10.1016/j.knee.2012.01.004

60. Hospital C, Bucharest E. EVOLUTION TOWARD NEW BIOABSORBABLE MATERIAL. 2016;51(2):190-198.

61. Nouri A, Rohani A, Li Y, Wen C. Biodegradable metallic suture anchors : A review. *Smart Mater Manuf*. 2022;(May):100005. doi:10.1016/j.smmf.2022.100005

62. Easley J, Puttlitz C, Hackett E, et al. A prospective study comparing tendon-to-bone interface healing using an interposition bioresorbable scaffold with a vented anchor for primary rotator cuff repair in sheep. *J Shoulder Elb Surg*. 2020;29:157-166.

63. Randelli P, Spennacchio P, Ragone V, Arrigoni P, Casella A, Cabitza P. Complications associated with arthroscopic rotator cuff repair : a literature review. *Musculoskeletal Surg*. 2012;(96):9-16. doi:10.1007/s12306-011-0175-y

64. Lacheta L, Dekker TJ, Anderson N, Goldenberg B, Millett PJ. Arthroscopic Knotless, Tensionable All-Suture Anchor Bankart Repair. *Arthrosc Tech*. 2019;8(6):e647-e653. doi:10.1016/j.eats.2019.02.010

65. Kholinne E, Hwang J, Kwak J-M, Sun Y, Koh K-H, Jeon I-H. Serial magnetic resonance imaging evaluation of the early reaction of all-suture anchors in arthroscopic rotator cuff repair. *ACTA Orthop Trumatologica Turc*. 2022;56(2):111-115. doi:10.5152/j.aott.2022.20167

66. Pandey RK, Panda SS. Drilling of bone : A comprehensive review. *J Clin Orthop Trauma*. 2013;4(1):15-30. doi:10.1016/j.jcot.2013.01.002

67. Timon C, Keady C. Thermal Osteonecrosis Caused by Bone Drilling in Orthopedic Surgery : A Literature Review. *Cureus*. 2019;11(7):1-7. doi:10.7759/cureus.5226

68. Weller J, Birkner B, Schneider KN, Durchholz H. Anchor Site Fracture Following Arthroscopic Rotator Cuff Repair – A Case Report and Review of the Literature. *J Orthop Case Reports*. 2021;11(5):104-108. doi:10.13107/jocr.2021.v11.i05.2228

69. Hossen MR, Dadoo N, Holomakoff DG, Co A, Gramlich WM, Mason MD. Wet stable and mechanically robust cellulose nano fibrils (CNF) based hydrogel. *Polymer (Guildf)*. 2018;151:231-241. doi:10.1016/j.polymer.2018.07.016

70. Jorfi M, Foster EJ. Recent advances in nanocellulose for biomedical applications. 2015;41719:1-19. doi:10.1002/app.41719

71. Lin N, Dufresne A. Nanocellulose in biomedicine : Current status and future prospect. *Eur Polym J*. 2014;59:302-325. doi:10.1016/j.eurpolymj.2014.07.025

72. Eatemadi A, Daraee H, Zarghami N, Yar HM, Akbarzadeh A. Nanofiber: Synthesis and biomedical applications. *Artif Cells, Nanomedicine Biotechnol*. 2016;44(1):111-121. doi:10.3109/21691401.2014.922568

73. Nechyporchuk O, Belgacem MN, Bras J. Production of cellulose nanofibrils: A review of recent advances. *Ind Crops Prod*. 2016;93:2-25. doi:10.1016/j.indcrop.2016.02.016

74. Villegas DF, Donahue TLH, Villegas DF, Donahue TLH. Collagen morphology in human meniscal attachments : A SEM study Collagen morphology in human meniscal attachments : A SEM study. *Connect Tissue Res*. 2010;51:327-336. doi:10.3109/03008200903349639

75. Parenteau-bareil R, Gauvin R, Berthod F. Collagen-Based Biomaterials for Tissue Engineering Applications. 2010:1863-1887. doi:10.3390/ma3031863

76. Siqueira P, Siqueira É Der, Lima AE De, et al. Three-Dimensional Stable Alginate-Nanocellulose Gels for Biomedical Applications : Towards Tunable Mechanical Properties and Cell Growing. 2019:1-22. doi:10.3390/nano9010078

77. Yong K, Mooney DJ. Progress in Polymer Science Alginate : Properties and biomedical applications. *Prog Polym Sci*. 2012;37(1):106-126. doi:10.1016/j.progpolymsci.2011.06.003

78. Martins M, Barros AA, Quraishi S, et al. The Journal of Supercritical Fluids Preparation of macroporous alginate-based aerogels for biomedical applications. *J Supercrit Fluids*. 2015;106:152-159. doi:10.1016/j.supflu.2015.05.010

79. Jayakumar R, Menon D, Manzoor K, Nair S V, Tamura H. Biomedical applications of chitin and chitosan based nanomaterials — A short review. *Carbohydr Polym*. 2010;82(2):227-232. doi:10.1016/j.carbpol.2010.04.074

80. Anitha A, Sowmya S, Kumar PTS, et al. Progress in Polymer Science Chitin and chitosan in selected biomedical applications. *Prog Polym Sci*. 2014;39(9):1644-1667. doi:10.1016/j.progpolymsci.2014.02.008

81. Jayakumar R, Prabaharan M, Nair S V, Tamura H. Novel chitin and chitosan nano fibers in biomedical applications. *Biotechnol Adv*. 2010;28(1):142-150. doi:10.1016/j.biotechadv.2009.11.001

82. Dufresne A. 1. Cellulose and potential reinforcement. In: *Nanocellulose: From Nature to High Performance Tailored Materials*. 2nd ed. De Gruyter; 2017:1-46. doi:10.1515/9783110480412-002

83. Sharma A, Thakur M, Bhattacharya M, Mandal T. Commercial application of cellulose nano-composites – A review. *Biotechnol Reports*. 2019;(2018):e00316. doi:10.1016/j.btre.2019.e00316

84. Chesley MP. Characterization of Nano-Cellulose Based Composites For Biomedical Applications. *Electron Theses Diss*. 2019;3083(August).

85. MATERIALS ASFTA. ASTM D638-14-Standard Test Method for Tensile Properties of Plastics. *Annu B ASTM Stand*. 2019:1-17. doi:10.1520/D0638-14.1

86. MATERIALS ASFTA. ASTM D695-15-Standard Test Method for Compressive Properties of Rigid Plastics. *Annu B ASTM Stand*. 2019:1-8. doi:10.1520/D0695-15.2

87. AMERICAN SOCIETY FOR TESTING AND MATERIALS. ASTM D790 − 17 - Flexural Properties of Unreinforced and Reinforced Plastics and Electrical Insulating Materials. *Annu B ASTM Stand*. 2017:12. doi:10.1520/D0790-17.2

88. ASTM International. ASTM D256-06: Standard Test Methods for Determining The Izod Pendulum Impact Resistance of Plastics. *Annu B ASTM Stand*. 2010;08(01):20.

89. International Organization of Standards. International Organization of Standards [ISO] 10993-5:2009: Evaluation of Medical Devices - Part 5: Test for In Vitro Cytotoxicity.

90. International Organization of Standards. International Organization of Standards [ISO] 10993-12:2021: Evaluation of Medical Devices - Part 12: Sample Preparation and Reference Materials.

91. International Organization of Standards. International Organization of Standards [ISO] 10993-13:2010: Evaluation of Medical Devices - Part 13: Identification and Quantification of Degradation Products from Polymeric Medical Devices.

92. International Organization of Standards. International Organization of Standards [ISO] 10993-14:2001: Evaluation of Medical Devices - Part 14: Identification and Quantification of Degradation Products from Ceramics.

93. International Organization of Standards. International Organization of Standards [ISO] 10993-15:2019: Evaluation of Medical Devices - Part 15: Identification and Quantification of Degradation Products from Metals and Alloys.

94. International Organization of Standards. International Organization of Standards [ISO] 10993-16:2017: Evaluation of Medical Devices - Part 16: Toxicokinetic Study Design for Degradation Products and Leachables.

95. International Organization of Standards. International Organization of Standards [ISO] 10993-19:2020: Evaluation of Medical Devices - Part 19: Physico-chemical, Morphological and Topographical Characterization of Materials.

96. Zhang ZL, Ødegård J, Søvik OP. Determining true stress - strain curve for isotropic and anisotropic materials with rectangular tensile bars : method and verifications. *Comput Mater Sci*. 2001;20:77-85.

97. Tan SC, Cheng S. Failure Criteria For Fibrous Anisotropic Materials. *J Mater Civ Eng*. 1993;5(2):198-211.

98. Duda JC, Smoyer JL, Norris PM, Hopkins PE. Extension of the diffuse mismatch for thermal boundary conductance between isotropic and anisotropic materials. *Appl Phys Lett*. 2009;95(3):1-3. doi:10.1063/1.3189087

99. Alonso MI, Garriga M. Optical properties of anisotropic materials : an experimental approach. *Thin Solid Films*. 2004;456(4):124-131. doi:10.1016/j.tsf.2003.12.061

100. Li K, Clarkson CM, Wang L, et al. Alignment of Cellulose Nanofibers: Harnessing Nanoscale Properties to Macroscale Benefits. *ACS Nano*. 2021;(15):3646-3673.

101. Holomakoff DG. NANOCELLULOSE FIBERS AS A POTENTIAL MATERIAL FOR ORTHOPEDIC IMPLANTATION APPLICATION. *Electron Theses Diss*. 2017;2773(August).

102. Endes C, Espinosa SC, Mueller S, et al. A critical review of the current knowledge regarding the biological impact of nanocellulose. 2016:1-14. doi:10.1186/s12951-016-0230-9

103. Dufresne A. *Nanocellulose: From Nature to High Performance Tailored Materials*.; 2017. doi:10.1515/9783110480412-002

104. Peng Y, Gardner DJ, Han Y, Kriziltas A, Cai Z, Tshabalala MA. Influence of drying method on the material properties of nanocellulose I : thermostability and crystallinity. *Cellulose*. 2013;20(August):2379-2392.

105. Sharmila N, Ariffin H. Cellulose nanofibrils for biomaterial applications. *Mater Today Proc*. 2019;16:1959-1968. doi:10.1016/j.matpr.2019.06.074

106. Langdon SP. *Cancer Cell Culture*.; 2014.

107. Izumiya M, Haniu M, Ueda K, et al. Evaluation of MC3T3-E1 Cell Osteogenesis in Different Cell Culture Media. 2021:1-12.

108. Wang M. Developing bioactive composite materials for tissue replacement. *Biomaterials*. 2003;24(1):2133-2151. doi:10.1016/S0142-9612(03)00037-1

109. Wetzel B, Haupert F, Friedrich K, Zhang MQ, Rong MZ. Impact and Wear Resistance of Polymer Nanocomposites. *Polym Eng Sci*. 2002;42(9):1919-1927.

110. Paul EL, Atiemo-obeng VA, Kresta SM. *HANDBOOK OF INDUSTRIAL MIXING SCIENCE AND PRACTICE*.; 2004.

111. Dlamini DS, Li J, Mamba BB. Critical review of montmorillonite / polymer mixed-matrix filtration membranes : Possibilities and challenges. *Appl Clay Sci*. 2019;168(2):21-30. doi:10.1016/j.clay.2018.10.016

112. Halliwell SM. *Polymer Composites in Construction*.; 2000.

113. Kierys A, Zaleski R, Buda W, Pikus S. Nanostructured polymer – titanium composites and titanium oxide through polymer swelling in titania precursor. *Colloid Polym Sci*. 2013;291(6):1463-1470. doi:10.1007/s00396-012-2881-x

114. Harsányi G. Tutorial Polymer films in sensor applications : a review of present uses and future possibilities. *Sens Rev*. 2000;20(2):98-105.

115. Šupová M. Problem of hydroxyapatite dispersion in polymer matrices : A review Problem of hydroxyapatite dispersion in polymer matrices : a review. *J Mater Sci Mater Med*. 2016;(March 2009). doi:10.1007/s10856-009-3696-2

116. Li J, Gao Y, Zhao J, Sun J, Li D. Homogeneous dispersion of chitin nanofibers in polylactic acid with different pretreatment methods. *Cellulose*. 2017;24(4):1705-1715. doi:10.1007/s10570-017-1216-y

117. Basch A, Beck F, Söderström T, Varlamov S, Catchpole KR. Enhanced light trapping in solar cells using snow globe coating. *Prog Photovoltaics*. 2012;20(November):837-842. doi:10.1002/pip.2240

118. Anikushin BM, Lagutin PG, Kanbetova AM, Novikov AA, Vindkirov VA. ZETA POTENTIAL OF NANOSIZED PARTICLES OF CELLULOSE AS A FUNCTION OF pH. *Chem Technol Fuels Oils*. 2022;57(6):41-43. doi:10.1007/s10553-022-01328-0

119. Demitri C, Sole R Del, Scalera F, et al. Novel Superabsorbent Cellulose-Based Hydrogels Crosslinked with Citric Acid. *J Appl Polym Sci*. 2008. doi:10.1002/app

120. Reddy N, Reddy R, Jiang Q. Crosslinking biopolymers for biomedical applications. *Trends Biotechnol*. 2015;33(6):362-369. doi:10.1016/j.tibtech.2015.03.008

121. Headley J, Udoetok IA, Dimmick RM, Wilson LD, Headley J V. Adsorption Properties of Cross-linked Cellulose-Epichlorohydrin Polymers in Aqueous Solution Adsorption properties of cross-linked cellulose-epichlorohydrin polymers in aqueous solution. *Carbohydr Polym*. 2015;136(September):329-340. doi:10.1016/j.carbpol.2015.09.032

122. Spoljaric S, Salminen A. Crosslinked nanofibrillated cellulose : poly (acrylic acid) nanocomposite films ; enhanced mechanical performance in aqueous environments. *Cellulose*. 2013:2991-3005. doi:10.1007/s10570-013-0061-x

123. Das D, Ghosh P, Dhara S, Panda AB, Pal S. Dextrin and Poly (acrylic acid) -Based Biodegradable , Non-Cytotoxic , Chemically Cross-Linked Hydrogel for Sustained Release of Ornidazole and Ciprofloxacin. *Appl Mater Interfaces*. 2015. doi:10.1021/am508712e

124. Chau TT, Bruckard WJ, Koh PTL, Nguyen A V. A review of factors that affect contact angle and implications for flotation practice. *Adv Colloid Interface Sci*. 2009;150(2):106-115. doi:10.1016/j.cis.2009.07.003

125. Krainer S, Hirn U. Contact angle measurement on porous substrates : Effect of liquid absorption and drop size. *Colloids Surfaces A Physicochem Eng Asp*. 2021;619(March):126503. doi:10.1016/j.colsurfa.2021.126503

126. Administration F. Overview of Medical Device Classification and Reclassification.

127. Jones III ADJ, Mi G, Webster TJ. Science & Society A Status Report on FDA Approval of Medical Devices Containing Nanostructured Materials. *Trends Biotechnol*. 2019;37(2):117-120. doi:10.1016/j.tibtech.2018.06.003

128. Sweet B V., Schwemm AK, Parson DM. Review of the Processes for FDA Oversight of Drugs, Medical Devices, and Combination Products. 2011;17(1).

129. Zuckerman DM, Brown P, Nissen SE. Medical Device Recalls and the FDA Approval Process. *Arch Intern Med*. 2011;171(11). doi:10.1001/archinternmed.2011.30

130. Barber AF, Herbert MA. All-Suture Anchors: Biomechanical Analysis of Pullout Strength, Displacement, and failure mode. *Arthroscopy*. 2016;33(6):1113-1121.

APPENDICES

APPENDIXA: STATISTICAL NORMALICY AND STATISTICAL TABLES OF BULK CNF

To view the statistical variance of all sample sets normal density of samples were displaced and viewed for bell curve nature. Shapiro-Wilk, ANOVA, and Tukey statistics were done on sample sets as a whole and individual samples to view contributing factors to variance.

Directional Films:

Normality Test (8/3/2022 17:07:04)
NormalityTest
Shapiro-Wilk

			DF	Statistic	p-value	Decision at level(5%)
Modulus	1D	50	5.000	0.851	0.196	Can't reject normality
		60	6.000	0.857	0.179	Can't reject normality
		70	6.000	0.959	0.810	Can't reject normality
		80	7.000	0.970	0.897	Can't reject normality
		90	5.000	0.813	0.103	Can't reject normality
		100	6.000	0.911	0.445	Can't reject normality
	2D	50	5.000	0.875	0.286	Can't reject normality
		60	6.000	0.943	0.682	Can't reject normality
		70	6.000	0.883	0.282	Can't reject normality
		80	7.000	0.794	0.036	Reject normality
		90	5.000	0.848	0.190	Can't reject normality
		100	6.000	0.816	0.082	Can't reject normality

Please refer to the "Decision at level" column for conclusion

Figure A.1: Shapiro-Wilk Table of Film Directionality Grouped by Direction.

Normality Test (8/3/2022 17:07:32)
NormalityTest
Shapiro-Wilk

			DF	Statistic	p-value	Decision at level(5%)
Modulus	50	1D	5.000	0.851	0.196	Can't reject normality
		2D	5.000	0.875	0.286	Can't reject normality
	60	1D	6.000	0.857	0.179	Can't reject normality
		2D	6.000	0.943	0.682	Can't reject normality
	70	1D	6.000	0.959	0.810	Can't reject normality
		2D	6.000	0.883	0.282	Can't reject normality
	80	1D	7.000	0.970	0.897	Can't reject normality
		2D	7.000	0.794	0.036	Reject normality
	90	1D	5.000	0.813	0.103	Can't reject normality
		2D	5.000	0.848	0.190	Can't reject normality
	100	1D	6.000	0.911	0.445	Can't reject normality
		2D	6.000	0.816	0.082	Can't reject normality

Please refer to the "Decision at level" column for conclusion

Figure A.2: Shapiro-Wilk Table of Film Directionality Modulus Grouped by Temperature.

Normality Test (8/3/2022 17:07:52)

NormalityTest

Shapiro-Wilk

			DF	Statistic	p-value	Decision at level(5%)
Tensile Strength	1D	50	5.000	0.964	0.836	Can't reject normality
		60	6.000	0.963	0.840	Can't reject normality
		70	6.000	0.795	0.052	Can't reject normality
		80	7.000	0.887	0.262	Can't reject normality
		90	5.000	0.913	0.489	Can't reject normality
		100	6.000	0.979	0.947	Can't reject normality
	2D	50	5.000	0.903	0.428	Can't reject normality
		60	6.000	0.959	0.813	Can't reject normality
		70	6.000	0.905	0.405	Can't reject normality
		80	7.000	0.971	0.908	Can't reject normality
		90	5.000	0.955	0.769	Can't reject normality
		100	6.000	0.939	0.654	Can't reject normality

Please refer to the "Decision at level" column for conclusion

Figure A.3: Shapiro-Wilk Table of Film Directionality Tensile Strength Grouped by Direction.

Normality Test (8/3/2022 17:08:11)

NormalityTest

Shapiro-Wilk

			DF	Statistic	p-value	Decision at level(5%)
Tensile Strength	50	1D	5.000	0.964	0.836	Can't reject normality
		2D	5.000	0.903	0.428	Can't reject normality
	60	1D	6.000	0.963	0.840	Can't reject normality
		2D	6.000	0.959	0.813	Can't reject normality
	70	1D	6.000	0.795	0.052	Can't reject normality
		2D	6.000	0.905	0.405	Can't reject normality
	80	1D	7.000	0.887	0.262	Can't reject normality
		2D	7.000	0.971	0.908	Can't reject normality
	90	1D	5.000	0.913	0.489	Can't reject normality
		2D	5.000	0.955	0.769	Can't reject normality
	100	1D	6.000	0.979	0.947	Can't reject normality
		2D	6.000	0.939	0.654	Can't reject normality

Please refer to the "Decision at level" column for conclusion

Figure A.4: Shapiro-Wilk Table of Film Directionality Tensile Strength Grouped by Temperature.

Compression:

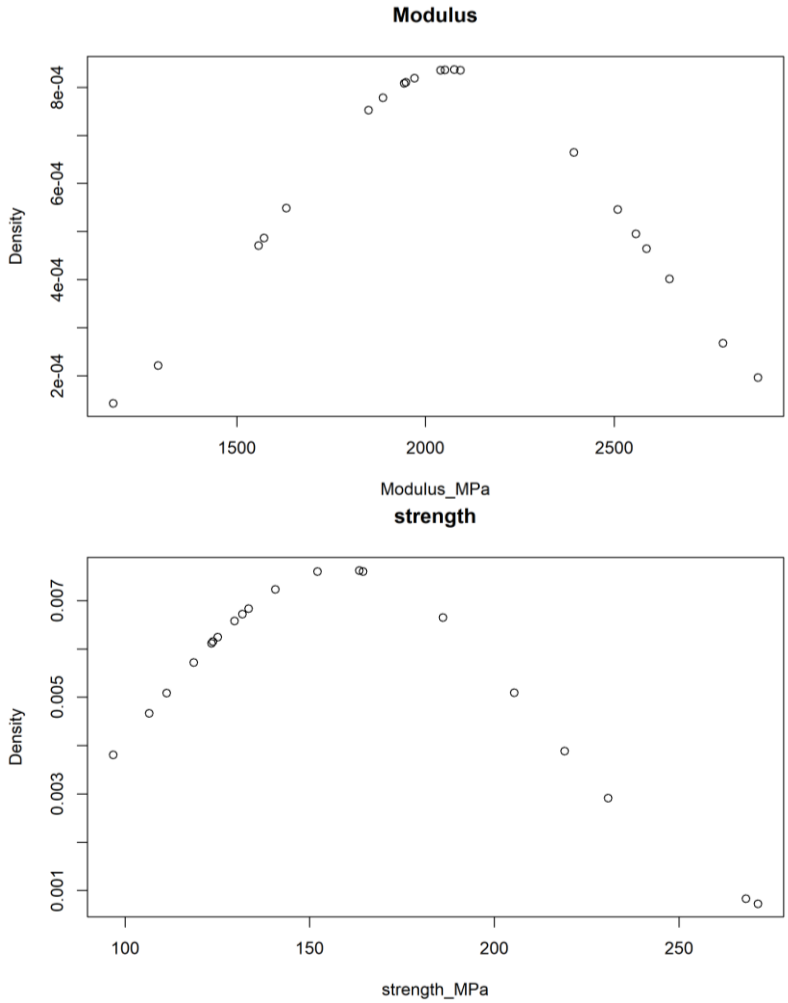

Figure A.5: Normality of All Direction Compression Testing.

Normality Test (7/6/2022 15:30:16)

NormalityTest

Shapiro-Wilk

		DF	Statistic	p-value	Decision at level(5%)
Modulus	1	7.000	0.817	0.061	Can't reject normality
	2	7.000	0.837	0.093	Can't reject normality
	3	7.000	0.956	0.783	Can't reject normality

Modulus(1): At the 0.05 level, the data was significantly drawn from a normally distributed population.
Modulus(2): At the 0.05 level, the data was significantly drawn from a normally distributed population.
Modulus(3): At the 0.05 level, the data was significantly drawn from a normally distributed population.

Histograms

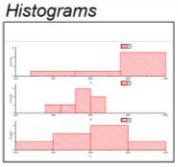

Figure A.6: Shapiro-Wilk Test of Compressive Modulus.

Normality Test (7/6/2022 15:31:12)

NormalityTest

Shapiro-Wilk

		DF	Statistic	p-value	Decision at level(5%)
Compressive Strength	1	7.000	0.972	0.911	Can't reject normality
	2	7.000	0.930	0.548	Can't reject normality
	3	7.000	0.950	0.727	Can't reject normality

Compressive Strength(1): At the 0.05 level, the data was significantly drawn from a normally distributed population.
Compressive Strength(2): At the 0.05 level, the data was significantly drawn from a normally distributed population.
Compressive Strength(3): At the 0.05 level, the data was significantly drawn from a normally distributed population.

Histograms

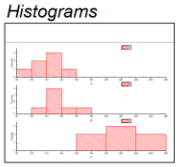

Figure A.7: Shapiro-Wilk Test of Compressive Strength.

Table A1: P Values of Compressional Modulus and Strength, Alpha=0.05 *=Significance

Category	Modulus (P value)	Strength (P value)
All Directions	0.114	$2.25e^{-6}$*
1Vs2	0.06	0.16
1Vs3	0.158	$4.32e^{-5}$*
2Vs3	0.76	0.0002*

Tensile Bulk:

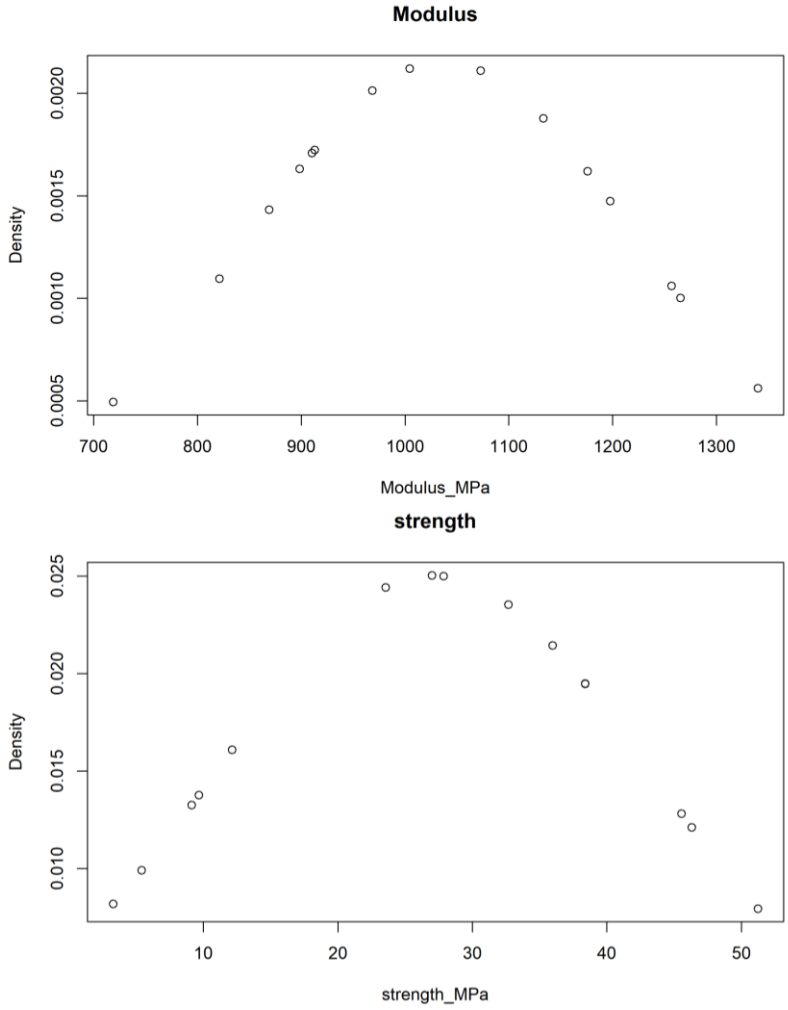

Figure A.8: Normality of All Tensile Testing.

lormality Test (7/6/2022 15:49:13)
NormalityTest
Shapiro-Wilk

		DF	Statistic	p-value	Decision at level(5%)
Modulus	1 Dir	5.000	0.902	0.420	Can't reject normality
	2 Dir	5.000	0.938	0.650	Can't reject normality
	3 Dir	5.000	0.946	0.712	Can't reject normality

Modulus(1 Dir): At the 0.05 level, the data was significantly drawn from a normally distributed population.
Modulus(2 Dir): At the 0.05 level, the data was significantly drawn from a normally distributed population.
Modulus(3 Dir): At the 0.05 level, the data was significantly drawn from a normally distributed population.

Histograms

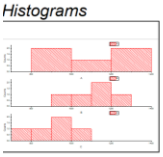

Figure A.9: Shapiro-Wilk for Bulk Tensile Modulus.

Normality Test (7/6/2022 15:50:15)

NormalityTest

Shapiro-Wilk

		DF	Statistic	p-value	Decision at level(5%)
Tensile Strength	1 Dir	5.000	0.888	0.347	Can't reject normality
	2 Dir	5.000	0.963	0.827	Can't reject normality
	3 Dir	5.000	0.953	0.758	Can't reject normality

Tensile Strength(1 Dir): At the 0.05 level, the data was significantly drawn from a normally distributed population.
Tensile Strength(2 Dir): At the 0.05 level, the data was significantly drawn from a normally distributed population.
Tensile Strength(3 Dir): At the 0.05 level, the data was significantly drawn from a normally distributed population.

Histograms

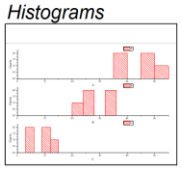

Figure A.10: Shapiro-Wilk Tensile Strength of Bulk Tensile.

Table A2: P Value of Tensile Modulus and Strength, Alpha=0.05 *=Significance

Category	Modulus (P value)	Strength (P value)
All Directions	0.11	$1.89e^{-7}$*
1Vs2	0.90	0.002*
1Vs3	0.12	$1.83e^{-6}$*
2Vs3	0.03*	$4.6e^{-5}$*

Flexure:

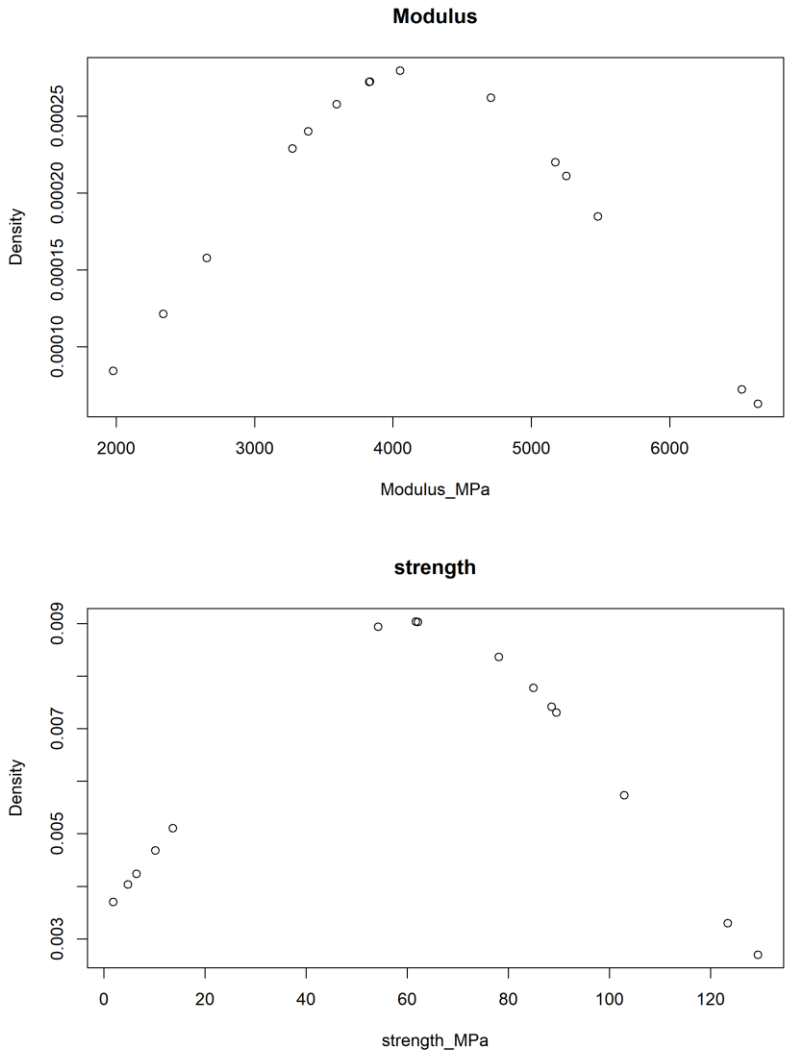

Figure A.11: Normality of All Flexure Testing.

Normality Test (7/26/2022 16:50:57)

NormalityTest

Shapiro-Wilk

		DF	Statistic	p-value	Decision at level(5%)
Modulus	1	5.000	0.892	0.365	Can't reject normality
	2	5.000	0.862	0.236	Can't reject normality
	3	5.000	0.975	0.906	Can't reject normality

Modulus(1): At the 0.05 level, the data was significantly drawn from a normally distributed population.
Modulus(2): At the 0.05 level, the data was significantly drawn from a normally distributed population.
Modulus(3): At the 0.05 level, the data was significantly drawn from a normally distributed population.

Histograms

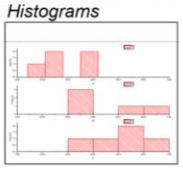

Figure A.12: Shapiro-Wilk for Modulus of Flexure Test.

Normality Test (7/6/2022 16:06:20)

NormalityTest

Shapiro-Wilk

		DF	Statistic	p-value	Decision at level(5%)
Flexural Strength	1	5.000	0.980	0.937	Can't reject normality
	2	5.000	0.853	0.203	Can't reject normality
	3	5.000	0.940	0.665	Can't reject normality

Flexural Strength(1): At the 0.05 level, the data was significantly drawn from a normally distributed population.
Flexural Strength(2): At the 0.05 level, the data was significantly drawn from a normally distributed population.
Flexural Strength(3): At the 0.05 level, the data was significantly drawn from a normally distributed population.

Histograms

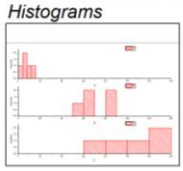

Figure A.13: Shapiro-Wilk for Flexural Strength of Flexure Test.

Table A3: P Value of Flexure Modulus and Flexure Strength, Alpha=0.05 *=Significance

Category	Modulus (P value)	Strength (P value)
All Directions	0.04*	$1.54e^{-6}$*
1Vs2	0.07	$2.26e^{-5}$*
1Vs3	0.02*	$1.01e^{-5}$*
2Vs3	0.50	0.02*

APPENDIX B: MIXING EXPERIMENT STATISTICAL ANALYSIS

Mixing Statistics

Normality Test (7/31/2022 15:50:54)
NormalityTest
Shapiro-Wilk

			DF	Statistic	p-value	Decision at level(5%)
Modulus	1 CNF	Hand	9.000	0.961	0.805	Can't reject normality
		Mixer	10.000	0.859	0.073	Can't reject normality
		Dilute	10.000	0.947	0.632	Can't reject normality
	2.5 CNF	Hand	10.000	0.958	0.768	Can't reject normality
		Mixer	10.000	0.910	0.282	Can't reject normality
		Dilute	10.000	0.960	0.783	Can't reject normality
	5 CNF	Hand	10.000	0.903	0.237	Can't reject normality
		Mixer	10.000	0.926	0.414	Can't reject normality
		Dilute	10.000	0.976	0.937	Can't reject normality
	1 10	Hand	10.000	0.980	0.964	Can't reject normality
		Mixer	10.000	0.947	0.630	Can't reject normality
		Dilute	10.000	0.885	0.149	Can't reject normality
	2.5 10	Hand	10.000	0.910	0.281	Can't reject normality
		Mixer	10.000	0.946	0.625	Can't reject normality
		Dilute	6.000	0.997	0.999	Can't reject normality
	5 10	Hand	10.000	0.911	0.290	Can't reject normality
		Mixer	10.000	0.916	0.328	Can't reject normality
		Dilute	10.000	0.881	0.134	Can't reject normality
	1 25	Hand	10.000	0.949	0.658	Can't reject normality
		Mixer	10.000	0.930	0.444	Can't reject normality
		Dilute	10.000	0.945	0.606	Can't reject normality
	2.5 25	Hand	10.000	0.886	0.151	Can't reject normality
		Mixer	10.000	0.945	0.609	Can't reject normality
		Dilute	10.000	0.906	0.254	Can't reject normality
	5 25	Hand	10.000	0.804	0.016	Reject normality
		Mixer	10.000	0.846	0.052	Can't reject normality
		Dilute	10.000	0.962	0.814	Can't reject normality

Please refer to the "Decision at level" column for conclusion

Figure A.14: Shapiro-Wilk Table of Modulus from Mixing Samples, Grouped by Type Then Mixing Style.

Normality Test (7/31/2022 15:50:15)
NormalityTest
Shapiro-Wilk

			DF	Statistic	p-value	Decision at level(5%)
Modulus	Hand	1 CNF	9.000	0.961	0.805	Can't reject normality
		2.5 CNF	10.000	0.958	0.768	Can't reject normality
		5 CNF	10.000	0.903	0.237	Can't reject normality
		1 10	10.000	0.980	0.964	Can't reject normality
		2.5 10	10.000	0.910	0.281	Can't reject normality
		5 10	10.000	0.911	0.290	Can't reject normality
		1 25	10.000	0.949	0.658	Can't reject normality
		2.5 25	10.000	0.886	0.151	Can't reject normality
		5 25	10.000	0.804	0.016	Reject normality
	Mixer	1 CNF	10.000	0.859	0.073	Can't reject normality
		2.5 CNF	10.000	0.910	0.282	Can't reject normality
		5 CNF	10.000	0.926	0.414	Can't reject normality
		1 10	10.000	0.947	0.630	Can't reject normality
		2.5 10	10.000	0.946	0.625	Can't reject normality
		5 10	10.000	0.916	0.328	Can't reject normality
		1 25	10.000	0.930	0.444	Can't reject normality
		2.5 25	10.000	0.945	0.609	Can't reject normality
		5 25	10.000	0.846	0.052	Can't reject normality
	Dilute	1 CNF	10.000	0.947	0.632	Can't reject normality
		2.5 CNF	10.000	0.960	0.783	Can't reject normality
		5 CNF	10.000	0.976	0.937	Can't reject normality
		1 10	10.000	0.885	0.149	Can't reject normality
		2.5 10	6.000	0.997	0.999	Can't reject normality
		5 10	10.000	0.881	0.134	Can't reject normality
		1 25	10.000	0.945	0.606	Can't reject normality
		2.5 25	10.000	0.906	0.254	Can't reject normality
		5 25	10.000	0.962	0.814	Can't reject normality

Please refer to the "Decision at level" column for conclusion

Figure A.15: Shapiro-Wilk Table of Modulus from Mixing Samples, Grouped by Mixing Style Then Type.

Normality Test (7/31/2022 15:52:08)
NormalityTest
Shapiro-Wilk

			DF	Statistic	p-value	Decision at level(5%)
Strength	1 CNF	Hand	9.000	0.969	0.882	Can't reject normality
		Mixer	10.000	0.952	0.693	Can't reject normality
		Dilute	10.000	0.928	0.430	Can't reject normality
	2.5 CNF	Hand	10.000	0.924	0.388	Can't reject normality
		Mixer	10.000	0.960	0.780	Can't reject normality
		Dilute	10.000	0.914	0.310	Can't reject normality
	5 CNF	Hand	10.000	0.906	0.252	Can't reject normality
		Mixer	10.000	0.977	0.948	Can't reject normality
		Dilute	10.000	0.947	0.635	Can't reject normality
	1 10	Hand	10.000	0.867	0.092	Can't reject normality
		Mixer	10.000	0.948	0.644	Can't reject normality
		Dilute	10.000	0.948	0.646	Can't reject normality
	2.5 10	Hand	10.000	0.981	0.970	Can't reject normality
		Mixer	10.000	0.884	0.145	Can't reject normality
		Dilute	6.000	0.843	0.139	Can't reject normality
	5 10	Hand	10.000	0.936	0.506	Can't reject normality
		Mixer	10.000	0.948	0.643	Can't reject normality
		Dilute	10.000	0.888	0.163	Can't reject normality
	1 25	Hand	10.000	0.879	0.126	Can't reject normality
		Mixer	10.000	0.801	0.015	Reject normality
		Dilute	10.000	0.923	0.384	Can't reject normality
	2.5 25	Hand	10.000	0.901	0.226	Can't reject normality
		Mixer	10.000	0.851	0.060	Can't reject normality
		Dilute	10.000	0.954	0.716	Can't reject normality
	5 25	Hand	10.000	0.908	0.267	Can't reject normality
		Mixer	10.000	0.900	0.217	Can't reject normality
		Dilute	10.000	0.941	0.564	Can't reject normality

Please refer to the "Decision at level" column for conclusion

Figure A.16: Shapiro-Wilk Table of Strength from Mixing Samples, Grouped by Type Then Mixing Style.

Normality Test (7/31/2022 15:51:36)
NormalityTest
Shapiro-Wilk

			DF	Statistic	p-value	Decision at level(5%)
Strength	Hand	1 CNF	9.000	0.969	0.882	Can't reject normality
		2.5 CNF	10.000	0.924	0.388	Can't reject normality
		5 CNF	10.000	0.906	0.252	Can't reject normality
		1 10	10.000	0.867	0.092	Can't reject normality
		2.5 10	10.000	0.981	0.970	Can't reject normality
		5 10	10.000	0.936	0.506	Can't reject normality
		1 25	10.000	0.879	0.126	Can't reject normality
		2.5 25	10.000	0.901	0.226	Can't reject normality
		5 25	10.000	0.908	0.267	Can't reject normality
	Mixer	1 CNF	10.000	0.952	0.693	Can't reject normality
		2.5 CNF	10.000	0.960	0.780	Can't reject normality
		5 CNF	10.000	0.977	0.948	Can't reject normality
		1 10	10.000	0.948	0.644	Can't reject normality
		2.5 10	10.000	0.884	0.145	Can't reject normality
		5 10	10.000	0.948	0.643	Can't reject normality
		1 25	10.000	0.801	0.015	Reject normality
		2.5 25	10.000	0.851	0.060	Can't reject normality
		5 25	10.000	0.900	0.217	Can't reject normality
	Dilute	1 CNF	10.000	0.928	0.430	Can't reject normality
		2.5 CNF	10.000	0.914	0.310	Can't reject normality
		5 CNF	10.000	0.947	0.635	Can't reject normality
		1 10	10.000	0.948	0.646	Can't reject normality
		2.5 10	6.000	0.843	0.139	Can't reject normality
		5 10	10.000	0.888	0.163	Can't reject normality
		1 25	10.000	0.923	0.384	Can't reject normality
		2.5 25	10.000	0.954	0.716	Can't reject normality
		5 25	10.000	0.941	0.564	Can't reject normality

Please refer to the "Decision at level" column for conclusion

Figure A.17: Shapiro-Wilk Table of Strength from Mixing Samples, Grouped by Mixing Style Then Type.

Table A4: Statistics of 10% and 25 Percent Titania Films Across All Mixing Styles for All Times, Alpha=0.05 *=Significance

Category	Modulus (P value) 10%	Strength (P Value) 10%	Modulus (P value) 25%	Strength (P Value) 25%
1 Minute Hand vs Mixer 1D	0.41	0.16	0.13	0.06
1 Minute Hand vs Mixer 2D	0.086	0.27	0.219	0.06
2.5 Minute Hand vs Mixer 1D	0.818	0.03*	0.211	0.561
2.5 Minute Hand vs Mixer 2D	0.04*	0.25	0.24	0.12
5 Minute Hand vs Mixer 1D	0.016*	0.018*	0.506	0.082
5 Minute Hand vs Mixer 2D	0.936	0.355	0.032*	0.391
Mixer 1 Minute vs 2.5 Minute 1D	0.002*	0.03*	0.0042*	0.206
Mixer 1 Minute vs 2.5 Minute 2D	0.14	0.80	0.008*	0.635
Mixer 2.5 Minute vs 5 Minute 1D	0.04*	0.352	0.09	0.014*

Mixer 2.5 Minute vs 5 Minute 2D	0.006*	0.003*	0.561	0.389
Mixer 1 Minute vs 5 Minute 1D	0.191	0.012*	0.609	0.251
Mixer 1 Minute vs 5 Minute 2D	0.58	0.027*	0.021*	0.6
Mixer vs Dilute 1D	0.00106*	0.001*	0.0076*	0.001*
Mixer vs Dilute 2D	0.025*	0.025*	$9.55e^{-6}$*	$9.55e^{-6}$*

APPENDIX C: POLYCUP STATISTICAL ANALYSIS

Polycup:

Normality Test (7/30/2022 00:56:12)
NormalityTest
Shapiro-Wilk

			DF	Statistic	p-value	Decision at level(5%)
Modulus	1	CNF	5.000	0.904	0.430	Can't reject normality
		0.25	3.000	0.987	0.784	Can't reject normality
		1	5.000	0.901	0.418	Can't reject normality
		2.5	5.000	0.939	0.660	Can't reject normality
		5	5.000	0.974	0.898	Can't reject normality
	2	CNF	5.000	0.932	0.611	Can't reject normality
		0.25	3.000	0.862	0.272	Can't reject normality
		1	5.000	0.879	0.304	Can't reject normality
		2.5	5.000	0.981	0.938	Can't reject normality
		5	5.000	0.818	0.112	Can't reject normality

Modulus(1,CNF): At the 0.05 level, the data was significantly drawn from a normally distributed population.
Modulus(1,0.25): At the 0.05 level, the data was significantly drawn from a normally distributed population.
Modulus(1,1): At the 0.05 level, the data was significantly drawn from a normally distributed population.
Modulus(1,2.5): At the 0.05 level, the data was significantly drawn from a normally distributed population.
Modulus(1,5): At the 0.05 level, the data was significantly drawn from a normally distributed population.
Modulus(2,CNF): At the 0.05 level, the data was significantly drawn from a normally distributed population.
Modulus(2,0.25): At the 0.05 level, the data was significantly drawn from a normally distributed population.
Modulus(2,1): At the 0.05 level, the data was significantly drawn from a normally distributed population.
Modulus(2,2.5): At the 0.05 level, the data was significantly drawn from a normally distributed population.
Modulus(2,5): At the 0.05 level, the data was significantly drawn from a normally distributed population.

Figure A.18: Shapiro-Wilk Table on Modulus of Polycup Specimens Grouped by Direction.

Normality Test (7/30/2022 00:52:05)
NormalityTest
Shapiro-Wilk

			DF	Statistic	p-value	Decision at level(5%)
Modulus	CNF	1	5.000	0.904	0.430	Can't reject normality
		2	5.000	0.932	0.611	Can't reject normality
	0.25	1	3.000	0.987	0.784	Can't reject normality
		2	3.000	0.862	0.272	Can't reject normality
	1	1	5.000	0.901	0.418	Can't reject normality
		2	5.000	0.879	0.304	Can't reject normality
	2.5	1	5.000	0.939	0.660	Can't reject normality
		2	5.000	0.981	0.938	Can't reject normality
	5	1	5.000	0.974	0.898	Can't reject normality
		2	5.000	0.818	0.112	Can't reject normality

Modulus(CNF,1): At the 0.05 level, the data was significantly drawn from a normally distributed population.
Modulus(CNF,2): At the 0.05 level, the data was significantly drawn from a normally distributed population.
Modulus(0.25,1): At the 0.05 level, the data was significantly drawn from a normally distributed population.
Modulus(0.25,2): At the 0.05 level, the data was significantly drawn from a normally distributed population.
Modulus(1,1): At the 0.05 level, the data was significantly drawn from a normally distributed population.
Modulus(1,2): At the 0.05 level, the data was significantly drawn from a normally distributed population.
Modulus(2.5,1): At the 0.05 level, the data was significantly drawn from a normally distributed population.
Modulus(2.5,2): At the 0.05 level, the data was significantly drawn from a normally distributed population.
Modulus(5,1): At the 0.05 level, the data was significantly drawn from a normally distributed population.
Modulus(5,2): At the 0.05 level, the data was significantly drawn from a normally distributed population.

Figure A.19: Shapiro-Wilk Table on Modulus of Polycup Specimens Grouped by Sample Type.

Normality Test (7/30/2022 01:12:45)
NormalityTest
Shapiro-Wilk

			DF	Statistic	p-value	Decision at level(5%)
Strength	1	CNF	5.000	0.910	0.468	Can't reject normality
		0.25	3.000	0.849	0.239	Can't reject normality
		1	5.000	0.989	0.975	Can't reject normality
		2.5	5.000	0.885	0.333	Can't reject normality
		5	5.000	0.962	0.822	Can't reject normality
	2	CNF	5.000	0.996	0.996	Can't reject normality
		0.25	3.000	0.994	0.846	Can't reject normality
		1	5.000	0.906	0.445	Can't reject normality
		2.5	5.000	0.851	0.199	Can't reject normality
		5	5.000	0.827	0.133	Can't reject normality

Strength(1,CNF): At the 0.05 level, the data was significantly drawn from a normally distributed population.
Strength(1,0.25): At the 0.05 level, the data was significantly drawn from a normally distributed population.
Strength(1,1): At the 0.05 level, the data was significantly drawn from a normally distributed population.
Strength(1,2.5): At the 0.05 level, the data was significantly drawn from a normally distributed population.
Strength(1,5): At the 0.05 level, the data was significantly drawn from a normally distributed population.
Strength(2,CNF): At the 0.05 level, the data was significantly drawn from a normally distributed population.
Strength(2,0.25): At the 0.05 level, the data was significantly drawn from a normally distributed population.
Strength(2,1): At the 0.05 level, the data was significantly drawn from a normally distributed population.
Strength(2,2.5): At the 0.05 level, the data was significantly drawn from a normally distributed population.
Strength(2,5): At the 0.05 level, the data was significantly drawn from a normally distributed population.

Figure A.20: Shapiro-Wilk Table on Strength of Polycup Specimens Grouped by Direction.

Normality Test (7/30/2022 01:11:32)
NormalityTest
Shapiro-Wilk

			DF	Statistic	p-value	Decision at level(5%)
Strength	CNF	1	5.000	0.910	0.468	Can't reject normality
		2	5.000	0.996	0.996	Can't reject normality
	0.25	1	3.000	0.849	0.239	Can't reject normality
		2	3.000	0.994	0.846	Can't reject normality
	1	1	5.000	0.989	0.975	Can't reject normality
		2	5.000	0.906	0.445	Can't reject normality
	2.5	1	5.000	0.885	0.333	Can't reject normality
		2	5.000	0.851	0.199	Can't reject normality
	5	1	5.000	0.962	0.822	Can't reject normality
		2	5.000	0.827	0.133	Can't reject normality

Strength(CNF,1): At the 0.05 level, the data was significantly drawn from a normally distributed population.
Strength(CNF,2): At the 0.05 level, the data was significantly drawn from a normally distributed population.
Strength(0.25,1): At the 0.05 level, the data was significantly drawn from a normally distributed population.
Strength(0.25,2): At the 0.05 level, the data was significantly drawn from a normally distributed population.
Strength(1,1): At the 0.05 level, the data was significantly drawn from a normally distributed population.
Strength(1,2): At the 0.05 level, the data was significantly drawn from a normally distributed population.
Strength(2.5,1): At the 0.05 level, the data was significantly drawn from a normally distributed population.
Strength(2.5,2): At the 0.05 level, the data was significantly drawn from a normally distributed population.
Strength(5,1): At the 0.05 level, the data was significantly drawn from a normally distributed population.
Strength(5,2): At the 0.05 level, the data was significantly drawn from a normally distributed population.

Figure A.21: Shapiro-Wilk Table on Strength of Polycup Specimens Grouped by Sample

Normality Test (7/30/2022 00:32:05)
NormalityTest
Shapiro-Wilk

		DF	Statistic	p-value	Decision at level(5%)
Water Gain	CNF	18.000	0.979	0.940	Can't reject normality
	0.250	18.000	0.952	0.465	Can't reject normality
	1.000	18.000	0.886	0.032	Reject normality
	2.500	18.000	0.972	0.831	Can't reject normality
	5.000	18.000	0.947	0.383	Can't reject normality

Water Gain(CNF): At the 0.05 level, the data was significantly drawn from a normally distributed population.
Water Gain(0.250): At the 0.05 level, the data was significantly drawn from a normally distributed population.
Water Gain(1.000): At the 0.05 level, the data was not significantly drawn from a normally distributed population.
Water Gain(2.500): At the 0.05 level, the data was significantly drawn from a normally distributed population.
Water Gain(5.000): At the 0.05 level, the data was significantly drawn from a normally distributed population.

Figure A.22: Shapiro-Wilk Table of Water Gain of Polycup Specimens.

Table A5: P Values of Polycup Films Mechanical Tests, Alpha=0.05 *=Significance

Category	Modulus (P value)	Strength (P value)
1 Direction All composites	0.005*	0.328
2 Direction All Composite	0.26*	0.3

Table A6: ANOVA P Values From Time Point 10 Minutes Alpha=0.05 *=Significance

Category	P value
5% Polycup vs CNF 10 Minute	0.004**
5% Polycup vs 0.25% Polycup 10 Minute	0.04*
5% Polycup vs 1% Polycup 10 Minute	0.01*
5% Polycup vs 2.5% Polycup 10 Minute	0.16
2.5% Polycup vs CNF 10 Minute	0.001**
2.5% Polycup vs 0.25% Polycup 10 Minutes	0.016*
2.5% Polycup vs 1% Polycup 10 Minutes	0.0024*

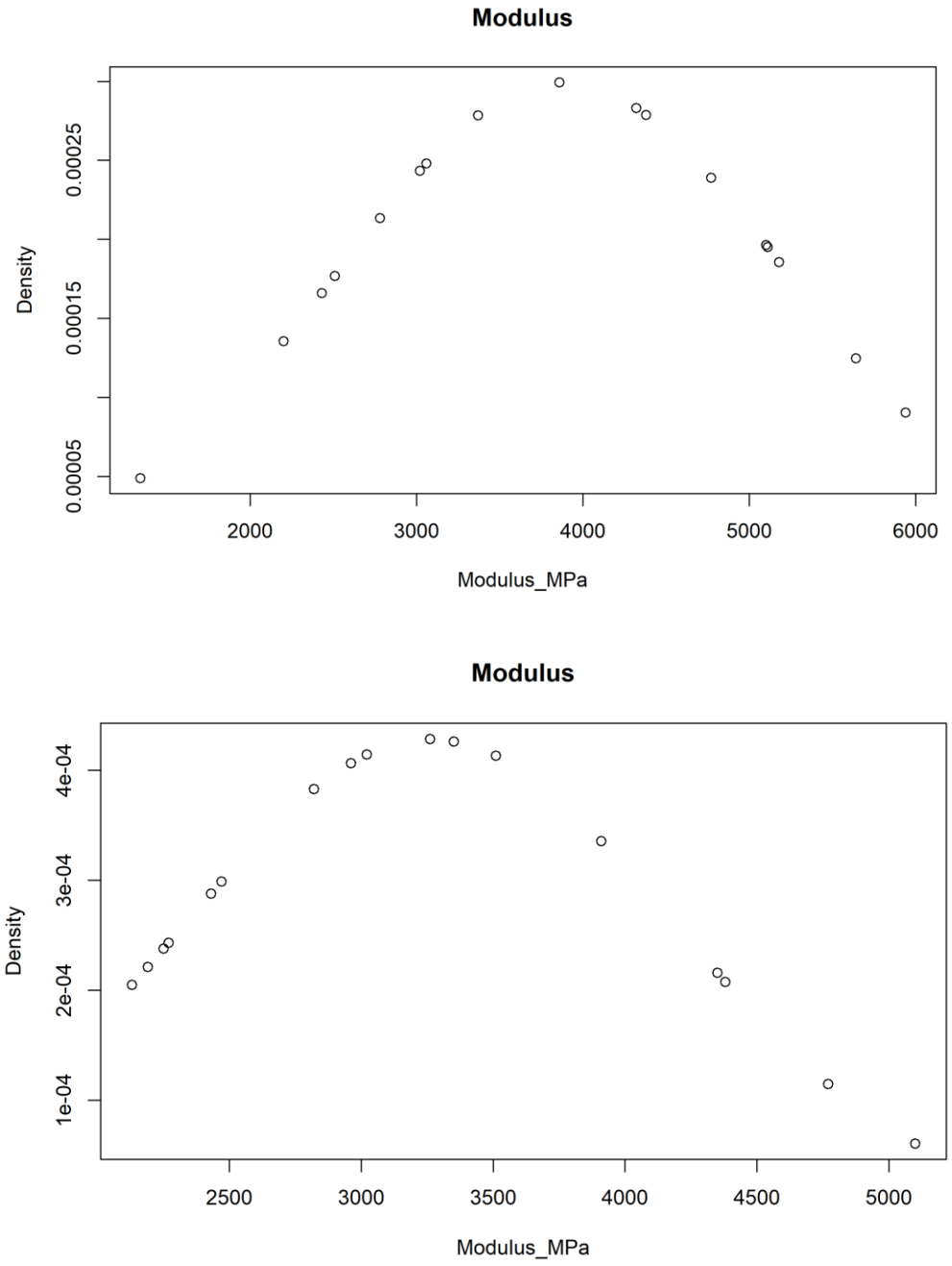

Figure A.23: Normality of Modulus Across All PolyCup wt% (Top 1 Direction, Bottom 2 Direction).

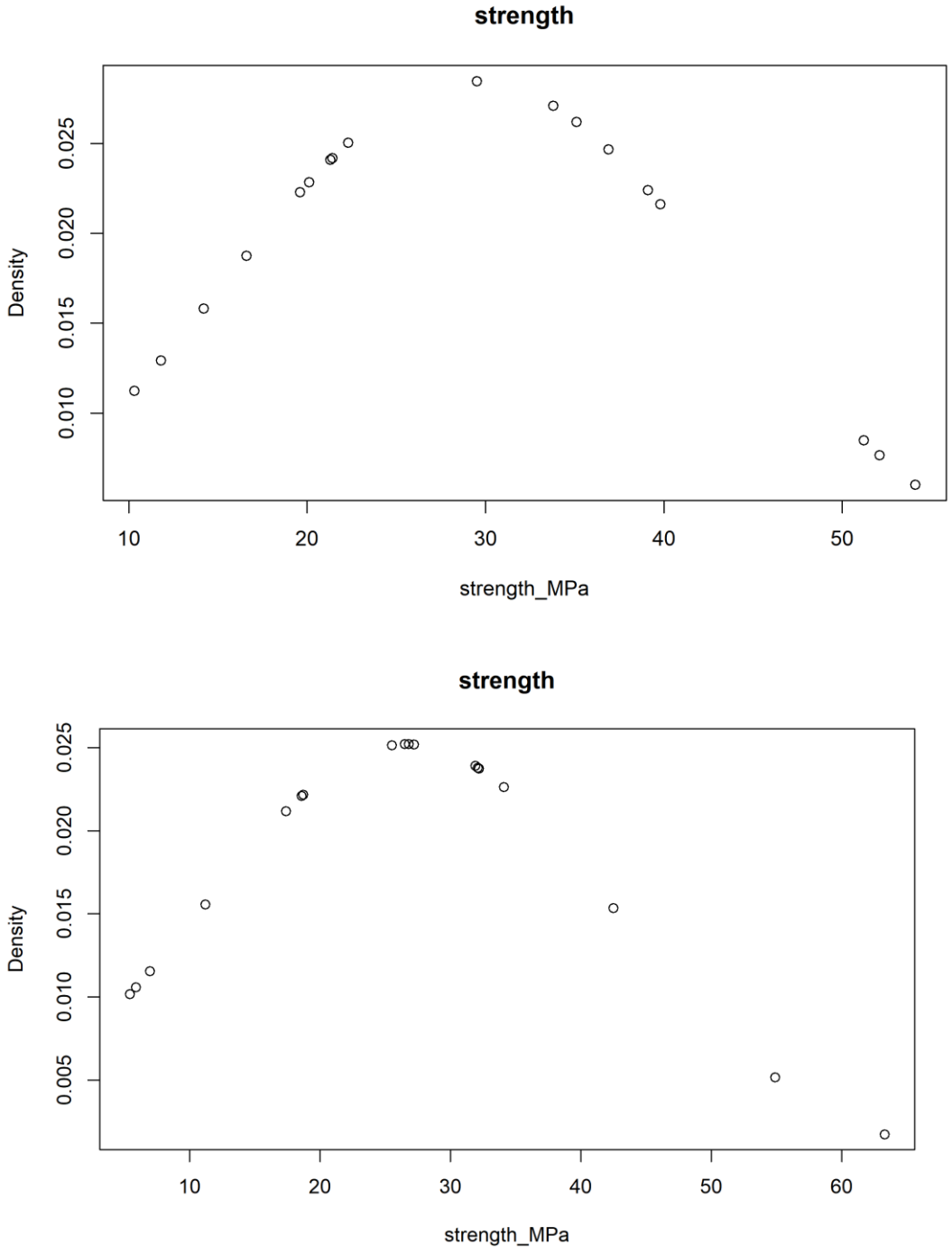

Figure A.24: Normality of Strength Across All Polycup wt% (Top 1 Direction, Bottom 2 Direction).

BOIGROPHY OF AUTHOR

Mitchell Chesley was born in Waterville on January 1st, 1995. He graduated from Gardiner Area High School spring of 2013, before continuing on for a Bachelor's in Bioengineering at The University of Maine. In the spring of 2017 he graduated from The University of Maine with his Bachelor's in bioengineering and proceeded to work on campus with the Mason lab as a Research Specialist. In the spring of 2018 he began his graduate career in biomedical engineering at the University of Maine. In the August of 2019 he completed his master's degree in biomedical engineering from The University of Maine and started his IPh.D. in the fall 2019. In Spring of 2020 he received his candidacy and became a Ph.D. candidate. He is a Candidate for the Interdisciplinary Doctor of Philosophy degree in biomaterial engineering from the University of Maine in August 2022.